Long-term Performance of Activated Carbon in Cyclic Adsorption/Regeneration of VOCs: Experimental and Modeling Investigation of Fixed Bed Adsorber

by

Amin Sadeghi Ardekani

A thesis submitted in partial fulfillment of the requirements for the degree of

Master of Science

in

Environmental Engineering

Department of Civil and Environmental Engineering

University of Alberta

Abstract

Activated carbon (AC) has attracted tremendous interest in adsorption-based air treatment. Nonetheless, a major challenge associated with the use of ACs is the decline in adsorption capacity with time due to heel build-up (i.e., accumulation of non-desorbed species). Designing a reliable adsorption system requires a deeper understanding of the changes occurring during the long-term use of ACs. For this purpose, the effect of ACs' properties such as porosity and operational conditions such as purge gas flow rate on the long-term performance of ACs requires further investigation.

 The objective of the present work was two-fold: first, to study the simultaneous effect of purge gas flowrate and activated carbon's porosity during prolonged cyclic adsorption/regeneration of three different ACs. Secondly, develop a model that can predict the long-term performance of ACs during adsorption/regeneration of a representative volatile organic compound (VOC). This section itself comprised two main stages: 1) Modeling the impact of heel on AC's pore size distribution (PSD), adsorption isotherm, and capacity, and 2) verifying the model using cyclic adsorption-desorption of 1,2,4-trimethyl benzene (TMB). The model predicts the cyclic adsorption capacity of AC by applying the Dubinin-Radushkevich-Langmuir (D-R-L) isotherm based on AC's limiting pore volume and adsorbate-adsorbent affinity coefficient.

For the long-term experimental study, six scenarios were investigated by varying the dry air purge gas flow rates 0.5 and 5 SLPM and the porosity of adsorbent used (44%, 60%, and 86% microporosity). The cyclic adsorption/regeneration experiment results indicated that the cumulative heel and the adsorption capacity followed ascending and descending trends with cycle number, respectively. Initially, the porosity and micropore volume of the adsorbents played a more

important role in their performance. However, at higher cycle numbers, the effect of purge gas flow rate was more determinant in the performance of ACs. In the first five cycles, the two adsorbents with the highest micropore volume, G-70R, and B101412, showed similar heel build-up formation rates while B100772 with lower micropore volume ($0.43\ \frac{cm^3}{g}$ as opposed to $0.50\ \frac{cm^3}{g}$) had slightly lower heel build-up. Alternatively, at the 20th cycle, purge gas flow rate had a clear effect on the performance and cumulative heel build-up of all three ACs regardless of their porosity. For all three adsorbents used in this study, samples regenerated with 0.5 SLPM all had an average cumulative heel of 31 %. Those regenerated with 5 SLPM Had a cumulative heel build-up average of 21%. The presence of mesopores and a hierarchal pore structure certainly helped reduce heel build-up in the micropores. DTG analysis of the samples showed that with an increase in purge gas flow rate, the nature of heel build-up starts to change and transform into heavier chemically formed compounds.

In the second part, two machine learning (ML) algorithms, multivariate linear regression (MLR) and Decision tree, were applied to predict Micropore volume reduction because of volatile organic compounds (VOCs) cyclic heel build-up on activated carbons (ACs). A dataset of 100 experimental tests of cyclic adsorption/regeneration of different VOCs on ACs with distinct properties was used. It was observed that micropore volume reduction could be predicted with acceptable accuracy with an R2 of 0.85 ± 0.08 using the MLR algorithm by considering the adsorbent characteristics, adsorbate properties, and regeneration conditions. The micropores prediction results were then combined with several mathematical equations to predict the pore size distribution of a used activated carbon. To verify the model, its results were tested against nine samples with various stages of heel build-up. The micropore and PSD were predicted with a mean relative absolute error (MRAE) of 3.5%, 10.8%, and 12.0% for G-70R, B101412, and B100772,

respectively. The PSD prediction model was then utilized in conjunction with the DRL isotherm prediction model, and the adsorption capacity of samples at five concentrations of 0, 50, 100, 500, and 1000 ppm were predicted for each adsorbent. The prediction of adsorption capacity on the virgin G-70R, B101412, and B100772 had a MRAE of 0.6%, 8.9%, and 2.7, respectively while for the corresponding used samples the MRAE was 13.2%, 10.1%, and 10.0%. The results of this study are beneficial in improving the long-term performance of activated carbons and making them last longer.

DEDICATIONS

*Dedicated to the loving memory of my aunt, **Neda**.*

May you rest in peace.

"Only in silence the word,

Only in dark the light,

Only in dying life:

Bright the hawk's flight

On the empty sky."

Ursula K.Le Guin

Acknowledgements

First and foremost, I must give thanks to my outstanding advisor, Professor Zaher Hashisho, whose fatherly guidance and motivations kept me on track and inspired me to continue my work. I cannot express enough gratitude for everything you taught me through these years. I will remember your teaching in both my academic and personal life.

In addition, I would like to thank my amazing parents, Bita and Mohammadreza; your continued support gave me the warmth to survive many cold nights away from home. Additionally, I want to give a loving thanks to my second family in Edmonton, Keivan, Marjan, and Vahab. Thank you for making me feel I belong and for briefly making me forget how far I was from everyone I knew. Your care and compassion was the only reason I had to keep pushing forward and try to do better. Thank you for putting up with me for more than two years. No matter where we each might end up, you will always be a part of me.

I appreciate my colleagues and friends in the Air Quality Characterization Lab for their valuable help, contributions, and, more importantly, their friendship: Arman Peyravi, Sina Esfandiarpour, and Saied Alizadeh.

Last but not least, I want to give special thanks to Dr. Alireza Haghighat, who was always there when I needed him the most. Thank you for giving me the comfort of mind and motivation to keep going and believing in myself.

TABLE OF CONTENTS

LIST OF TABLES

LIST OF FIGURES

LIST OF ACRONYMS

1,2,4-TMB	1,2,4-trimethylbenzene
AC	Activated carbon
ACF	Activated carbon fibers
ARE	Absolute relative error
BAC	Beaded activated carbon
CEPA	Canadian environment protection act
DAC	Data acquisition and control
DFT	Density function theory
DRL	Dubinin-Radushkevich-Langmuir
DRL	Dubinin-Radushkevich
DTG	Derivative thermogravimetric
EPA	Environmental protection agency
GAC	Granular activated carbon
IUPAC	International union of pure and applied chemistry
LSM	Least squared method
MAE	Mean absolute error
MFC	Mass flow controller
ML	Machine learning
MLR	Multivariate linear regression
MRAE	Mean relative absolute error
MRAE	Mean relative absolute error
PAC	Powdered activated carbon
PCC	Pearson correlation coefficient
PID	Photoionization detectors
PSA	Pressure swing adsorption
PSD	Pore size distribution
QSAR	Quantitative structure-activity relationship
QSDFT	Quenched solid density function theory
RMSE	Root mean squared error
SLPM	Standard liter per minute
TGA	Thermogravimetric analysis
TSA	Thermal swing adsorption
VOC	Volatile organic compound

Recognition of contributions

The research conducted in this work is an original study done by myself Amin Sadeghi Ardekani. I was responsible for proper initial planning, designing, and performing the experiments required for this study. Subsequently, data acquisition and interpretation were also performed by me under the careful supervision of Dr. Zaher Hashisho. The automated setup utilized for the long-term cyclic experimental investigation, explained in detail in Chapter 3, was originally developed by Dr. Alireza Haghighat. He was responsible for the logic and the design of the setup.

Furthermore, he initiated the building of this device's prototype, which was later completed and improved upon by me under Dr. Zaher Hashisho's supervision. Many parts of the original prototype were replaced and recalibrated during these improvements so the setup could perform with utmost efficiency. Data acquisition and calculation methods were also developed by me to ease the use of this device.

1. CHAPTER 1: Introduction

1.1 Volatile Organic Compounds

Several Definitions for Volatile Organic Compounds (VOCs) are used by various governmental entities. These definitions differ based on which characteristic of VOC is targeted[1]. The U.S Environmental Protection Agency (EPA) defines VOCs based on the potential for photochemical reaction. It identifies VOCs as any carbon compound that can participate in the atmospheric photochemical reaction, excluding carbon monoxide, carbon dioxide, carbonic acid, metallic carbides or carbonates, ammonium carbonate, and those it designates as having negligible photochemical reactivity[2]. Prior to 2001, the European Union (E.U.) defined VOCs as any organic compound, at 293.15 K, having a vapor pressure of 0.01 KPa or more. Subsequently, a new definition more aligned with their U.S. counterpart was brought forth that defined VOCs as all anthropogenic organic compounds, excluding methane, which have the potential for photochemical oxidants production due to reaction with nitrogen oxide in the presence of sunlight[3,4]. Similarly, the Canadian Environment Protection Act (CEPA) describes VOCs as organic compounds with one or more carbon atoms that can readily evaporate into the atmosphere, excluding photo-chemically non-reactive compounds such as methane, ethane and the chlorofluorocarbons (CFCs)[5]

The U.S EPA categorizes a large number of VOCs as human carcinogens, irritants, and toxicants. Moreover, recent studies suggest that not only a link exists between the development of several respiratory diseases and VOC exposure, but also they could exasperate existing conditions in patients[6,7]. In addition, VOCs being precursors in the formation of particulate matter ($PM_{2.5}$) and ground-level ozone, through photochemical reactions with NO_x, can facilitate smog formation [8].

VOC sources can be categorized into two major groups of anthropogenic sources and natural sources. Natural sources include volcanic eruptions, vegetation emissions, and forest fires[1],while

human-made sources refer to transportation (i.e., vehicle exhaust emissions), oil refining, and many industrial activities[9]. VOC emissions from the aforementioned major sources vary greatly. On a global scale, natural sources release significantly more VOC than human-made sources[10,11] However, in most industrialized countries such as China, both sources produce almost the same level of VOC emission[12]. In Canada, the amount of anthropogenic VOCs remained almost the same from 1990 to 1998, averaging 2867 kilotonnes of VOC per year, but since then, with the enactment of new control methods and regulations, these amounts have continuously declined and have reached values as low as 1675 kilotonnes by 2019. In that order, the primary sectors contributing to VOC emissions in 2019 were the oil and gas, paints and solvents, and commercial/residential/institutional [13].

As stated, the paints and solvents sector has been ranked the second primary anthropogenic source of VOC emission in Canada and produced about 300 kilotonnes of VOC in 2019 alone, where surface coating operations contributed to about 22 % of it [13]. These emissions results from the solvent-based paints being generally used, which contain various organic compounds such as aromatic and aliphatic hydrocarbons, esters, ketones, and alcohols. Many efforts have been made to replace these solvent-based paints with water-based paints and powdered paints; alas, these efforts have mainly been unsuccessful thus far because of encountering two issues: (i) they are not 100% organic solvent-free and still emit a considerable amount of VOCs, and (ii) the final quality of the paint is negatively affected, which cannot meet the market requirement[9]. As a result, mitigation methods are still the main approach for controlling VOC emissions.

1.2 VOC mitigation methods

There exists a wide variety of methods for the control of VOC emissions. However, these techniques can be categorized into two general groups: (i) methods that require modifications in

3

the equipment and materials used in the process or even changes in the process itself, with VOC emission reduction in mind, and (ii) add-on control techniques aiming to regulate emissions. Even though the former techniques can be effective, their usage is limited because modifications are not always possible. Add-on control techniques can further be classified into two main sub-groups: (i) destructive and (ii) non-destructive methods [14].

As the name suggests, the central common factor in destructive methods is eliminating VOCs, whether with the help of oxidation as in thermal and catalytic oxidation or digestion by microorganisms as is the case in bio-filtration [14]. Thermal oxidation is generally used when recovery of energy is of high importance since energy recovery up to 85% is possible. In this method, VOCs are directly combusted and converted mainly into carbon dioxide and water. Catalytic oxidation functions similarly to thermal oxidation, with the major difference of operating at much lower temperatures (370-480 °C as opposed to 700 to 980 °C). Biofiltration operates by directing the VOC-laden air stream over biologically active compost or soil and thus oxidizing the VOCs with the biological activity of the bed. Although this method requires less capital investment and produces safer secondary waste, it is limited by its sluggishness and selectivity of the microorganisms towards different VOCs [15].

Non-Destructive methods are used when the target is the recovery of the VOC rather than its removal [15]. In comparison with destructive methods, recovery methods are more economical because they realize recovery of VOCs, which could be re-used down the line. Furthermore, the high temperatures used in destructive methods will inadvertently result in toxic byproducts such as NO_x [16] . Recovery methods consist of condensation, adsorption, absorption, and membrane separation, each with its own advantages and limitations. [14,15] **Figure 1.1.1** Illustrates various VOC mitigation methods most commonly used.
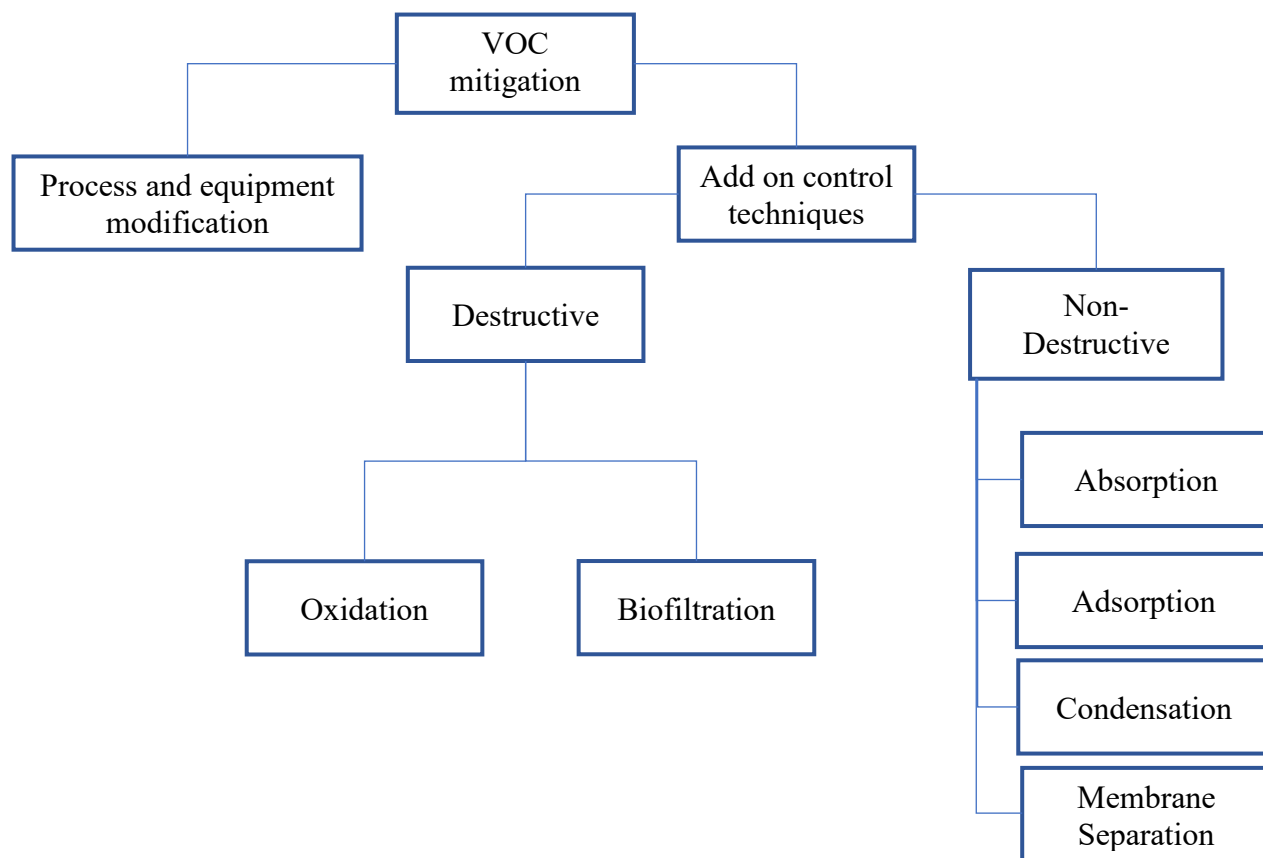
Figure 1.1 Classification of VOC abatement methods[14]

Adsorption is extensively applied for VOC capture and recovery and is the most favorable mitigation method due to its low cost and high efficiency [16,17]. Selecting a proper adsorbent is crucial for an efficient adsorption process. An ideal adsorbent is expected to possess specific characteristics such as high adsorption capacity, high hydrophobicity to be competitive with water vapor present in flue gas, easy regeneration, and high thermal stability to make sure it can withstand cyclic adsorption/regeneration[17]. Activated carbon is one of the most widely used adsorbents due to its low-cost production, considerable adsorption capacity, and thermal stability [16]. In industries, standard practice follows the adsorption stage with a regeneration stage to re-use the activated carbon and make it a financially viable method for VOC capture and removal [18].

Several regeneration methods are available, including thermal[19], chemical[20] and biological[21]. In most industrial processes, thermal regeneration is conducted at temperatures not exceeding 300 °C to regenerate activated carbon adsorbents loaded with VOCs from a contaminated gas stream [22]. However, this regeneration cannot always completely restore the adsorbent to its virgin state, and heel build-up, i.e., accumulation of non-desorbed species and their byproducts on the surface of the adsorbent, occurs after each regeneration step. Heel build-up significantly impacts the adsorption capacity of activated carbon and, as a result, its lifespan and forces an inevitable replacement of the adsorbent, which results in an increased cost of the process [23]. It follows that knowing the heel formation rate and factors affecting it is essential.

1.3 Research Significance

Laboratory and pilot-plant testing have traditionally been the building block of adsorption system design. As with any experimental method, prior to conducting the experiments, specific goals are determined and parameters are set to study the aforementioned goal. These selected parameters such as regeneration temperature, adsorbate used and type of flow gas for the experimental conditions, as valuable as they are, limit the results obtained to that specific experimental condition. This limitation entails that one needs to conduct separate experiments for each different experimental condition and scenario one has in mind. In the case of cyclic adsorption experiments, investigating one specific adsorption scenario itself takes a long time and requires repetition of the adsorption/regeneration experiment to study changes occurring with consecutive usage. Additionally, in each experimental cycle, depending on the nature of the experiment, energy and chemicals are consumed. As a result, if multiple experimental scenarios are needed to be studied, the stress put on resources both from an economic and environmental perspective is worsened [24].

For long-term investigation of the adsorption/regeneration cyclic experiment in which the goal is to lifespan of the adsorbent, the difficulties above worsen to the point of making the study almost unachievable. Especially if for better comparison of the results, there is a need to run the test again with a different adsorbate or vary the experimental parameters. These issues might be why there are so few studies investigating changes occurring during the long-term performance of activated carbon adsorbents.

Alternatively, a mathematical model can simplify the design of a full-scale adsorption system by reducing the number of tests required under various operating conditions. These models are usually calibrated by a few well-designed and controlled laboratory bench-scale tests. Having been verified, the model itself can be used as a means of primary data development in place of the experiments. Ultimately, a verified model can be used to extrapolate other non-tested variables and avoid unnecessary time and expenses generally associated with pilot-scale testing to a reasonable extent. For the case of long-term performance, if a verified model existed, testing the effect of different experimental conditions on the performance of the selected adsorbent would be much easier and the difference between a five-cycle experiment and a 50 cycles experiment would be reduced to mere seconds rather than weeks and months.

1.4 Objectives

This study was conducted with two main objectives in mind:

1. Study the effect of activated carbon's (AC) microporosity on its long-term performance under two extreme purge gas flow rates.

2. Develop a mathematical model to predict changes in pore size distribution and performance of the activated carbon after long-term cyclic experiments.

In the experimental stage, three different activated carbons with various microporosities underwent consecutive cyclic adsorption/regeneration experiments using two different purge gas flowrates to study heel formation rates and capacity reduction for each case. For the modeling section, a dataset of 100 experimental tests of VOCs on activated carbon was collected from both existing literature and long-term cyclic experiments conducted in the first stage. Multivariable linear regression was applied to the data set in conjunction with the mathematical models existing in the literature to predict the effect of cumulative heel build-up on the pore size distribution and adsorption capacity given the adsorbents characteristics and adsorbents initial physical properties.

1.5 Thesis Outline

This thesis is divided into five chapters. Chapter 1 gives a general introduction of the topic and its objectives. Chapter 2 includes a detailed literature review on related topics such as adsorption, regeneration, heel formation, machine learning, and its application in adsorption. Chapter 3 includes a description of the materials and methods used. Chapter 4 presents the experimental and modeling results and their relevant discussions. Finally, in chapter 5 conclusions of the research as well as recommendations for future works are provided.

1.6 References

1. HaiLin W, Lie N, Jing L, et al. Characterization and assessment of volatile organic compounds (VOCs) emissions from typical industries. *Chinese Science Bulletin*. 2013;58(7):724-730. doi:10.1007/s11434-012-5345-2

2. Technical Overview of Volatile Organic Compounds | US EPA. Accessed September 19, 2021. https://www.epa.gov/indoor-air-quality-iaq/technical-overview-volatile-organic-compounds

3. EUR-Lex - 31999L0013 - EN - EUR-Lex. Accessed September 19, 2021. https://eur-lex.europa.eu/legal-content/EN/TXT/?uri=celex%3A31999L0013

4. EUR-Lex - 32001L0081 - EN - EUR-Lex. Accessed September 19, 2021. https://eur-lex.europa.eu/legal-content/EN/TXT/?uri=celex%3A32001L0081

5. Toxic substances list: volatile organic compounds - Canada.ca. Accessed September 19, 2021. https://www.canada.ca/en/environment-climate-change/services/management-toxic-substances/list-canadian-environmental-protection-act/volatile-organic-compounds.html

6. Nurmatov UB, Tagiyeva N, Semple S, Devereux G, Sheikh A. Volatile organic compounds and risk of asthma and allergy: a systematic review. *European Respiratory Review*. 2015;24(135):92-101. doi:10.1183/09059180.00000714

7. Paciência I, Madureira J, Rufo J, Moreira A, Fernandes E de O. A systematic review of evidence and implications of spatial and seasonal variations of volatile organic compounds (VOC) in indoor human environments. *http://dx.doi.org/101080/1093740420151134371*. 2016;19(2):47-64. doi:10.1080/10937404.2015.1134371

8. Canada Gazette, Part 1, Volume 153, Number 27: Volatile Organic Compound Concentration Limits for Certain Products Regulations. Accessed September 19, 2021. https://gazette.gc.ca/rp-pr/p1/2019/2019-07-06/html/reg1-eng.html

9. Kim BR. VOC Emissions from Automotive Painting and Their Control: A Review. *Environmental Engineering Research*. 2011;16(1):1-9. doi:10.4491/eer.2011.16.1.001

10. Piccot SD, Watson JJ, Jones JW. A Global Inventory of Volatile Organic Compound Emissions From Anthropogenic Sources. *Journal of Geophysical Research: Atmospheres*. 1992;97(D9). doi:10.1029/92JD00682

11. Guenther A, Hewitt CN, Erickson D, et al. A global model of natural volatile organic compound emissions. *Journal of Geophysical Research: Atmospheres*. 1995;100. doi:10.1029/94JD02950

12. Tie X, Li G, Ying Z, Guenther A, Madronich S. Biogenic emissions of isoprenoids and NO in China and comparison to anthropogenic emissions. *Science of the Total Environment*. 2006;371:238-251. doi:10.1016/j.scitotenv.2006.06.025

13. Canada's Air Pollutant Emissions Inventory - Open Government Portal. Accessed September 19, 2021. https://open.canada.ca/data/en/dataset/fa1c88a8-bf78-4fcb-9c1e-2a5534b92131

14. Khan FI, Kr Ghoshal A. Removal of Volatile Organic Compounds from polluted air. *Journal of Loss Prevention in the Process Industries*. 2000;13(6):527-545. doi:10.1016/S0950-4230(00)00007-3

15. Rani Parmar G, Rao NN. Emerging Control Technologies for Volatile Organic Compounds. *Critical Reviews in Environmental Science and Technology*. 2008;39(1):41-78. doi:10.1080/10643380701413658

16. Zhang X, Gao B, Creamer AE, Cao C, Li Y. Adsorption of VOCs onto engineered carbon materials: A review. *Journal of Hazardous Materials*. 2017;338:102-123. doi:10.1016/J.JHAZMAT.2017.05.013

17. Yang C, Miao G, Pi Y, et al. Abatement of various types of VOCs by adsorption/catalytic oxidation: A review. *Chemical Engineering Journal*. 2019;370:1128-1153. doi:10.1016/J.CEJ.2019.03.232

18. Carratalá-Abril J, Lillo-Ródenas MA, Linares-Solano A, Cazorla-Amorós D. Regeneration of activated carbons saturated with benzene or toluene using an oxygen-containing atmosphere. *Chemical Engineering Science*. 2010;65(6):2190-2198. doi:10.1016/J.CES.2009.12.017

19. Moreno-Castilla C, Rivera-Utrilla J, Joly JP, López-Ramón M v., Ferro-García MA, Carrasco-Marín F. Thermal regeneration of an activated carbon exhausted with different substituted phenols. *Carbon*. 1995;33(10):1417-1423. doi:10.1016/0008-6223(95)00090-Z

20. Martin RJ, Ng WJ. Chemical regeneration of exhausted activated carbon—I. *Water Research*. 1984;18(1):59-73. doi:10.1016/0043-1354(84)90048-4

21. Ivancev-Tumbas I, Dalmacija B, Tamas Z, Karlovic E. Reuse of biologically regenerated activated carbon for phenol removal. *Water Research*. 1998;32(4):1085-1094. doi:10.1016/S0043-1354(97)00337-0

22. Hwang KS, Choi DK, Gong SY, Cho SY. Adsorption and thermal regeneration of methylene chloride vapor on an activated carbon bed. *Chemical Engineering Science*. 1997;52(7):1111-1123. doi:10.1016/S0009-2509(96)00470-8

23. Jahandar Lashaki M, Hashisho Z, Phillips JH, Crompton D, Anderson JE, Nichols M. Mechanisms of heel buildup during cyclic adsorption-desorption of volatile organic compounds in a full-scale adsorber-desorber. *Chemical Engineering Journal*. 2020;400:124937. doi:10.1016/J.CEJ.2020.124937

24. Weber WJ, Smith EH. Simulation and design models for adsorption processes. *Environmental Science and Technology*. 1987;21(11):1040-1050. doi:10.1021/ES00164A002

2. CHAPTER 2: Literature review

2.1 Adsorption

Adsorption is a separation process in which gas or solutes are transferred and accumulated onto solid surfaces [1,2]. Unbalanced molecular forces exist on all surfaces; when a substance collides with that surface, the existing unbalanced forces attract the substance and maintain it near the interface. This phenomenon results in a more prominent presence of the gas or liquid in the vicinity of the solid surface than the bulk phase, regardless of gas or liquids' nature [3]. The gas or vapor accumulated on the solid, which is in the adsorbed state, is usually referred to as "adsorbate," and the space it occupies is aptly named "adsorption space" [4].

Based on the nature of forces involved, adsorption can be divided into two main categories: physical adsorption (physisorption) and chemical adsorption (chemisorption). Physisorption is produced by the reversible interaction of weak van der Waals forces among adsorbed species and adsorbent surface. Chemical Adsorption, on the other hand, involves the transfer or sharing of electrons resulting in the formation of chemical bonds[3,5]. The chemical bonds formed are relatively more robust than the intermolecular forces existing in physisorption. Therefore, the enthalpy changes in chemisorption are more substantial and in the order of 40 to 400 KJ, while it does not usually exceed 20 K.J. for physisorption [3,5].

Furthermore, physisorption is non-selective and can occur between any adsorbate-adsorbent system, whereas chemisorption only takes place in specific system combinations. Finally, because of the selectivity involved in chemisorption, it can only form unimolecular layers; conversely, physisorption does not suffer this limitation and can form multimolecular layers [6]. It should be noted that chemical and physical adsorption are not isolated and often co-occur [7].

In the case of separation processes, research has shown physical adsorption to be the more significant of the two. Physisorption can further be categorized into Thermal swing adsorption

(TSA) and Pressure swing adsorption (PSA), which is solely dependent on how the operation is performed [2].

2.2 Activated Carbon

First records of activated carbon usage in human history go back as far as 1600 B.C in Egypt where wood chars had a medicinal purpose. There have been many instances of activated carbon being used as an adsorbent in the recorded history, but practical usage of it only began in the 20th century during the world wars where the need for gas masks' development intensified adsorption research [1]. Activated carbon is an excellent adsorbent for most pollutants due to its highly porous structure, hydrophobicity, and large specific surface area. It can be produced by pyrolysis of nearly all carbonaceous organic material such as wood, husks, and coconut shells [7].

Activated Carbons, in general, have strongly developed internal surfaces and a porous structure made up of pores of various shapes and sizes [3]. Several methods have been suggested to determine the shape of the pores, which resulted in a diverse outcome such as slit-shaped, V-shaped capillaries, and many more [83]. The most common classification of pores, introduced by Dubinin and adopted by the International Union of Pure and Applied Chemistry (IUPAC), is based on the pores' width (W). The pore width is defined as the distance of the two adjacent walls for a slit-shaped pore or the radius of a cylindrical pore [3]. Based on Dubinins' classification, the porous structure of activated carbon is tri-dispersed and is made up of micropores, mesopores, and macropores.

Micropores, if slit-shape, are two-dimensional spaces in between two graphite-like walls and if cylindrical are the three-dimensional space within a cylinder with the cylinder diameter representing the pore width; however, whereas in graphite, the distance between two neighboring planes is a constant 3.76 Å (0.376 nm), in activated carbon, this distance is varied and mostly

greater than 3.76 Å since it can accommodate much larger adsorbate molecules [1]. In fact, micropores have pore widths of up to 20 Å (2nm). Another important parameter of micropores is their large surface areas. Because adsorption forces from opposite walls overlap in micropores, they have much larger adsorption energy than mesopores, and thus they are where a vast majority of adsorption takes place. The adsorption process, in micropores, is exclusively done through volume filling rather than capillary condensation [3].

Mesopores (also known as transitional pores) have dimensions in the range of 20 to 500 Å and typically only makeup 5% of the carbon's total surface area. Capillary condensation is the primary source of adsorption in these pores. Finally, macropores have a negligible contribution to the total surface area of the adsorbent [3].

Commercial activated carbon can often be found in one of two forms: powdered activated carbon (PAC) and granular activated carbon (GAC). PACs are produced from sawdust, and their average size is in the range of 15 to 25 μm. Alternatively, GACs are produced from pulverized powders and then bound together using tar. GACs sizes vary based on their application. [1]

2.3 Adsorption parameters

Adsorption parameters such as adsorption capacity and adsorption kinetics are influenced by a variety of factors. Although the affecting factors are many, they can mainly be divided into three categories: (i) operational conditions under which adsorption is conducted, (ii) adsorbent's chemical and physical property, and (iii) adsorbate's characteristics. Improving and optimizing industrial adsorption processes requires a thorough understanding of the aforementioned factors and their corresponding effects on the adsorption process [9].

Prior to delving deeper into the above categories, a few definitions are needed. Adsorption capacity (also known as loading) is the mass of adsorbate captured by the unit mass of adsorbent[10]. At any

given temperature, adsorption capacity, either as a function of its partial pressure or concentration, is described by the adsorption isotherm [11]. Adsorption capacity can be determined in many ways, two of the more important methods are: 1. Utilizing the gravimetric methods and weighting the adsorbent both before and after the adsorption process, and 2. Through the integration of the breakthrough curve.

The breakthrough curve is a plot that illustrates the concentration of the adsorbate existing in the effluent stream at any time since the initiation of the experiment. As long as the adsorbent has the capacity, the adsorbate vapor is wholly captured, and thus, the effluent stream is void of any vapor trace. When saturation of the adsorbent is imminent, vapor concentration in the effluent stream begins to rise. The time at which 5% of the influent concentration is reached is called "breakthrough time." The rise in vapor concentration continues, and saturation time is reached when 100% of inlet concentration is observed, and no more adsorption occurs[12,13].

2.3.1 Adsorption Conditions

One of the most critical factors affecting the adsorption process is the temperature at which it takes place. Adsorption, being an exothermic reaction, is adversely affected by temperature increase[14,15]. Raising the adsorption temperature can provide the activation energy required to form chemical bonds and thus promotes chemisorption[16,17]. Additionally, higher temperature means faster adsorption kinetic and, as a result, shorter breakthrough time [18]. Lastly, by providing the molecules with more energy (i.e., increase in temperature), their kinetic energy and motion increase, resulting in easier diffusion into smaller pores [18]. Jahandar Lashaki et al.[16], in a study on the effect of adsorption and regeneration temperature on heel build-up on activated carbon, examined the effect of adsorption temperature on adsorption of 1-butanol, n-decane, and a mixture of chemicals typically emitted from automobile painting operations. It was reported that a 20°C increase in

adsorption temperature (from 25°C to 45°C) resulted in nearly 30% capacity loss for 1-butanol since it was physisorbed. However, for n-decane and the mixture in which chemisorption at 25°C was suspected, the increase in temperature caused a negligible difference in adsorption capacity. In conclusion, it appears that high temperatures is undesirable for adsorption since it decreases the adsorption capacity of the physisorbed compounds while at the same time promoting chemisorption, which can result in severe loss of capacity in future cycles.

Purge gas flowrate is another effective parameter that plays a role in heel buildup. Niknaddaf et al.[19], conducted a study where they investigated the combined effect of purge gas flowrate and heating rate. It was reported that that decreasing heating rate and/or increasing purge gas flow rate decreases heel buildup. The justification for this was that with an increased in purge gas flowrate, the resident time of adsorbates in micropores are reduced and thus they are exposed to high temperatures for shorter durations. Babu et all[20], also reported that with four times increase in flowrate, the breakthrough curve became steeper and the breakthrough time was almost halved. This was attributed to shorter residence time of the adsorbate in the bed which was not long enough to allow for adsorption equilibrium to be reached.

Adsorption duration is an essential element in multi-component gas adsorption. As the adsorption duration lengthens, heavier compounds replace the lighter ones leading to an increase in irreversible adsorption. [18]

2.3.2 Adsorbent's properties

The adsorption capability of activated carbons is dependent on several factors, including their physical properties such as their pore size distribution, surface area, total pore volume, and surface functional groups [21,22]. The aforementioned properties are highly influenced by the precursor organic material and the activation method and conditions chosen [23].

Cal et al. [24], investigated the adsorption of acetone and benzene on three activated carbon fibers (ACFs) with different porosity. It was reported that for a specific adsorbate, at low concentrations, the adsorbent with the narrower pores demonstrated better adsorption compared with the ACF with larger pores, even though the former had significantly lower surface area and total pore volume. However, the situation is reversed with increased inlet concentration, in which case total pore volume seems to play a more crucial role in adsorption capacity. Similar results were also reported by Mangun et al.[25], in a study where adsorption of alkanes with a different number of carbons, ranging from methane to pentane, on four varied ACF was studied. This study illustrated that at a low concentration for alkane with low boiling points, the molecule does not condense in the narrow micropore and remains in a tightly bound gas phase. As a result, it does not occupy a large volume, and the available pore volume is not a limiting parameter.

On the other hand, with an increase in the concentration and boiling point of the alkane, the adsorbate prefers to condense inside the larger mesopores; in this case, the available pore volume becomes an essential factor that affects adsorption capacity. As stated by Mangun et al.[25], the ideal adsorbent would be one with very narrow micropores and thus influential overlapping forces and sizeable total pore volume, facilitating adsorption in a broad range of VOC concentrations. From the previous study, it can be concluded that a pore size/ pore volume effect must be considered to optimize adsorbent performance.

Lillo-Ródenas et al.[23], performed a comprehensive study on the effect of microporosity on adsorption of benzene and toluene at low concentrations. They compared toluene and benzene adsorption capacity at low concentrations (200 ppmv) on ten different activated carbons. A high correlation was reported between CO_2 micropore volume, which shows micropore volume of

smaller micropores below 7 Å, and the adsorption capacity. Their conclusions for activated carbon are in good agreement with previous experiments conducted on ACF.

Comparable studies were conducted by Huang et al.[26], where three types of activated carbons adsorbed acetone and n-hexane. They showed that since BET surface area and pore volume are closely related, it is better to study adsorption capacity per unit BET area for practical purposes. This method simplifies observing the effect of micropore size differences on adsorption capacity. It was reported that the adsorption capacity per unit of BET area for acetone decreases for all three adsorbents when the porosity increases. The results are in agreement with previous studies. Since acetone has a low boiling point, it remains in the gas phase inside the pores, and the smaller pores, having stronger overlapping forces, can accumulate more acetone within than their larger counterparts.

The effect of porosity on adsorption capacity was also investigated by Lashaki et al.[27], in a study involving a mixture of VOCs and five different beaded activated carbons. The mixture involved many compounds with a high boiling point which would condense inside the meso and macro pores, requiring large volumes. As a result, a greater correlation of adsorption capacity with total pore volume than with micropore volume was reported (R^2 of 0.87 and R^2 of 0.70, respectively).

Feizbakhshan et al.[28], studied the effect of activated carbon's pore size distribution on its performance in cyclic process. Three different activated carbons were investigated, using 1,2,4-trimethyl benzene as adsorbent. Two of the adsorbents, namely ACFC-20-N and G-70R-V, were highly microporous (97% and 85.5% microporosity, respectively), while the last one, B-100777-V, had much lower micropore volume (37% microporosity). At first, the results might appear contradictory with previous studies since the first cycle adsorption capacity shows a weak correlation with total pore volume (R^2 of 0.72). However, by normalizing by surface area and

gaining the adsorption capacity per surface area, there is a significant correlation with total pore volume as suggested by previous studies (R^2 of 0.99).

Surface characteristics such as acidity, polarity, and chemical reactivity are heavily influenced by carbon-oxygen surface groups present. These carbon-oxygen surface compounds result from oxygen gas reactions with activated carbon at temperatures below 400 °C since these reactions predominantly develop during chemisorption of oxygen. The carbon-oxygen surface groups can be divided into three categories: (i) acidic, (ii) basic, and (iii) neutral[3]. Lillo-Ródenas et a [23] reported that samples with reduced carbon-oxygen surface groups had higher adsorption of toluene and benzene compared to their pristine counterparts. This phenomenon was hypothesized to result from the specific interaction between π electron-rich regions of the graphene layer with the aromatic ring of the adsorbate.

2.3.3 Adsorbate's properties

The physical and chemical properties of the adsorbate also play an important role in the adsorption process. Some of these prominent properties are molecular weight, functional groups, polarity, and boiling point of the adsorbate[29]. Mangun et al.[25], reported that for each specific ACF used in the experiment, the amount of alkane adsorbed is positively related to its boiling point. Canet et al.[30] showcased that adsorbates with large molecular volume have limited access to narrower micropores, and as a result, the adsorbent is underutilized, and adsorption capacity is reduced.

2.4. Adsorption isotherm models

Equilibrium adsorption isotherms are an invaluable tool in designing an adsorption system [31]. When adsorbate containing gas stream has been in contact with the adsorbent surface for an adequate amount of time, the adsorbate concentration ends up in a dynamic balance with the solid interface concentration. This balance is usually referred to as adsorption equilibrium [32]. Adsorption

isotherms illustrate the equilibrium mentioned above at a certain temperature[33]. In the upcoming section, we will discuss some of the more common adsorption isotherm models developed.

2.4.1. Langmuir isotherm model

Langmuir adsorption isotherm is a simplified isotherm model initially developed to describe the adsorption of gases onto solid-phase adsorbents, specifically activated carbons[34]. In the formulation of this model, several assumptions are made regarding the nature of the adsorption process. Firstly, a finite number of adsorption sites are considered to exist on the adsorbent surface. These sites are presumed to be identical. Secondly, monolayer adsorption onto these homogenous adsorption sites is assumed. Lastly, the adsorbed molecules are assumed to have no sideways interaction[35]. The Langmuir adsorption isotherm model can be presented as[36]:

$$q_e = \frac{q_m bC}{1+bC} \qquad \text{2-1}$$

And

$$b = b_0 \exp\left(\frac{-\Delta H_{ad}}{RT}\right) \qquad \text{2-2}$$

Where q_e is adsorbent equilibrium capacity, q_m is the adsorbent maximum equilibrium capacity, b is the temperature-dependent Langmuir affinity coefficient (m^3/kg), C is the gas phase concentration, b_0 is the pre-exponential constant (m^3/kg), ΔH_{ad} is the heat of Adsorption, R is the ideal gas constant, and T is the temperature. It can be observed that the above equation can be reduced to Henry's law isotherm at low concentration and low pressure and is thus thermodynamically consistent in this region[37].

2.4.2 Freundlich isotherm model

Freundlich isotherm model[38] is the earliest known example of a relationship defining non-ideal reversible adsorption. Historically it was developed for adsorption on animal charcoal[34]. As

opposed to the Langmuir isotherm model, this isotherm model does not rely on an assumption of uniformity of heat and affinities. The isotherm model expression itself demonstrates the heterogeneity of the surface[37]. Freundlich isotherm model is empirical and, as such, lacks a fundamental thermodynamic basis. The model is not valid for a wide range of adsorption data since it does not approach Henry's law constant at low pressures, and at high pressures, it does not have a finite limit [34,37]. However, despite these limitations, it has wide applications in heterogeneous systems such as activated carbons [37]. [39]

Freundlich adsorption isotherm model can be presented as[38]:

$$q_e = K_f C^{\frac{1}{n}} \qquad \text{2-3}$$

Where K_f and n, for a given adsorbent-adsorbate system, are constant at a specific temperature [34]. 1/n is a measure of the intensity of adsorption or surface heterogeneity. 1/n values in the range of 0 to 1 indicate favorable adsorption, while 1/n values greater than one represent unfavorable adsorption [37].

2.4.3 Dubinin-Radushkevich isotherm model

Dubinin-Radushkevich isotherm is a semi-empirical model based on Polanyi's potential[39]. It was originally developed with the adsorption of gases on microporous adsorbents in mind[37]. However, its usage soon expanded to include many adsorbents with heterogeneous surfaces and a Gaussian energy distribution[37]. Unlike Freundlich isotherm, the D-R isotherm model maintains a core thermodynamic basis and, as a result, is highly regarded [36]. It has been often demonstrated to work exceptionally well for intermediate and high concentration data ranges but, similar to the Freundlich isotherm model, fails to approach Henry's law constant at low concentrations [34]. The D-R adsorption isotherm model can be presented as[39]:

$$W = W_0 \, exp(-kA^2) \qquad 2\text{-}4$$

And

$$A = RT \, ln(P_0/P) \qquad 2\text{-}5$$

Where W represents the volumetric adsorption capacity expressed as adsorbed liquid volume per unit mass of adsorbent; A is the adsorption potential; W_0 is the limiting pore volume; R is the universal gas constant; T is the absolute temperature; P_0 is the saturated vapor pressure at temperature T, and P is the partial pressure of the adsorbate.

k is the D-R equation parameter for the target compound, if we were to choose a reference adsorbate, the following equation can estimate the k value:

$$k = \frac{k_s}{\beta} \qquad 2\text{-}6$$

Where k_s is the value of k for reference adsorbate, and β is the affinity coefficient for target adsorbate [39]. There have been many approximation methods suggested for β such as (i) ratio of molar volumes of the target adsorbate to that of reference compound (V/V_s), (ii) ratio of molecular parachors of the target adsorbate to that of reference compound and (iii) ratio of the polarities ($\frac{\alpha}{\alpha_s}$) for polar organic adsorbates[40]. The reference adsorbate chosen for β is usually benzene for which $\beta \equiv 1.0$[41].

The most significant advantage of the D-R isotherm is that it only requires two parameters, namely W_0 and k, to make predictions for the adsorption capacity of any adsorbate-adsorbent system[39]. Urano et al. [40], conducted a study on seven different activated carbon samples and 13 organic adsorbents to find an association between D-R equation parameters and properties of AC samples. Previously Dubinin had reported W_0 to be related to the micropore volume [37]. However, after their investigation, Urano et al.[40], empirically found that values of W_0 can be predicted from the volume

of pores below 3.2 nm (32Å) plus 0.055 mL. Crittenden et al.[42], also arrived at the same conclusion that W_0 values are solely dependent on the adsorbent.

For prediction of β, several approaches have been presented in the literature. Dubinin himself suggested the use of either molar volume ratios or parachors ratios[43]. Reucroft et al.[44], selected 15 chemicals and subsequently categorized them into three groups based on their respective polarity. A reference adsorbate was arbitrarily chosen from each group to approximate β and it was demonstrated that the ratio of electronic polarities leads to better estimation for β. Moreover, it was reported that if a single compound were chosen to represent the entire data set, the error value for the predicted β vs the experimental β would be too high. Conversely, Urano et al.[40] observed that when benzene is used as the reference adsorbate, k_S and β values had a negligible variation with the change in adsorbent type and averaged $2.7 \pm 0.3 \times 10^{-3}$. Additionally, satisfactory predictions of β could be made for all 13 chemicals involved in the study. Noll et al.[45] also investigated the influence of adsorbates' selection on β prediction via various methods. In their study, isotherm data for ten organic compounds, ranging from nonpolar to strongly polar, were developed. It was reported that to gain optimum accuracy in β prediction, it is best to choose a reference adsorbate with similar polarity. The previous studies demonstrate no concurrence for selecting a reference adsorbate, and the choice is often made arbitrarily.

Furthermore, depending on the method chosen for calculating , some experimental measurement is unavoidable. Given the limitations mentioned above, Prakash et al .[43] proposed using a quantitative structure-activity relationship (QSAR) method to predict k directly with no need for a reference adsorbate. QSAR approach asserts that a given chemical's physical and biological properties are closely related to its molecular structure; thus, with the help of some "molecular descriptors, "one can derive statistical relationships between the chemical's properties and its

topological features [46]. Nirmalakhandan et al. [46], had previously used this method and the molecular connectivity descriptor to predict AC adsorption capacity successfully. Prakash et al. [43] conducted linear regression of the k values present in the literature vs. the first-order valance molecular connectivity index and reported a single variable model capable of predicting k value with a R^2 of 0.924. The model can be presented as:

$$\log k = 1.585 - 0.442 \; {}^1\chi^v \qquad \text{2-7}$$

Qi et al.[41] further investigated the QSAR model proposed by Prakash et al. [43]. k values for benzene, acetone and methyl ethyl ketone (MEK) adsorption on three different activated carbon fibers were obtained experimentally. These experimental values were compared against their corresponding QSAR model-produced counterparts. It was reported that for two of the activated carbon fibers utilized, the results agreed with a maximum difference of 16%. The model showed some divergence (63-96%) from experimental values for the last ACF. This divergence was hypothesized to be due to a specific adsorbent-adsorbate interaction for that particular ACF.

Hung et al. [39], employed all the above-mentioned estimation methods for D-R equation parameters and developed a mathematical model capable of predicting ACs' adsorption capacity. In this method, having knowledge of the adsorbent's structure and adsorbate's pore size distribution is sufficient to make predictions regarding capacity. However, since at low concentration ranges D-R equation overestimates adsorption capacity and does not approach Henry's law constant, the D-R equation was modified. Through experiments on various AC samples, it was reported that at relative pressure between 1.5×10^{-3} and 0.01, both the D-R isotherm model and Langmuir isotherm model generate similar isotherms. Thus, the parameters required for Langmuir isotherm can be determined by fitting the isotherm obtained from the D-R equation. Finally, an isotherm model was developed to overcome the limitations of the D-R model. This new isotherm model

utilized Langmuir isotherm for relative pressures below 1.5×10^{-3} and D-R model for relative pressures beyond it. The newly developed isotherm model was fittingly named the D-R-L isotherm model. The D-R-L isotherm model's predictive capabilities were tested against experimentally obtained adsorption capacity values. An average discrepancy of 9.7% and 2.5% was reported for benzene adsorption onto the selected ACs at low and high relative pressure.

It is essential to mention that all the above studies were conducted on freshly prepared and virgin AC samples, and to the best of our knowledge, no study has been done to modify the D-R-L predictive model to accommodate used ACs. In industrial applications, AC is often used in a cyclic adsorption/regeneration process where its physical properties constantly change. As a result, modifications are inevitable to make the D-R-L model better suited for practical industrial usage. The most crucial change in the physical property of AC regarding isotherm prediction are changes occurring in its pore size distribution due to the accumulation of heel-buildup in the pores. Were a model to be developed which could predict PSD after cyclic heel build-up, ACs' adsorption capacity throughout the long-term cyclic process could be predicted.

2.5. Regeneration

As the cyclic adsorption process goes on, the target adsorbate is continuously accumulated on the surface of the adsorbent. This accumulation of adsorbate reduces the working adsorption capacity of the adsorbent with each cycle. A suitable regeneration stage can preserve the porosity and internal structure of the adsorbent while eliminating the adsorbed species leading to the adsorbents reuse[47]. Various techniques are available for the regeneration of VOC-laden adsorbents, including but not limited to thermal regeneration [48], chemical regeneration47, and bio-regeneration[50].

2.5.1. Thermal Regeneration

Thermal regeneration is the more commonly used method, and comprises heating the adsorbent bed to increase its temperature while a purge gas flow passes through it, carrying the desorbed species away[51]. Alternatively steam or hot purge gas can be used to heat the bed and thus regenerate it. The purge gas used is usually an inert gas, such as N_2, to avoid any potential reactions among desorbed compounds and impurities in the gas[52]. To provide heating to the adsorbent bed, traditionally, hot purge gas or steam is applied. However, many novel methods have been proposed and utilized, including conductive, microwave, and resistive heating[53–55].

2.5.2. Chemical Regeneration

Thermal regeneration methods are effective yet energy-intensive approaches for the re-use of adsorbents. This high energy consumption motivated researchers to look for methods that could increase the regeneration efficiency while consuming less energy, and thus chemical regeneration methods came to be. Chemical regeneration techniques are many, and they differ in the regeneration mechanism employed and the regeneration agents used[52]. The most well-known of these regenerative methods are solvent, NaOH, supercritical, and oxidative regeneration[52]. As with any method, there are advantages and drawbacks involved with all chemical regeneration techniques named above. Solvent regeneration, for example, causes much less damage to the porous structure of the adsorbent[56]. However, it employs the use of hazardous organic compounds that, if not disposed of properly, can have environmental consequences[57]. Consequently, the use of chemical regeneration methods needs to be considered on a case-by-case basis.

2.5.3. Bio-Regeneration

Bio-regeneration is defined as using microbial activities to re-new activated carbon[58]. It involves mixing bacteria with the loaded activated carbon in a closed batch system[59]. In the literature, two

mechanisms have been proposed for the bio-regeneration of activated carbon. The first mechanism requires the desorption of organic compounds from carbon into the liquid phase due to a concentration gradient. Subsequently, the released compounds are then degraded by microbial activity[60]. The second mechanism hypothesizes the presence of extra-cellular enzymes excreted by microorganisms which can then enter the pores of activated carbon and degrade the adsorbed species [61]. However, this hypothesis has been challenged since, for enzymes to react with adsorbate, they first need to be adsorbed into the carbon pores. The adsorption of the enzyme into small pores might prove challenging since the average molecular diameter of a monomeric enzyme is above 31 Å, which would exclude all micropores and even some mesopores. This exclusion is contradictory to observations made in experiments [58]. One factor that strongly limits the use of bio-regeneration is the biodegradability of the adsorbate. Having a recalcitrant organic compound as adsorbate can hamper the biodegradation process and reduce its efficiency [58].

2.6. Heel-build up

One of the main challenges associated with the adsorption of VOCs using activated carbon is heel-build up. Heel refers to the accumulation of strongly adsorbed species that can thwart complete regeneration of adsorbent and thus lower its adsorption capacity and reduces its operational lifespan. This reduction in capacity will force the operator to replace the adsorbent bed more frequently, increasing maintenance costs[62]. Several mechanisms have been suggested in the literature for heel-build-up: (i) non-desorbed physisorption, (ii) chemisorption of adsorbates or adsorbate's reaction by-products (iii) adsorbate decomposition (i.e., char formation). The occurrence of each of the mentioned mechanisms depends on a variety of factors, such as the nature of the VOCs involved and the extent of the cyclic adsorption/regeneration procces[62]. Jahandar Lashaki et al.[62], conducted a study on heel formation mechanisms in full-scale adsorber's

products and concluded that non-desorbed physisorption was the most important mechanism in the early cycles. Moreover, if carbon was exposed to oxygen impurities of the purge gas, thermal oxidation could play a significant role in heel-buildup. If no such exposure occurred, however, pyrolysis reactions were the main contributor instead.

Parameters affecting heel-build up have been the subject of many studies since heel-build up can have a major economic and environmental impact on the adsorption process. These studies helped to identify several impactful parameters and how they influence heel-build up. These parameters, similar to the ones affecting adsorption capacity mentioned before, can be divided into three major groups:

- Adsorbate's characteristics
- Adsorbent's properties.
- Operational conditions under which adsorption/regeneration is conducted.

With regards to adsorbate property. Wang et al. [63], investigated the adsorption of a mixture of organic compounds commonly found in vehicle painting booth operations. With the help of solvent extraction methods, they were able to identify the organic compounds and their respective concentration remaining on regenerated BAC. It was concluded that high boiling point compounds contribute more to heel build-up since they are harder to desorb. In special cases where compounds might have similar boiling points, their structure and functionality affect adsorption dynamics.

As for adsorbent properties, several independent investigations have been performed, a summary of which is included here. Jahandar Lashaki et al. [64], performed a thorough investigation on five activated carbon adsorbents to study the role of the pore size distribution (PSD) on heel formation. To isolate the contribution of PSD, the ACs were chosen meticulously to cover a wide range of physical properties (30-88% microporosity) while sharing similar surface chemistry. Next ACs

underwent 5 cycle adsorption/regeneration experiments. Adsorbents were characterized both before and after cyclic experiments. Based on the reports, the heel was linearly correlated (R^2=0.91) with BAC micropore volume. Furthermore, adsorbents with the highest share of mesopores exhibited the best adsorption performance. This was attributed to the fact that mesopores contribute to adsorption but not to heel formation. From their reports, it can be concluded that a balance of mesopores and micropores is needed to have adsorbents with sufficient adsorption capabilities and low heel formation. It should be noted that regeneration was done in the absence of oxygen.

Feizbakhshan et al. [65] explored the role of PSD on heel formation in the presence of oxygen impurity in the purge gas. For this study, three activated carbon samples with various physical properties were chosen. They arrived at the same conclusion that samples with higher microporosity exhibit higher amounts of heel build-up. It was also suggested that a hierarchal pore structure is beneficial in the presence of oxygen and simplifies the desorption process. This was attributed to the fact that larger pores (mesopores and macropores) help overcome the transport limitation present in micropores. The role of BACs surface oxygen groups was investigated by Jahandar Lashaki et al. [64], and it was reported that samples with higher surface oxygen groups result in higher heel build-ups.

The impact of regeneration parameters on heel-build-up is highly dependent on the regeneration method chosen. One of the first parameters studied was the temperature in which desorption was completed. Jahandar Lashaki et al. [66], firstly investigated the influence of adsorption temperature on heel build-up. It was reported that an increase of 10 °C from (25 to 35 °C) increased heel build-up by 30%, regardless of the consecutive regeneration temperature. Conversely, a further increase

31

from 35 to 45 °C had no effect. The reasoning behind this phenomenon was suggested to be a shift from physisorption to chemisorption at some point in between 25 to 35 °C. Additionally, cumulative heel build-up for activated carbons regenerated at 288 and 400 °C was also assessed. The use of higher regeneration temperature resulted in a 60% reduction in mass balance cumulative heel. The reduction is due to the greater difference between regeneration temperature and boiling point of the adsorbates, which translates to a greater driving force for desorption. However, it should be heeded that the experiments mentioned above were all done in the absence of oxygen. As Feizbakhshan et al. [67] later demonstrated, the increased temperature can facilitate reactions amongst adsorbates and oxygen impurity, resulting in higher heel build-up.

A more in-depth study on the effect of desorption purge gas's oxygen content was performed by Jahandar Lashaki et al [68]. In this study, different concentrations of oxygen impurity ($\leq 5 - 10,000 \; ppm$) were used in N_2 desorption purge gas. It was reported that an increase in oxygen impurity was accompanied by an increase in mass balance cumulative heel up to 35%. This result was argued to be due to a shift from pure physisorption to a combination of physisorption and chemisorption with an increase in oxygen impurity. The subsequent derivative thermogravimetric analysis confirmed their claims.

Niknaddaf et al. [69] illustrated that in addition to the regeneration temperature, the heating rate used to achieve such a high temperature also plays a role in the heel build-up rate. Their study used resistive heating on activated fiber cloth at several heating rates ranging from 5 to 100 °C/min. It was reported that an increase in heating rate was accompanied by an increase in heel build-up from 4.6 to 10.4 (wt.%). In the same study, Niknaddaf et al. [69], investigated the effect of purge gas flow rate and described that a 50 fold increase in purge gas flow rate (from 0.1 to 5) resulted in a ten-fold decrease in heel build-up (from 14 to 1.4%). They supported these results by claiming that a

surge in heating rate or a reduction in flow rate both allow a higher concentration of adsorbate to be in contact with increased temperatures for a longer duration, which will result in an increased adsorbate decomposition and coke formation on the adsorbent surface.

The above-mentioned studies primarily focused on a limited number of cycles (up to 5). This limitation reduces the opportunity for further heel formation and even heel transformation from physisorbed species into higher molecular weight non-desorbed species. Additionally, the heel formation trends have only been confirmed in the studied cycles, and any heel trend for higher cycles is currently only speculation. There are still gaps in research on what happens in higher cycle numbers. This gap is problematic since, in full-scale abetment systems, hundreds of cycles are typically completed on individual BAC batch [62].

2.7. Machine-learning method

In recent years, machine learning (ML) has become an invaluable tool in developing computational algorithms. It has been influential in recent discoveries in the fields of artificial intelligence, computer science, and chemistry[70]. Machine learning's primary goal is to make accurate predictions of y from x. One advantage that machine learning methods offer is their ability to discover complex structures without prior knowledge. These methods enable us to fit very complex functions onto the dataset without the risk of occurrence of overfitting.[71].

Machine learning's application in environmental engineering has been a topic of interest recently. These methods have already been utilized in various fields such as waste-to-energy conversion[72], municipal solid-waste treatment[73], biochar for organic compound sorption72, and adsorption processes. Application of ML in adsorption is generally centered around one of the topics below:

- Inverse design of adsorbent material [75]
- Performance prediction[76]

- Adsorption process optimization [77]

Yuan et al. [78] applied several tree-based models to predict CO_2 adsorption as a function of textural and compositional properties of biomass waste-derived porous carbons To that end, they complied a data set including 527 data points and applied ML methods to them. Out of the various models assessed, it was reported that gradient boosting decisions (GBDTs) demonstrated the best predictive performance with R^2 of 0.98 and 0.84 on training and test data, respectively. Subsequently, feature importance analysis was done on the GBDT method, which was recognized as the most accurate. The pressure and temperature of the adsorption experiment were reported as the most influential parameters.

Xiao et al. [79], investigated the optimization of a layered bed pressure swing adsorption for hydrogen purification using ML methods. Published experimental results showcased a contradiction between hydrogen purity and recovery; therefore, multiple target optimization was needed. To that purpose, polynomial regression (PNR) and artificial neural network (ANN) were used to predict the performance of a two-bed six-step process designed for purification. Following this step, a combination of two ANN models and a sequence quadratic program algorithm were used to achieve multi-level optimization. Final optimization results were validated with Aspen Adsorption cycle model. It was concluded that ANN, rather than PNR, is a better choice for optimizing the purification performance of hydrogen.

Even though an increasing number of studies have been pursued in adsorption, no studies, to the best of our knowledge, are using ML techniques to predict changes in adsorbent porosity caused by heel formation. As previously mentioned, heel build-up can significantly change the porous structure of the activated carbon adsorbent, resulting in reduced adsorption capacity. Thus having

a PSD prediction model can help us predict adsorption capacities of ACs during cyclic adsorption/regeneration experiments and avoid unwarranted replacement of adsorbent bed.

2.8 References

1.   Suzuki M, Suzuki M. *Adsorption Engineering*. Vol 14. Kodansha; 1990. Accessed September 21, 2021. https://www.academia.edu/download/56981223/AdsorptionEngineering.pdf

2.   Khan FI, Kr. Ghoshal A. Removal of Volatile Organic Compounds from polluted air. *Journal of Loss Prevention in the Process Industries*. 2000;13(6):527-545. doi:10.1016/S0950-4230(00)00007-3

3.   Bansal RC, Goyal M. Activated Carbon Adsorption. Published online May 24, 2005. doi:10.1201/9781420028812

4.   Thommes M, Kaneko K, Neimark A v., et al. Physisorption of gases, with special reference to the evaluation of surface area and pore size distribution (IUPAC Technical Report). *Pure and Applied Chemistry*. 2015;87(9-10):1051-1069. doi:10.1515/PAC-2014-1117

5.   Rufford T, Zhu J, Hulicova-Jurcakova D. *Green Carbon Materials: Advances and Applications*.; 2019.

6.   Bansal RC, Goyal M. Activated Carbon Adsorption. Published online May 24, 2005. doi:10.1201/9781420028812

7.   Hu H, Xu K. Physicochemical technologies for HRPs and risk control. *High-Risk Pollutants in Wastewater*. Published online January 1, 2020:169-207. doi:10.1016/B978-0-12-816448-8.00008-3

8.   Barrer RM, McKenzie N, Reay JSS. Capillary condensation in single pores. *Journal of Colloid Science*. 1956;11(4-5):479-495. doi:10.1016/0095-8522(56)90164-7

9.   Huang MC, Chou CH, Teng H. Pore-size effects on activated-carbon capacities for volatile organic compound adsorption. *AIChE Journal*. 2002;48(8):1804-1810. doi:10.1002/AIC.690480820

10. Mokhatab S, Poe WA, Mak JY. Handbook of natural gas transmission and processing: Principles and practices. *Handbook of Natural Gas Transmission and Processing: Principles and Practices*. Published online January 1, 2018:1-826. doi:10.1016/C2017-0-03889-2

11. Vidic RD, Suidan MT. Role of Dissolved Oxygen on the Adsorptive Capacity of Activated Carbon for Synthetic and Natural Organic Matter. *Environ Sci Technol*. 1991;25(9):1612-1618. doi:10.1021/ES00021A013

12. Carratalá-Abril J, Lillo-Ródenas MA, Linares-Solano A, Cazorla-Amorós D. Regeneration of activated carbons saturated with benzene or toluene using an oxygen-containing atmosphere. *Chemical Engineering Science*. 2010;65(6):2190-2198. doi:10.1016/J.CES.2009.12.017

13. Marsh H, Rodríguez-Reinoso F. Characterization of Activated Carbon. *Activated Carbon*. Published online January 1, 2006:143-242. doi:10.1016/B978-008044463-5/50018-2

14. Huang ZH, Kang F, Liang KM, Hao J. Breakthrough of methyethylketone and benzene vapors in activated carbon fiber beds. *Journal of Hazardous Materials*. 2003;98(1-3):107-115. doi:10.1016/S0304-3894(02)00284-4

15. Das D, Gaur V, Verma N. Removal of volatile organic compound by activated carbon fiber. *Carbon*. 2004;42(14):2949-2962. doi:10.1016/J.CARBON.2004.07.008

16. Lashaki MJ, Fayaz M, Wang H (Helena), et al. Effect of Adsorption and Regeneration Temperature on Irreversible Adsorption of Organic Vapors on Beaded Activated Carbon. *Environmental Science and Technology*. 2012;46(7):4083-4090. doi:10.1021/ES3000195

17. Jr KS, Dunn R, Ternes M. *Air Pollution Control Technology Handbook*. Vol 62.; 2015. doi:10.1595/205651318X696657

18.   Wang H, Lashaki MJ, Fayaz M, et al. Adsorption and Desorption of Mixtures of Organic Vapors on Beaded Activated Carbon. *Environmental Science and Technology*. 2012;46(15):8341-8350. doi:10.1021/ES3013062

19.   Niknaddaf S, Atkinson JD, Gholidoust A, et al. Influence of Purge Gas Flow and Heating Rates on Volatile Organic Compound Decomposition during Regeneration of an Activated Carbon Fiber Cloth. Published online 2020. doi:10.1021/acs.iecr.9b06070

20.   Babu B v, Gupta S. Modeling and Simulation of Fixed bed Adsorption column: Effect of Velocity Variation. *Engineering Technology*. Published online 2005:30923-34748. Accessed December 21, 2021. http://discovery.bits-pilani.ac.in/discipline/chemical/BVb/index.html;

21.   Aktaş Ö, Çeçen F. Effect of type of carbon activation on adsorption and its reversibility. *Journal of Chemical Technology and Biotechnology*. 2006;81(1):94-101. doi:10.1002/JCTB.1363

22.   Leng CC, Pinto NG. Effects of surface properties of activated carbons on adsorption behavior of selected aromatics. *Carbon*. 1997;35(9):1375-1385. doi:10.1016/S0008-6223(97)00091-2

23.   Lillo-Ródenas MA, Cazorla-Amorós D, Linares-Solano A. Behaviour of activated carbons with different pore size distributions and surface oxygen groups for benzene and toluene adsorption at low concentrations. *Carbon*. 2005;43(8):1758-1767. doi:10.1016/J.CARBON.2005.02.023

24.   Cal MP, Larson SM, Rood MJ. Experimental and modeled results describing the adsorption of acetone and benzene onto activated carbon fibers. *Environmental Progress*. 1994;13(1):26-30. doi:10.1002/EP.670130114

25.   Mangun C, Daley M, Braatz R, Economy J. Effect of pore size on adsorption of hydrocarbons in phenolic-based activated carbon fibers. *Carbon*. 1998;36(1-2):123-129. doi:10.1016/S0008-6223(97)00169-3

26.	Huang MC, Chou CH, Teng H. Pore-size effects on activated-carbon capacities for volatile organic compound adsorption. *AIChE Journal*. 2002;48(8):1804-1810. doi:10.1002/AIC.690480820

27.	Jahandar Lashaki M, Atkinson JD, Hashisho Z, Phillips JH, Anderson JE, Nichols M. The role of beaded activated carbon's pore size distribution on heel formation during cyclic adsorption/desorption of organic vapors. *Journal of Hazardous Materials*. 2016;315:42-51. doi:10.1016/J.JHAZMAT.2016.04.071

28.	Feizbakhshan M, Hashisho Z, Crompton D, Anderson JE, Nichols M. Effect of Activated Carbon's Pore Size Distribution on Oxygen Induced Heel Build-up. *Journal of Hazardous Materials*. 2021;409. doi:10.1016/J.JHAZMAT.2021.126905

29.	TIPNIS PR, HARRIOTT P. THERMAL REGENERATION OF ACTIVATED CARBONS. *Chemical Engineering Communications*. 1986;46(1-3):11-28. doi:10.1080/00986448608911393

30.	Canet X, Gilles F, Su BL, de weireld guy, Frere M. Adsorption of alkanes and aromatic compounds on various faujasites in the Henry domain. 1. Compensating cation effect on zeolites Y. *Journal of Chemical & Engineering Data* . 2007;52(6):2127-2137. doi:10.1021/je700214v

31.	Ghiaci M, Abbaspur A, Kia R, Seyedeyn-Azad F. Equilibrium isotherm studies for the sorption of benzene, toluene, and phenol onto organo-zeolites and as-synthesized MCM-41. *Separation and Purification Technology*. 2004;40(3):217-229. doi:10.1016/J.SEPPUR.2004.03.001

32.	Vasanth Kumar K, Sivanesan S. Sorption isotherm for safranin onto rice husk: Comparison of linear and non-linear methods. *Dyes and Pigments*. 2007;72(1):130-133. doi:10.1016/J.DYEPIG.2005.07.020

33.	El-Khaiary MI. Least-squares regression of adsorption equilibrium data: Comparing the options. *Journal of Hazardous Materials*. 2008;158(1):73-87. doi:10.1016/J.JHAZMAT.2008.01.052

34. Foo KY, Hameed BH. Insights into the modeling of adsorption isotherm systems. *Chemical Engineering Journal*. 2010;156(1):2-10. doi:10.1016/J.CEJ.2009.09.013

35. Langmuir I. THE CONSTITUTION AND FUNDAMENTAL PROPERTIES OF SOLIDS AND LIQUIDS. PART I. SOLIDS. *Journal of the American Chemical Society*. 2002;38(11):2221-2295. doi:10.1021/JA02268A002

36. Do D. *Adsorption Analysis: Equilibria and Kinetics (with Cd Containing Computer MATLAB Programs)*. Vol 2. World Scientific; 1998.

37. Al-Ghouti MA, Da'ana DA. Guidelines for the use and interpretation of adsorption isotherm models: A review. *Journal of Hazardous Materials*. 2020;393:122383. doi:10.1016/J.JHAZMAT.2020.122383

38. Freundlich H. Über die Adsorption in Lösungen. *Zeitschrift für Physikalische Chemie*. 1907;57U(1):385-470. doi:10.1515/ZPCH-1907-5723

39. Hung HW, Lin TF. Prediction of the Adsorption Capacity for Volatile Organic Compounds onto Activated Carbons by the Dubinin–Radushkevich–Langmuir Model. *Journal of the Air & Waste Management Association*. 2012;57(4):497-506. doi:10.3155/1047-3289.57.4.497

40. Urano K, Omori S, Yamamoto E. Prediction Method for Adsorption Capacities of Commercial Activated Carbons in Removal of Organic Vapors. *Environmental Science and Technology*. 1982;16(1):10-14. doi:10.1021/ES00095A006

41. Qi S, Hay KJ, Rood MJ, Cal MP. Carbon Fiber Adsorption Using Quantitative Structure-Activity Relationship. *Journal of Environmental Engineering*. 2000;126(9):865-868. doi:10.1061/(ASCE)0733-9372(2000)126:9(865)

42. Crittenden JC, Cortright RD, Rick B, Tang SR, Perram D. Using GAC to Remove VOCs From Air Stripper Off-Gas. *Journal - American Water Works Association*. 1988;80(5):73-84. doi:10.1002/J.1551-8833.1988.TB03040.X

43. Prakash J, Nirmalakhandan N, Speece RE. Prediction of Activated Carbon Adsorption Isotherms for Organic Vapors. *Environmental Science and Technology*. 1994;28(8):1403-1409. doi:10.1021/ES00057A005

44. Reucroft PJ, Simpson WH, Jonas LA. Sorption properties of activated carbon. *Journal of Physical Chemistry*. 1971;75(23):3526-3531. doi:10.1021/J100692A007

45. Noll K. *Adsorption Technology for Air and Water Pollution Control*. CRC Press; 1991.

46. Nirmalakhandan NN, Speece RE. Prediction of Activated Carbon Adsorption Capacities for Organic Vapors Using Quantitative Structure—Activity Relationship Methods. *Environmental Science and Technology*. 1993;27(8):1512-1516. doi:10.1021/ES00045A004

47. Jahandar Lashaki M, Atkinson JD, Hashisho Z, et al. Effect of desorption purge gas oxygen impurity on irreversible adsorption of organic vapors. *Carbon*. 2016;99:310-317. doi:10.1016/J.CARBON.2015.12.037

48. Moreno-Castilla C, Rivera-Utrilla J, Joly JP, López-Ramón M v., Ferro-García MA, Carrasco-Marín F. Thermal regeneration of an activated carbon exhausted with different substituted phenols. *Carbon*. 1995;33(10):1417-1423. doi:10.1016/0008-6223(95)00090-Z

49. Martin RJ, Ng WJ. Chemical regeneration of exhausted activated carbon—I. *Water Research*. 1984;18(1):59-73. doi:10.1016/0043-1354(84)90048-4

50. Ivancev-Tumbas I, Dalmacija B, Tamas Z, Karlovic E. Reuse of biologically regenerated activated carbon for phenol removal. *Water Research*. 1998;32(4):1085-1094. doi:10.1016/S0043-1354(97)00337-0

51. Friday DK, LeVan MD. Hot purge gas regeneration of adsorption beds with solute condensation: Experimental studies. *AIChE Journal*. 1985;31(8):1322-1328. doi:10.1002/AIC.690310811

52. Salvador F, Martin-Sanchez N, Sanchez-Hernandez R, Sanchez-Montero MJ, Izquierdo C. Regeneration of carbonaceous adsorbents. Part I: Thermal Regeneration. *Microporous and Mesoporous Materials*. 2015;202:259-276. doi:10.1016/J.MICROMESO.2014.02.045

53. Niknaddaf S, Atkinson JD, Shariaty P, et al. Heel formation during volatile organic compound desorption from activated carbon fiber cloth. *Carbon*. 2016;96:131-138. doi:10.1016/J.CARBON.2015.09.049

54. Fayaz M, Shariaty P, Atkinson JD, et al. Using Microwave Heating To Improve the Desorption Efficiency of High Molecular Weight VOC from Beaded Activated Carbon. *Environmental Science and Technology*. 2015;49(7):4536-4542. doi:10.1021/ES505953C

55. Ania CO, Parra JB, Menéndez JA, Pis JJ. Microwave-assisted regeneration of activated carbons loaded with pharmaceuticals. *Water Research*. 2007;41(15):3299-3306. doi:10.1016/J.WATRES.2007.05.006

56. Guo D, Shi Q, He B, Yuan X. Different solvents for the regeneration of the exhausted activated carbon used in the treatment of coking wastewater. *Journal of Hazardous Materials*. 2011;186(2-3):1788-1793. doi:10.1016/J.JHAZMAT.2010.12.068

57. Martin RJ, Ng WJ. The repeated exhaustion and chemical regeneration of activated carbon. *Water Research*. 1987;21(8):961-965. doi:10.1016/S0043-1354(87)80014-3

58. Aktaş Ö, Çeçen F. Bioregeneration of activated carbon: A review. *International Biodeterioration & Biodegradation*. 2007;59(4):257-272. doi:10.1016/J.IBIOD.2007.01.003

59. Goeddertz JG, Matsumoto MR, Scott Weber A. Offline Bioregeneration of Granular Activated Carbon. *Journal of Environmental Engineering*. 1988;114(5):1063-1076. doi:10.1061/(ASCE)0733-9372(1988)114:5(1063)

60. Kim DJ, Miyahara T, Noike T. Effect of C/N ratio on the bioregeneration of biological activated carbon. *Water Science and Technology*. 1997;36(12):239-249. doi:10.1016/S0273-1223(97)00720-8

61. Sirotkin AS, Koshkina LY, Ippolitov KG. The BAC-process for treatment of waste water Containing non-ionogenic synthetic surfactants. *Water Research*. 2001;35(13):3265-3271. doi:10.1016/S0043-1354(01)00029-X

62. Jahandar Lashaki M, Hashisho Z, Phillips JH, Crompton D, Anderson JE, Nichols M. Mechanisms of heel buildup during cyclic adsorption-desorption of volatile organic compounds in a full-scale adsorber-desorber. *Chemical Engineering Journal*. 2020;400:124937. doi:10.1016/J.CEJ.2020.124937

63. Wang H, Jahandar Lashaki M, Fayaz M, et al. Adsorption and desorption of mixtures of organic vapors on beaded activated carbon. *Environmental Science and Technology*. 2012;46(15):8341-8350. doi:10.1021/ES3013062

64. Jahandar Lashaki M, Atkinson JD, Hashisho Z, Phillips JH, Anderson JE, Nichols M. The role of beaded activated carbon's surface oxygen groups on irreversible adsorption of organic vapors. *Journal of Hazardous Materials*. 2016;317:284-294. doi:10.1016/J.JHAZMAT.2016.05.087

65. Feizbakhshan M, Hashisho Z, Crompton D, Anderson JE, Nichols M. Effect of Activated Carbon's Pore Size Distribution on Oxygen Induced Heel Build-up. *Journal of Hazardous Materials*. Published online August 13, 2021:126905. doi:10.1016/J.JHAZMAT.2021.126905

66. Jahandar Lashaki M, Fayaz M, Wang H, et al. Effect of Adsorption and Regeneration Temperature on Irreversible Adsorption of Organic Vapors on Beaded Activated Carbon. *Environmental Science and Technology*. 2012;46:7. doi:10.1021/es3000195

67. Feizbakhshan M, Amdebrhan B, Hashisho Z, et al. Effects of oxygen impurity and desorption temperature on heel build-up in activated carbon. *Chemical Engineering Journal*. 2021;409:128232. doi:10.1016/J.CEJ.2020.128232

68. Jahandar Lashaki M, Atkinson JD, Hashisho Z, et al. Effect of desorption purge gas oxygen impurity on irreversible adsorption of organic vapors. *Carbon*. 2016;99:310-317. doi:10.1016/J.CARBON.2015.12.037

69. Niknaddaf S, Atkinson JD, Shariaty P, et al. Heel formation during volatile organic compound desorption from activated carbon fiber cloth. *Carbon*. 2016;96:131-138. doi:10.1016/J.CARBON.2015.09.049

70. Jiang W, Xing X, Li S, Zhang X, Wang W. Synthesis, characterization and machine learning based performance prediction of straw activated carbon. *Journal of Cleaner Production*. 2019;212:1210-1223. doi:10.1016/J.JCLEPRO.2018.12.093

71. Mullainathan S, Spiess J. Machine Learning: An Applied Econometric Approach. *Journal of Economic Perspectives*. 2017;31(2):87-106. doi:10.1257/JEP.31.2.87

72. Li J, Zhu X, Li Y, Tong YW, Ok YS, Wang X. Multi-task prediction and optimization of hydrochar properties from high-moisture municipal solid waste: Application of machine learning on waste-to-resource. *Journal of Cleaner Production*. 2021;278:123928. doi:10.1016/J.JCLEPRO.2020.123928

73. Guo H nan, Wu S biao, Tian Y jie, Zhang J, Liu H tao. Application of machine learning methods for the prediction of organic solid waste treatment and recycling processes: A review. *Bioresource Technology*. 2021;319:124114. doi:10.1016/J.BIORTECH.2020.124114

74. Zhu X, Wang X, Ok YS. The application of machine learning methods for prediction of metal sorption onto biochars. *Journal of Hazardous Materials*. 2019;378:120727. doi:10.1016/J.JHAZMAT.2019.06.004

75. Kim B, Lee S, Kim J. Inverse design of porous materials using artificial neural networks. *Science Advances*. 2020;6(1). doi:10.1126/SCIADV.AAX9324

76. Zhang K, Zhong S, Zhang H. Predicting Aqueous Adsorption of Organic Compounds onto Biochars, Carbon Nanotubes, Granular Activated Carbons, and Resins with Machine Learning. *Environmental Science & Technology*. 2020;54(11):7008-7018. doi:10.1021/ACS.EST.0C02526

77. Foroughi M, Ahmadi Azqhandi MH, Kakhki S. Bio-inspired, high, and fast adsorption of tetracycline from aqueous media using Fe3O4-g-CN@PEI-β-CD nanocomposite: Modeling by response surface methodology (RSM), boosted regression tree (BRT), and general regression neural network (GRNN). *Journal of Hazardous Materials*. 2020;388:121769. doi:10.1016/J.JHAZMAT.2019.121769

78. Yuan X, Suvarna M, Low S, et al. Applied Machine Learning for Prediction of CO2 Adsorption on Biomass Waste-Derived Porous Carbons. *Environmental Science & Technology*. 2021;55(17):11925-11936. doi:10.1021/ACS.EST.1C01849

79. Xiao J, Li C, Fang L, et al. Machine learning–based optimization for hydrogen purification performance of layered bed pressure swing adsorption. *International Journal of Energy Research*. 2020;44(6):4475-4492. doi:10.1002/ER.5225

3. CHAPTER 3: Materials and Methods

3.1 Experimental Set-up and Materials

In the first section of this chapter, we go over the materials and methods used in the long-term adsorption/regeneration experiments to understand the factors affecting activated carbon's performance in extended cyclic processes. Firstly, the three adsorbents used in the experiments are introduced, accompanied by their physical and chemical properties. Then there is a detailed explanation of the automated setup developed exclusively for extended cyclic experiments, and finally, a brief description of the characteristic tests conducted to fulfill the objectives of this research work.

3.1.1 Adsorbents and Adsorbate

Three BACs (B101412, B100772 supplied by Blucher GmbH, and G-70R provided by Kureha Corporation) were tested. The BACs all shared similar surface chemical composition (**Table 3.1**) while having distinct physical properties, including a wide range of microporosities. As a result, the effect of porosity on the long-term performance of the mentioned samples can be isolated. A summary of all the relevant physical properties for the tested adsorbents can be seen in **Table 3.2**; Ahead of the experiments, all BACs were preheated at 300°C with a purge gas flow of 1 SLPM N_2 (99.9984% pure, Praxair, for 3 hours to remove any adsorbed impurity. The adsorbate used for all experiments was 1,2,4-trimethyl benzene (1,2,4-TMB, 98%, Sigma-Aldrich). 1,2,4-TMB has a boiling point of 171°C, and a kinetic diameter of 0.68 nanometers [1]. The reason for using 1,2,4-TMB is two-fold: first, this compound can typically be found in most vehicle painting and coating operations and thus can act as an effective surrogate for VOCs from paints and solvents[2]. Second: due to its large kinetic diameter, it will fill up the micropores fast and thus promotes heel build-up and makes the changes in adsorption capacity much easier to observe.[3] For regeneration of the

adsorbent, dry air (99.999% pure, Praxair and high purity N_2 (99.9984% pure, Praxair) were utilized.

Table 3.1. The surface chemical composition (atomic %) of virgin activated carbons obtained from XPS analysis

Adsorbent	Carbon (%)	Oxygen (%)	Sulfur (%)
B101412_Virgin	92.81	6.45	0.74
B100772_Virgin	92.03	7.22	0.74
G-70R_Virgin	93.41	6.59	Negligible

Table 3.2. Physical properties of the virgin adsorbents gained through N_2 adsorption at 77.15 K

Adsorbent	B101412_Virgin	B100772_Virgin	G-70R_Virgin
Microporosity %	44.00	60.00	86.00
Micropore Volume (cm^3/g)	0.49	0.43	0.50
Total pore Volume (cm^3/g)	1.10	0.72	0.58
BET surface area (m^2/g)	1640	1400	1331

3.1.2 Experimental Set-up and Methods

The main obstacle to overcome in studying cyclic adsorption/regeneration experiments is ensuring that each consecutive cycle is conducted as similar to the last one as possible. The challenge is mainly due to the number of parameters involved in the experiments. One must check the inlet concentration for each cycle and ensure a steady-state concentration of pollutants being injected into the inlet air stream, temperatures of the reactor where adsorption, or regeneration, are taking place need to be closely monitored as well. Additionally, the endpoint of the experiment, be it when a specific concentration is reached or a defined duration of time has passed, is another critical factor to be cautious about. As with any other experiment, despite the operator's precision, human errors are inevitable.

All the issues mentioned above are exacerbated as the number of consecutive adsorption/regeneration cycles increases. Thus, there was a need to automate the experiment to a large extent for investigation beyond the usual five cycles. To achieve this and obtain reliable results for long-term adsorption/regeneration experiments, an automated adsorption/regeneration experimental setup, shown in **Figure 3.1**, was developed. The automated setup was devised to run a large number of consecutive adsorption/regeneration experiments. Using this setup allows us to obtain a heel build-up trend for any adsorbate-adsorbent system quickly.
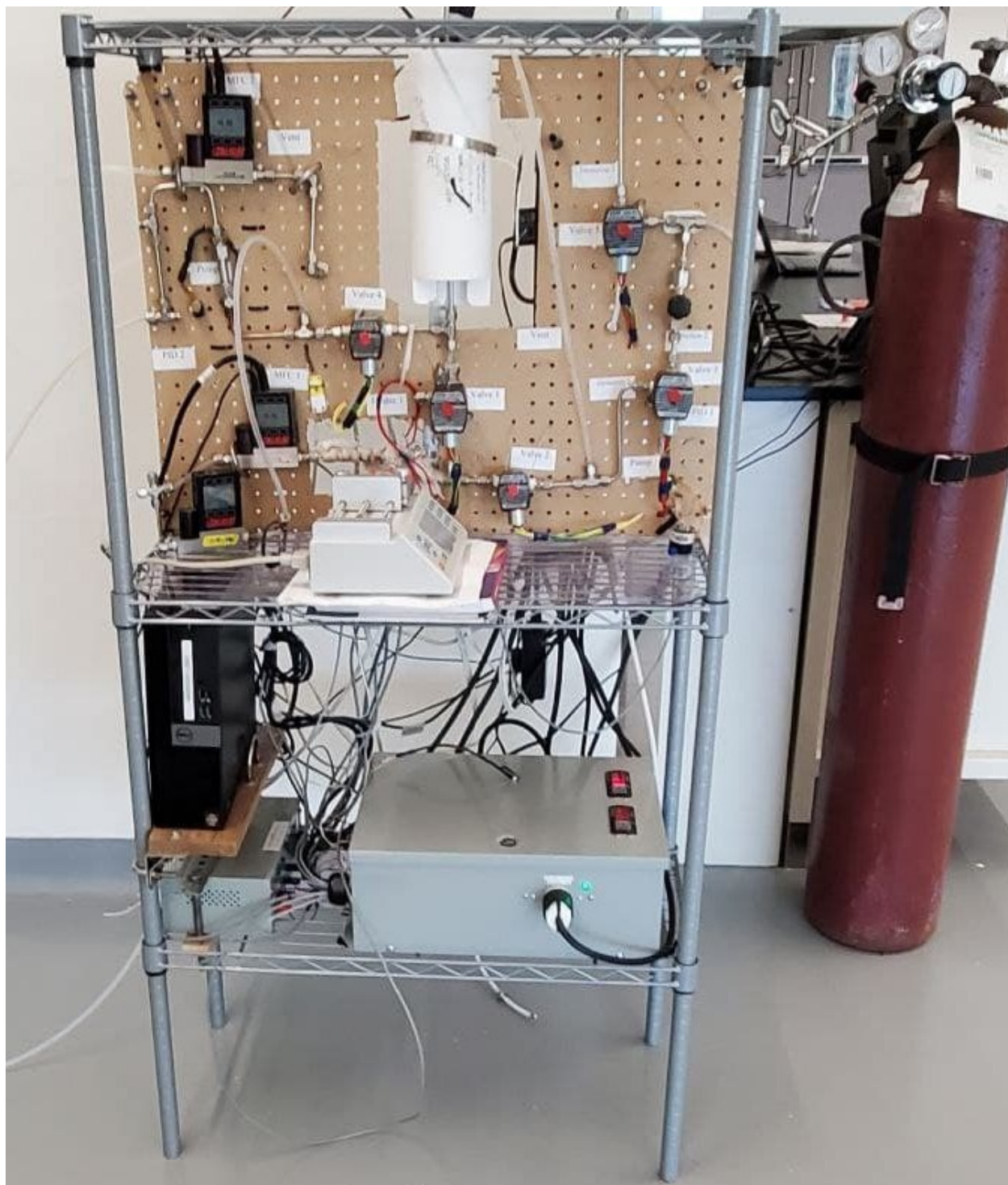
Figure 3.1. Automated setup designed for long-term cyclic adsorption/regeneration experiments

The automated setup's hardware (**Figure 3.2**) comprises an adsorption/regeneration tube, an adsorbate generation system, an organic vapor detection system, a regeneration system consisting of two half-cylinder ceramic heating element and a thermocouple, and a data acquisition and control (DAC) system. The adsorption/regeneration tube consisted of a stainless-steel tube (5mm inner diameter, 155 mm length) containing 2.000 ± 0.001 gr of dried BAC held in place by quartz wool at the bottom and top of the tube. A thermocouple (Omega; K type) was placed exactly in the center of the adsorption/regeneration tube cylinder to measure temperature changes inside the bed. The thermocouple was carefully measured to be exactly in the center of the AC bed.
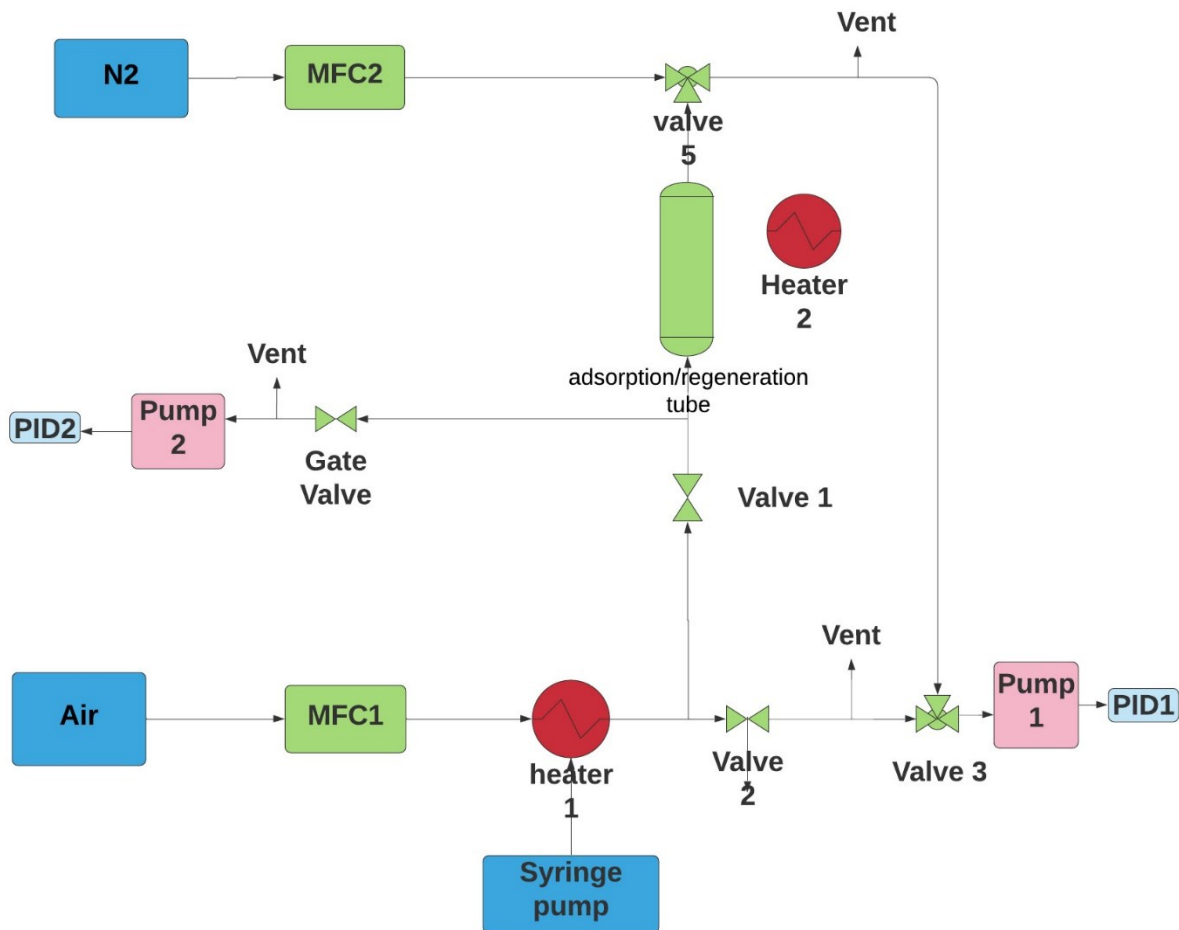
Figure 3.2. Schematic of the automated adsorption/regeneration setup developed for long-term cyclic experiments.

As for the adsorbate generation system, it consisted of a syringe pump (Chemyx Inc, Fusion 100), a mass flow controller (Alicat Scientific) and a fiberglass heating tape (Omega). The vapor stream of adsorbate is generated by injecting the target adsorbate into an air stream controlled with a mass flow controller. Additionally, the injection site is heated using the heating tape to help evaporate the adsorbate quicker. In this case the inlet stream into the adsorption tube consisted of 10 standard

liters per minute of dry air (SLPM) with a concentration of 100 ppmv. The syringe pump injected 1,2,4-TMB at a rate of 5.62 µl/min. To achieve a steady concentration, quartz glass wool was placed inside the injection port, and the port itself was slightly heated using a fiberglass heater tape to reach $40 \pm 1°C$. The vapor detection system consisted of two photoionization detectors which were used to measure the concentration of the VOC in the inlet and outlet stream (PID; Baseline-Mocon Inc. piD-TECH eVx purple) for the adsorption stage and in the outlet stream (PID; Baseline-Mocon Inc. piD-TECH eVx green) for the regeneration.

For regeneration, two semi-cylinder ceramic heating elements (Omega) were utilized to heat the regeneration tube. The DAC system and the LabVIEW program controlled the applied power to the heating unit to maintain the regeneration temperature at 288 °C for 3 hours. The regeneration parameters were chosen to simulate the industrial operation as closely as possible while optimizing the desorption of the adsorbate and minimizing adsorbent structural damage[4,5]. A type K thermocouple (1.6 mm outer diameter ungrounded, Omega) was used to measure the regeneration temperature at the center of the adsorbent bed. In order to study the effect of purge gas flow rate on the long-term performance of several BACs, two regeneration flowrates (0.5 and 5 SLPM) of dry air were chosen. The outlet concentration of the desorbed species was measured and recorded with the help of a second Photoionization detector (PID; Baseline-Mocon Inc. piD-TECH eVx green).

The DAC system was interfaced with the mass flow controller, adsorption/regeneration tube's thermocouple, and PIDs. All the necessary data was fed into a LabVIEW program, explained in detail in the next paragraph, and the values were controlled against the predefined parameters. All adsorption experiments were conducted until saturation, when the outlet concentration reaches the inlet concentration.

The setup utilized a specially designed LabVIEW program (**Figure 3.3**) to monitor adsorption/regeneration's progress and make decisions regarding the state of the cycle based on several predefined parameters. As a result, the operator's involvement is minimized only to setting the initial experimental parameters and ensuring the program is functioning as intended. With the program's help, it is possible to run a cyclic experiment 24/7 and reduce the chance of operational error.
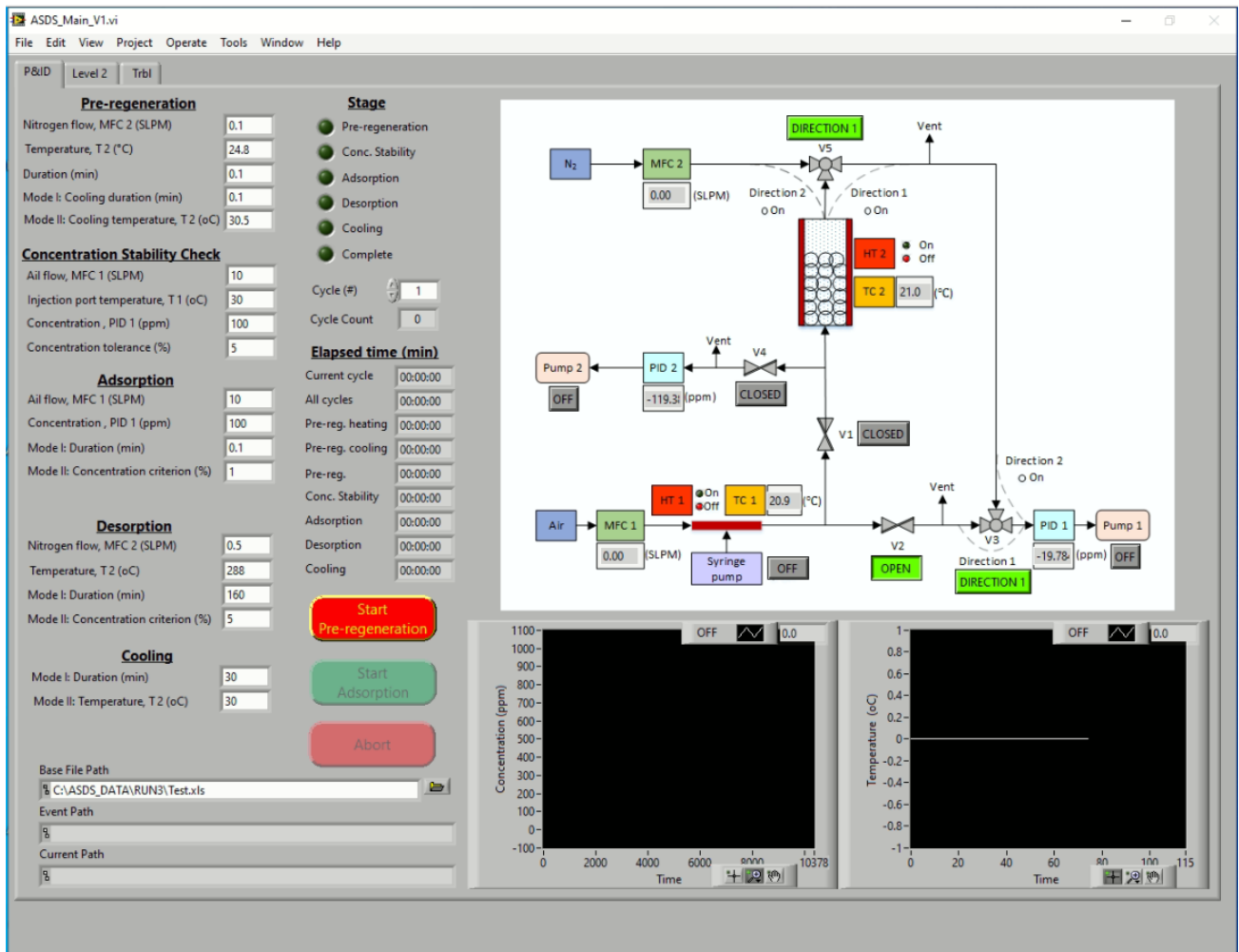
Figure 3.3. LabVIEW program interface used for controlling and monitoring the operation of cyclic adsorption/regeneration experiments

Prior to start of each cyclic test, the adsorption generation system was utilized in conjunction with vapour detection system to calibrate the PID. The calibration was done at a concentration of 200 ppmv of 1,2,4-TMB and a flow rate of 10 SLPM dry air. The calibration stage usually lasted around 30 minutes to allow for stabilization of the inlet concentration. After PID calibration, the system moved to the next stage which was the adsorption stage. This stage, as mentioned before, lasted until full saturation of the adsorbent bed was achieved. The Labview program checked saturation by comparing the effluent concentration data from the PID and comparing it against the inlet concentration of the bed. After adsorption stage, the regeneration begins by heating up the adsorption/regeneration tube until the target temperature, 288 °C, is reached. The system is kept at this temperature for 3 hours while dry air, at either 5 or 0.5 SLPM, purges the bed. After three hours, heating is stopped, but the air flow rate is maintained to cool the adsorption/regeneration tube to 25°C, which is required for the start of the next cycle. This is called the cooling stage. After cooling the whole procedure is repeated.

Two methods, integration of concentration curves and gravimetric methods, were used in conjunction to determine the heel build-up and adsorption capacity. For the integration method, firstly, with the data gathered by both PIDs, the breakthrough curves and desorption curves were drawn, and subsequent integration of the curves was done to obtain the required values. Integration of the breakthrough curves and desorption curves provides us with mass adsorbed and desorbed, respectively. Finally, adsorption capacity and heel build-up can be calculated as demonstrated:

$$q_{i(\%)} = \frac{IMA_i}{MI} \times 100 \qquad \text{3-1}$$

$$H_{i(\%)} = \frac{IMD_i - IMA_i}{MI} \times 100 \qquad \text{3-2}$$

Where q_i is the adsorption capacity and H_i is the cyclic heel build-up. IMA and IMD (g) are the integrated mass adsorbed and integrated mass desorbed in turn. The subscript i refers to cycle i, and MI is the weight of the preheated BAC.

Cumulative heel (H_T) defined as the total mass percentage accumulated on adsorbent after n consecutive adsorption/regeneration cycles, is calculated as follows:

$$H_T\,(\%) = \sum_{i=1}^{n} H_{i(\%)} \qquad \text{3-3}$$

To verify the above results and ensure calculations' accuracy, the above values were also calculated every three cycles based on gravimetric analysis. To that purpose, the adsorption/regeneration tube was weighted three times for the selected cycle. Before and after adsorption at the cycle and one final time after regeneration. The below equations were used to obtain the adsorption capacity and heel build-up via gravimetric analysis:

$$q_{i(\%)} = \frac{\text{Weight of BAC after adsorption} - \text{Weight of BAC before adsorption}}{\text{weight of preheated BAC}} \times 100 \qquad \text{3-4}$$

$$H_{i(\%)} = \frac{\text{Weight of BAC after regeneration} - \text{Weight of BAC before adsorption}}{\text{weight of preheated BAC}} \times 100 \qquad \text{3-5}$$

$$H_{T(\%)} = \frac{\text{Weight of BAC after last regeneration} - \text{Weight of BAC before first adsorption cycle}}{\text{weight of preheated BAC}} \times 100$$

$$\text{3-6}$$

Gravimetric analysis results of every third cycle were gathered and used as a base measure to normalize and calibrate the values obtained from the integration of the curves. Accordingly, the values obtained by integration were compared to the gravimetric results, and a correction factor was obtained. The correction factor was then used to calibrate the result of the next two cycles for

which no gravimetric results was present. This step was repeated every three cycle to get the most accurate results.

3.1.3 BACs Characterization

Several characterization tests were performed on BAC samples. These samples included virgin BAC gathered prior to the start of the experiments and ones collected at various points throughout the cyclic adsorption/regeneration experiments.

3.1.3.1 Micropore Surface Analysis

A micropore surface analyzer (Autosorb iQ2MP, Quantachrome.) was used to conduct surface analysis of several BAC samples and collect pore size distributions and BET surface areas. To this end, the device utilizes Nitrogen gas adsorption at 77 K with relative pressures ranging from 10^{-7} to 1. Before the Nitrogen gas adsorption, 30-60 mg of samples were placed inside specific 6 mm cells and degassed for 5 hours at 110 °C to remove all moisture present on the sample. To obtain the specific surface area of the samples, BET method was utilized at relative pressures ranging from 0.01 to 0.07. For micropore volume and total pore volume, the V-t method ($0.2 < \frac{p}{p_0} < 0.5$) and quench solid density functional theory (QSDFT) were used, respectively. QSDFT methods provided the pore size distribution as well.

3.1.3.2 Thermogravimetric Analysis (TGA)

Derivative thermogravimetric (DTG) analysis (TGA/DSC 1, Mettler Toledo) was performed on selected samples to investigate the thermal stability of the heel developed in the BAC pores. The samples were heated from 25 °C to 800 °C with a constant heating rate of 5 $\frac{°C}{min}$ and their weights was collected every second. 20 standard cm^3/min N$_2$ gas (99.999% pure, Praxair) was used to purge the desorbed species away.

3.1.3.3 X-ray photoelectron spectroscopy (XPS) Analysis

XPS was used to determine the three activated carbons' surface elemental composition (C, O, and S). With the help of the AXIS 165 spectrometer (Kratos Analytical), high-resolution scans of binding energies ranging from o to 1100 eV were gathered. The samples were selected to represent a start point, and endpoint of each adsorption/regeneration experiment for adsorbents. Subsequently, CasaXPS software was used to process the scans, and atomic concentration results were reported.

3.2 Pore size distribution model development

3.2.1 Introduction and Background

Hung et al. [6], developed a mathematical model capable of making predictions regarding the adsorption capacity of activated carbons at a wide range of relative pressures. Their model employed several estimation methods developed by previous researchers [7,8]. The final product was a D-R-L (Dubinin–Radushkevich-Langmuir) equation requiring only the pore size distribution of the adsorbent to be obtained experimentally. However, going through adsorption/regeneration experiments, the PSD of an adsorbent is subject to constant change. As it stands, one needs to conduct surface analysis for ACs after every adsorption/regeneration experiment and obtain the modified PSD. The surface analysis experiments require specific equipment and can take anywhere from a couple of days to a week to be completed. Having to conduct such a time-consuming experiment negates all the time saved by using a mathematical model in the first place. As a result, an addendum capable of making PSD predictions to the D-R-L model is needed. The D-R-L isotherm as explained in detail in chapter 2 is an expansion of the D-R equation which is a semi-empirical model based on Polayni's potential. The D-R isotherm has proven to work exceptionally well for intermediate and high concentration data ranges but fails to approach

Henry's law constant at low concentrations [6]. As a result of this shortcoming, Hung et al. [6] suggested to integrate the well-known D-R isotherm model with Langmuir isotherm. To this end experimental work was conducted and it was reported that for relative pressures below 1.5×10^{-3} Langmuir isotherm would fit best and for 1.5×10^{-3} and above the aforementioned D-R model could be utilized. However, to avoid the need for experimental investigations to obtain the Langmuir isotherm parameters, it was suggested that at relative pressure between 1.5×10^{-3} and 0.01, both the D-R isotherm model and Langmuir isotherm model generate similar isotherms. Thus, the parameters required for Langmuir isotherm can be determined by fitting the isotherm obtained from the D-R equation.

The D-R-L model proposed can be described as below [6]:

For $\frac{p}{p_0} < 1.5 \times 10^{-3}$ (Langmuir section):

$$q_e = \frac{q_m b C}{1 + bC} \qquad 3\text{-}7$$

Where q_m and b can be determined by fitting the isotherm obtained from the D-R equation.

For $1.5 \times 10^{-3} < \frac{p}{p_0} < 0.01$ (D-R section):

$W = W_0\, exp(-kA^2)$ 3-8

$W_0 = V_{32} + 0.055$ 3-9

$\log k = 1.585 - 0.442\ ^1\chi^v$ 3-10

$A = RT\, ln(P_0/P)$ 3-11

Where W represents the volumetric adsorption capacity expressed as equivalent liquid volume adsorbed per unit mass of adsorbent; A is the adsorption potential; W_0 is the pore limiting volume, V_{32} represents the volume of pore below 32 Å as defined by Urano et al. [7]; R is the universal gas constant; T is the absolute temperature; P_0 is the saturated vapor pressure at temperature T, and P

is the partial pressure of the adsorbate. k is the D-R equation parameter for the target compound. $^1\chi^v$ is the first-order valance molecular connectivity index of the targeted VOC. To obtain this parameter, first the hydrogen-suppressed molecular skeleton of 1,2,4- TMB was drawn, and each node was labeled. Then each node was given a valence value based on the atom located at the node and the type of bonds it had with surrounding atoms. For example, the carbon atom has a valence value equal to the number of bonds it has with surrounding molecules except hydrogen, so a fully saturated carbon atom has a valence value of 4. Subsequently $\prod v1, v2$ was calculated for each subgraph of the hydrogen-suppressed molecular skeleton. Finally, $^1\chi^v$ was calculated based on the following equation [6]:

$$^1\chi^v = \sum_1^n \prod v1, v2^{0.5} \qquad 3\text{-}12$$

Where n is the number of nodes on the skeleton.

To predict the PSD of an activated carbon sample that has gone through multiple cyclic adsorption/regeneration experiments. First, we need to determine how much available pore volume of the adsorbent has been reduced due to heel build-up within the pores. As previous investigations demonstrated, [9,10] heel build-up is primarily focused in the micropore region, and as such, almost all volume reduction will be exclusive to the volume of pores below 20 Å. Machine learning tools were chosen to predict micropore volume changes.

3.2.2 Data collection and preprocessing

The experimental data used in this study consisted of two main sections. The majority of the tests were compiled from already published investigations on cyclic adsorption/regeneration of VOCs on activated carbons[10–14]. The remaining experiments were selected from the long-term adsorption/regeneration cyclic tests conducted in this study. These experiments varied in many

ways, such as type of adsorbent, adsorbate, and purge gas, to name a few; however, they shared several essential similarities. For all test cases, adsorption was done using 10 SLPM air. Additionally, the adsorbate was a single compound, and no mixture was used; this is important since the developed isotherm prediction model had been designed for a single compound adsorbate. Three main parameter groups exist from which the input features for the ML model's development were chosen:

- **Adsorbent parameters:** physical properties of the initial fresh activated carbon, including pore volumes ($\frac{cm^3}{gr}$); micropore and total pore volume, BET surface area ($\frac{m^2}{gr}$).

- **Adsorbate parameters:** molecular weight ($\frac{gr}{mol}$), density ($\frac{gr}{ml}$), boiling point(°C), melting point(°C), electronic polarization, molecular parachors, molar volume ($\frac{cu\,m}{kmol}$), polarizability (Å³), Henrys Law Constant ($\frac{atm-m^3}{mol}$)

- **Parameters related to the operating condition of the cyclic experiment:** First cycle adsorption capacity (%wt.), final cycle's cumulative heel build-up (%wt.), purge gas oxygen content (ppm$_v$), and normalized purge gas flow rate.

Normalized purge gas flow rate ($\frac{SLPM}{cm^2}$) $= \frac{flow\,rate(SLPM)}{Cross-sectional\,area\,of\,AC\,bed\,(cm^2)}$

To account for the difference in the cross-sectional areas of the adsorbent beds between tests, purge gas flowrate was normalized by the cross-sectional area of each bed.

The targeted feature was defined as ($\frac{Final\,Micropore\,Volume}{Initial\,Micropore\,Volume} * 100$) to better represent changes occurring in the micropore volume of the adsorbent.

Pearson Correlation Coefficient (PCC) was used to measure the linear dependency between any two features. A correlation is a number ranging from -1 to +1 that measures the degree of

association between two attributes. Positive values for the correlation imply a positive association and vice versa, with +1 and -1 suggesting the presence of a strong positive and negative correlation, correspondingly. Values close to zero represent a very weak linear correlation, with 0 showing an absence of any linear correlation. When two features are highly correlated, one needs to be removed since they do not contribute any new information to the model. The cut-off point in this model was defined as 0.95; thus, features with an absolute PCC of 0.95 or higher were selected, and one was filtered out. PCC among two variables x and y can be calculated as follows:

$$r = \frac{\sum(x-\bar{X})(y-\bar{Y})}{\sqrt{\left[\sum(x-\bar{X})^2\right]\left[\sum(y-\bar{Y})^2\right]}}$$ 3-13

Where $\bar{X}$ or $\bar{Y}$ are the averages of variable x or y.

The PCCs between any two features used in this study are provided in **Figure 3.4**. In training and testing ML algorithms, two features, initial micropore volume and molecular parachors, were eliminated due to high linear correlation with virgin adsorbent BET surface area (PCC $_{Micropore}$ $_{volume~\&~BET}$ = 0.988) and molecular weight (PCC $_{Molecular~Parachors~\&~MW}$ = 0.964), respectively.

After removing highly correlated features, all the variables except the target value were normalized using the Z-transformation method into the range of 0.1-0.9. Normalization is critical when dealing with attributes of varying scales and units. For a fair comparison among all attributes, they should have the same scale and fit in a specific range. Z- transformation is a common normalization technique that is less influenced by outliers. This normalization subtracts the mean of the data from all values and divides them by standard deviation.
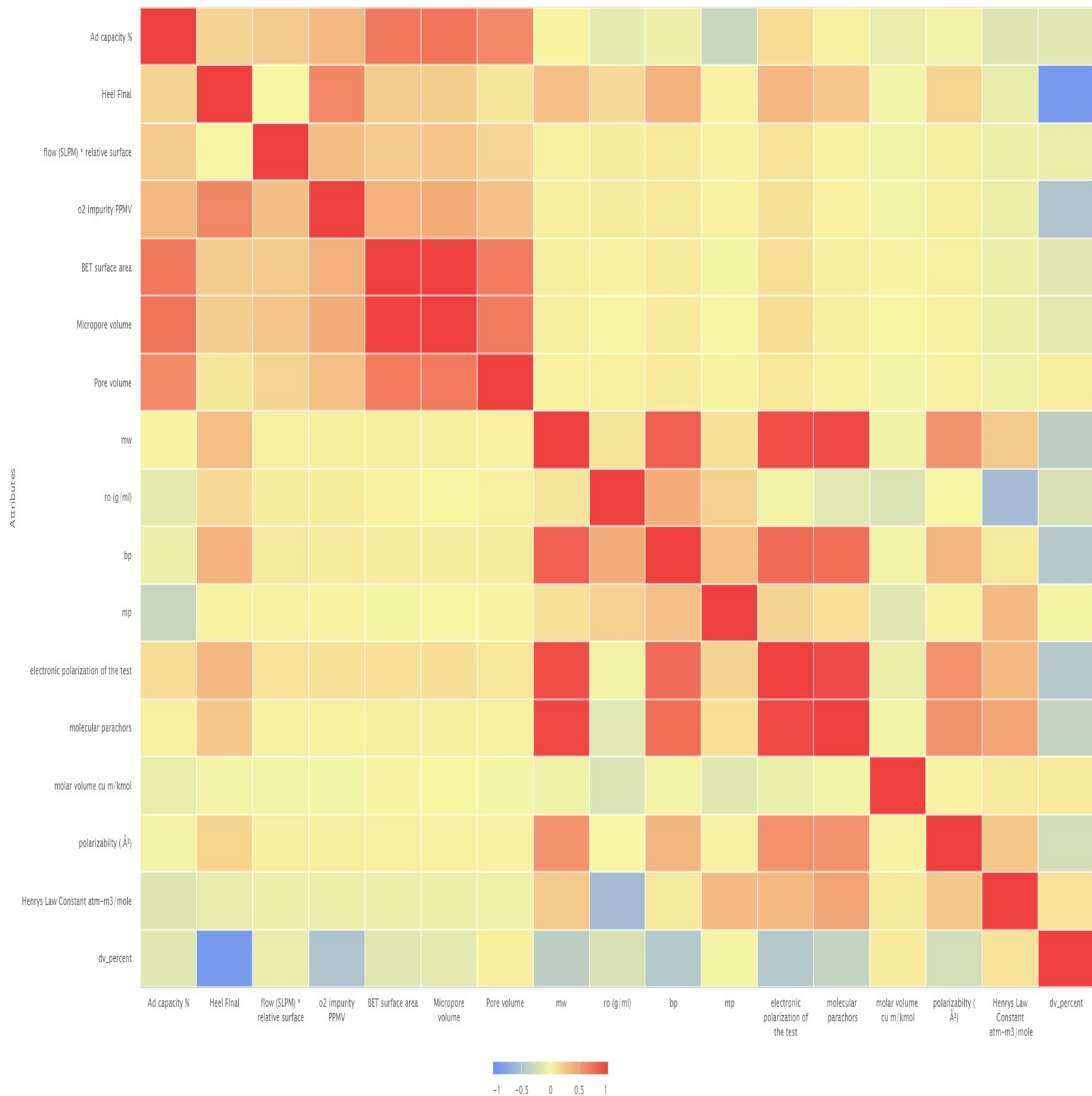
Figure 3.4. Pearson Coefficient matrix visualization.

3.2.3 Predictive model selection

The processed data, consisting of 100 data points gathered from both previous studies[10-14] and ones conducted in this research, was fed into the RapidMiner studio ™ program, a preliminary test was conducted using various predictive models such as Linear regression, Decision tree, Gradient boosted trees, and support vector machine, to identify models best suited for the dataset. Based on the program's performance results, the linear regression model and Decision tree were selected as the leading predictive models to be further investigated. The reason behind this selection was that the generalized linear model showed the highest correlation with a value of 0.807 and the lowest root mean squared error (RMSE) of 0.026, while the Decision tree was the fastest running model with a good correlation value of 0.769 and RMSE of 0.03. a comparison of the predictive models tested and their performance can be observed in **Table 3.3.**

Table 3.3. Predictive models performance

Model	Correlation	Standard Deviation	RMSE	Computation time (s)*
Generalized Linear Model	0.803	0.200	0.026	81
Decision Tree	0.769	0.160	0.030	50
Gradient Boosted Trees	0.775	0.122	0.037	6435
Support Vector Machine	0.615	0.290	0.049	609

* Obtained via AMD Ryzen 7 4800HS with a clockspeed of 2.9GHZ

3.2.3.1. Linear regression

Regression is a technique used to predict dependent variables' y' with the help of a range of independent variable values 'x'[15]. This statistical measure attempts to determine the strength of the relationship between one dependent variable (i.e., the label attribute) and a series of other changing variables known as independent variables (regular attributes). Based on the number of independent variables, a regression can be divided into Simple linear regression (one independent variable) and Multivariate linear regression (MLR)[15,16]. The basic MLR model can be described as follows:

$$y = \beta_0 + \beta_1 x_1 + \cdots + \beta_m x_m + \varepsilon \qquad \text{3-14}$$

$$\hat{\beta} = (X^T X)^{-1} X^T y \qquad \text{3-15}$$

$$\text{Where } \beta = \begin{bmatrix} \beta_0 \\ \beta_1 \\ \vdots \\ \beta_m \end{bmatrix}, X = \begin{bmatrix} 1 & x_{11} & \cdots & x_{1m} \\ 1 & x_{12} & \cdots & x_{2m} \\ \vdots & \vdots & \vdots & \vdots \\ 1 & x_{14} & \cdots & x_{nm} \end{bmatrix}, Y = \begin{bmatrix} Y_1 \\ Y_2 \\ \vdots \\ Y_n \end{bmatrix} \qquad \text{3-16}$$

The least squared method (LSM) attempts to find the matrix $b = \begin{bmatrix} b_0 \\ b_1 \\ \vdots \\ b_m \end{bmatrix}$ such that the cumulative squared distance from the real y_i and the values predicted $\beta_0 + \cdots + \beta_m x_m$ approaches the minimum possible. The least-square results for a basic linear regression can be obtained by solving this system [15].

$$\begin{bmatrix} \frac{\partial}{\partial \beta_0} \sum_{i=1}^{n} [y_i - (\beta_0 + \beta_1 x_i)]^2 \\ \vdots \\ \frac{\partial}{\partial \beta_m} \sum_{i=1}^{n} [y_i - (\beta_0 + \beta_1 x_i)]^2 \end{bmatrix} = 0 \qquad \text{3-17}$$

The resulting $\hat{y} = b_0 + b_1 x_1 + \cdots + b_m x_m$ can describe the relationship between x and y.

3.2.3.2. Decision tree

A decision tree comprises a collection of nodes aimed at creating a decision on values affiliation to a class or an approximation of a numerical target value. Each node contains a splitting rule for an attribute. In classification methods, this rule separates values into different classes, while for regression, this division is done to reduce error in an optimal way for the targeted criterion. Nodes are constantly created, and data is split until the targeted criteria are met. An approximation for a numerical value is obtained by averaging values in a leaf[15,16].

3.2.4. Cross-Validation

Cross-validation is a statistical method developed for the evaluation of learning algorithms. This is achieved by dividing the data into two segments: one part is used for training the model while the other is used to test the model against. In conventional cross-validation methods, the data sets cross over between both segments in successive rounds, and as a result, each data point will be validated against. The performance of the model is measured during the testing phase. K-fold cross-validation is the primary form of cross-validation typically utilized[17]. In k-fold cross-validation, the input Example Set is partitioned into *k* segments of equal size. One of those k segments is randomly chosen as the testing segment, and the remaining *k - 1* are used as a training data set (i.e., input of the Training subprocess). This process is repeated *k* times, and each time a different segment is designated as the test segment. The *k* results from the *k* iterations are averaged to produce a single estimation. Cross-validation is usually performed with one of the two goals in mind: (i) measure the generalizability of the algorithm (ii) compare the performance of several algorithms and decide which one is best suited for the available data set. The performance of the

selected model on an independent test is a reasonable approximation of its performance on unseen data sets. It is also to observe the occurrence of "overfitting" phenomena. Overfitting occurs when the model represents the testing data very well, but it does not generalize well for new data. Thus, the performance can be much worse on test data. A 5-fold cross-validation was chosen to test the generalizability of our models and compare MLR and decision tree methods. Thus the data points were separated into five equal-sized groups, and each time one group was selected as the test group, and the outcome of the other data points in the training group was validated against them. This process was repeated five times, and average performance parameters were reported for each model at the end.

Within the 5-fold cross-validation module and prior to the application of the select predictive model, the Forward selection technique was applied. Forward selection is a feature importance technique; Feature importance refers to techniques that assign a score to input features based on how useful they are at predicting a target variable; in this method, we start with one feature, and other features are added one by one to select the best combination of features for accurate prediction[18]. By applying this technique only, the features that played a major role in micropore volume changes are considered.

3.2.4. Models' performance

Models' performance evaluations for predictability and generalizability are acquired. The following three error types are used to evaluate the performance of each model and its accuracy.

$$R^2 = 1 - \frac{\sum_{i=i}^{N}(Y_i^{experiment} - Y_i^{prediction})^2}{\sum_{i=i}^{N}(Y_i^{experiment} - \hat{Y}_{average}^{prediction})^2} \qquad \text{3-18}$$

$$RMSE = \sqrt{\frac{1}{N}\sum_{i=i}^{N}(Y_i^{experiment} - Y_i^{prediction})^2} \qquad \text{3-19}$$

$$Percentage\ Error = \left| \frac{Y_i^{prediction} - Y_i^{experiment}}{Y_i^{experiment}} \right| * 100 \qquad\qquad 3\text{-}20$$

3.2.5. PSD prediction model

The Machine learning algorithm proposed in the previous section provides us the updated micropore volume of the activated carbon adsorbent containing heel build-up as a result of consecutive adsorption/regeneration experiments. Having the knowledge of new micropore volume, it is possible to predict the new pore size distribution of the adsorbent and make predictions regarding other PSD-related parameters such as the pore limiting volume parameter involved in the DRL isotherm prediction model. To that end, a new PSD needs to be devised that presents a new micropore volume equal to that predicted by the ML algorithm.

The first step is to gain a detailed PSD of the virgin adsorbent using the density function theory (DFT) method, as explained in the surface analysis section. Each point in the PSD represents a specific pore with its own pore width, and the area underneath it denotes the pore volume it contains. The target would be to reduce the PSD points until the area under the PSD in the micropore section (i.e., pores below 20Å) reach the updated micropore volume value predicted by the ML algorithm (**Figure 3.5**).

As demonstrated by the yellow arrows in **Figure 3.5**, each of the points below 20Å on the PSD of the virgin adsorbent needs to be reduced until they reach a new position. That position is decided by how much the micropore volume and thus the area within the micropore section needs to be reduced. To calculate the area, trapezoid sums calculation can be utilized. A straightforward method for point reduction would be to reduce all pores equally. In this method, the pores are all reduced simultaneously, and for an equally small amount, then the area can be calculated, and if the target has yet to be achieved, another reduction step is taken. However, based on previous

investigation and studies, it is known that adsorption is not done equally on all pores and different parameters affect the contribution of pores to adsorption and heel formation[5,19].
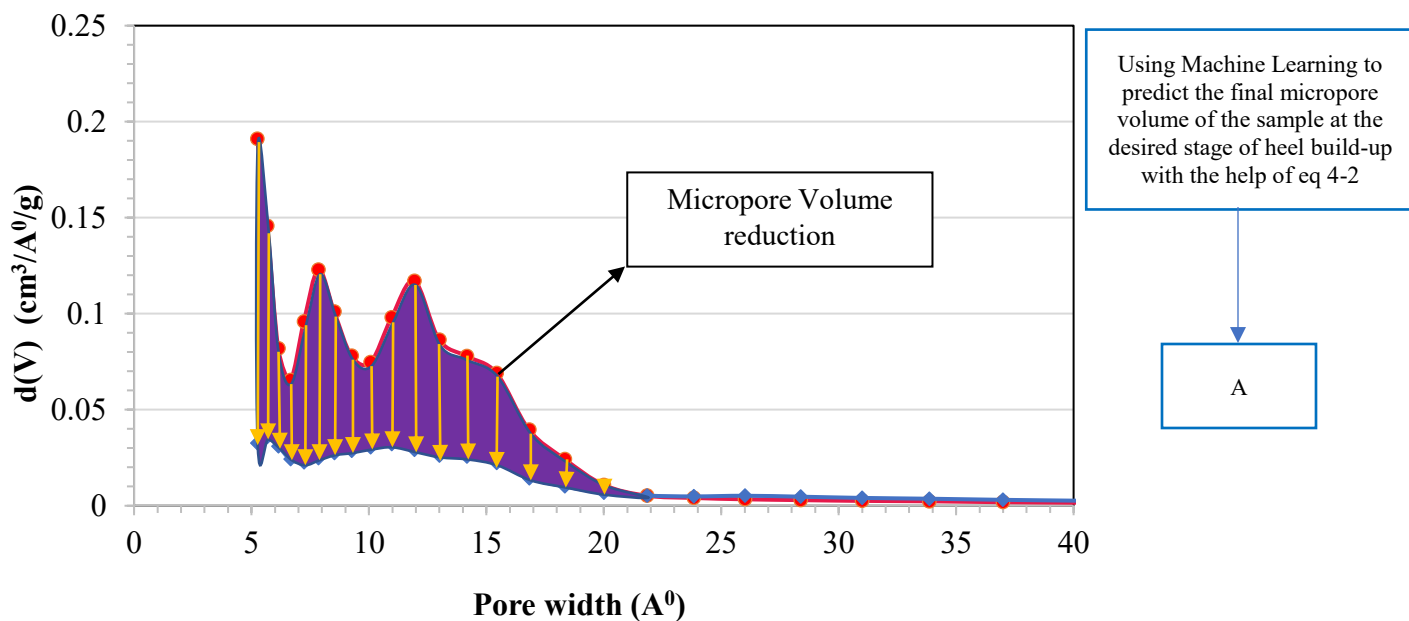
Figure 3.5. An example of micropore volume reduction required to obtain the new PSD. Purple shaded area represents the difference between new micropore volume and the virgin micropore volume.

To make the prediction of pore size distribution more accurate and better represent the real-world adsorption process, two new parameters were created to account for variation in different micropores' adsorption capabilities. S and E parameter representing volume of each pore and its characteristic energy, respectively. Firstly, in the micropore region, it is safe to assume that the larger the volume of an individual pore, the more adsorbate it can accommodate. This could also be considered as the frequency of each pore. To calculate this parameter trapezoid integration was used on the PSD to find out the volume of each pore size. The larger the area of the PSD plot under a specific pore size, the better its chance of adsorbing the target compound. These normalized factors were then used to represent the increased adsorption capabilities of relatively larger micropores. The result of these integrations were put inside the matrix S.

However, the available volume is not the only influential factor in the difference between adsorption of various pore sizes. Chen et al[20] conducted a thorough investigation on characteristic energy and pore size for adsorption in micropores. They concluded that characteristic energy is a complicated function of many factors, including pore size and temperature, but some approximation methods could still be used. These methods might not be suitable for the exact calculation of characteristic energy, but they are beneficial for comparing adsorption between various pores. One such approximation method was developed by, McEnaney[21] who proposed an empirical equation for characteristic energy (E_0) as a function of pore size L for activated carbon adsorbents as follows.

$$E_0 = 41.26 \exp(-1.120L) \qquad \text{3-21}$$

This function is only applicable for pore sizes in the range of 4 to 28 Å. However, this limitation does not affect the current work since we are only interested in pores below 20 Å. The characteristic energy of each pore below 20 Å was calculated with the above formula and a matrix of characteristic energies, named E, was formed. Matrix S and E were then multiplied to form a matrix named MSP which represents capability of each individual micropore in adsorbing the targeted VOC. With the help of the introduced parameters, the reduction amount for each PSD point was modified to represent its frequency and characteristic energy. The reduction was made until targeted micropore volume was achieved. The code utilized in MATLAB is presented in Appendix C.

Finally, having predicted a new PSD with the help of the ML algorithm and the PSD prediction model, we can gain new, previously unavailable information such as the volume of pores below 32 Å required for the DRL isotherm prediction. A summary of the modeling approach can be seen in **Figure 3.6**.
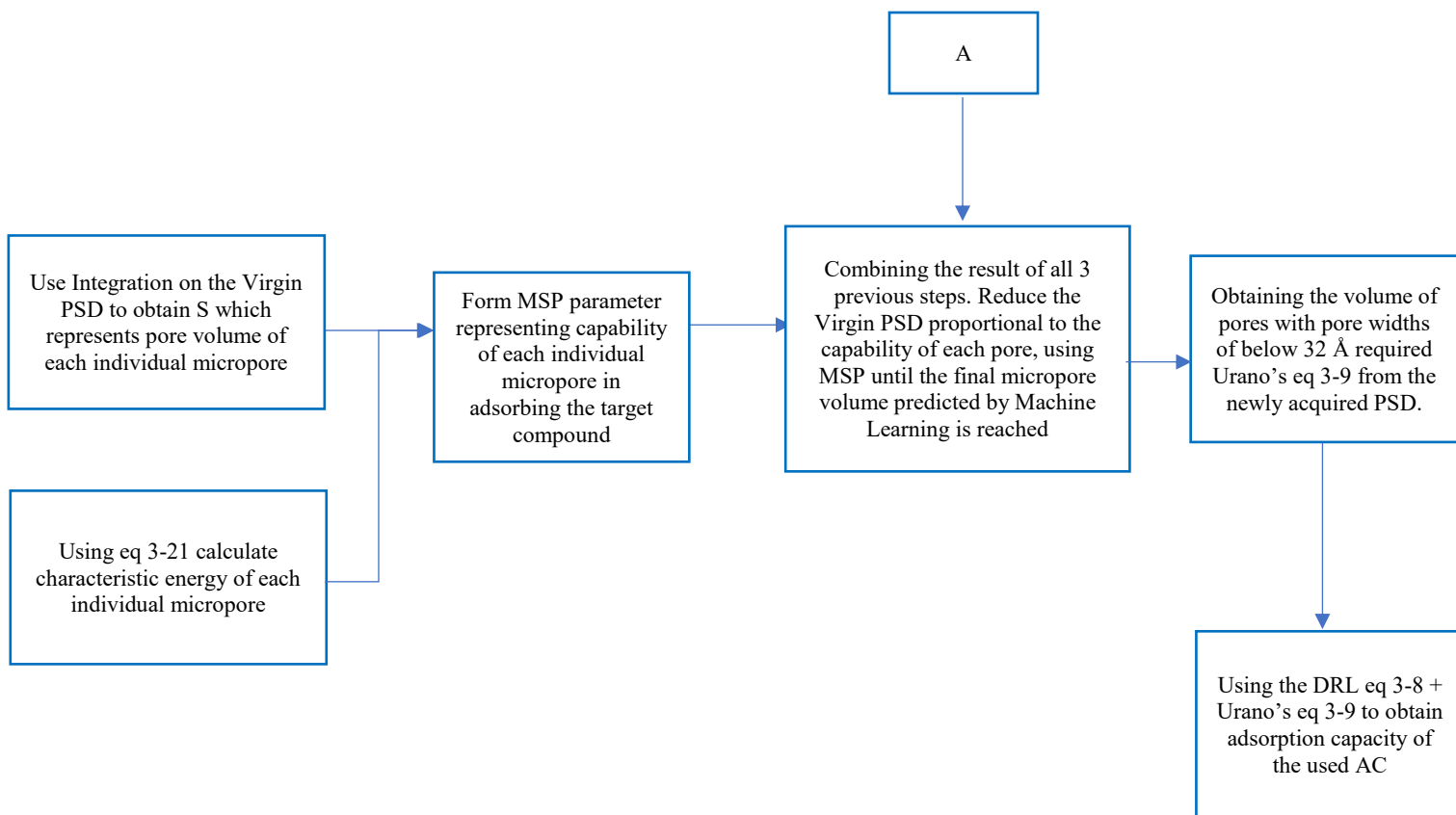
Figure 3.6. Flowchart of the modeling approach to obtain adsorption capacity of a used activated carbon sample containing heel.

3.3 References

1. Avhale A, Kaya D, Mabande GTP, et al. Defect-free zeolite membranes of the type BEA for organic vapour separation and membrane reactor applications. *Studies in Surface Science and Catalysis*. 2008;174(SUPPL. PART A):669-672. doi:10.1016/S0167-2991(08)80287-X

2. HaiLin W, Lie N, Jing L, et al. Characterization and assessment of volatile organic compounds (VOCs) emissions from typical industries. *Chinese Science Bulletin* . 2013;58(7):724-730. doi:10.1007/s11434-012-5345-2

3. Niknaddaf S, Atkinson JD, Shariaty P, et al. Heel formation during volatile organic compound desorption from activated carbon fiber cloth. *Carbon*. 2016;96:131-138. doi:10.1016/J.CARBON.2015.09.049

4. Salvador F, Martin-Sanchez N, Sanchez-Hernandez R, Sanchez-Montero MJ, Izquierdo C. Regeneration of carbonaceous adsorbents. Part I: Thermal Regeneration. *Microporous and Mesoporous Materials*. 2015;202:259-276. doi:10.1016/J.MICROMESO.2014.02.045

5. Jahandar Lashaki M, Atkinson JD, Hashisho Z, Phillips JH, Anderson JE, Nichols M. The role of beaded activated carbon's pore size distribution on heel formation during cyclic adsorption/desorption of organic vapors. *Journal of Hazardous Materials*. 2016;315:42-51. doi:10.1016/J.JHAZMAT.2016.04.071

6. Hung HW, Lin TF. Prediction of the Adsorption Capacity for Volatile Organic Compounds onto Activated Carbons by the Dubinin–Radushkevich–Langmuir Model. *Journal of the Air & Waste Management Association*. 2012;57(4):497-506. doi:10.3155/1047-3289.57.4.497

7. Urano K, Omori S, Yamamoto E. Prediction Method for Adsorption Capacities of Commercial Activated Carbons in Removal of Organic Vapors. *Environmental Science and Technology*. 1982;16(1):10-14. doi:10.1021/ES00095A006

8.	Qi S, Hay KJ, Rood MJ, Cal MP. Carbon Fiber Adsorption Using Quantitative Structure-Activity Relationship. *Journal of Environmental Engineering*. 2000;126(9):865-868. doi:10.1061/(ASCE)0733-9372(2000)126:9(865)

9.	Feizbakhshan M, Hashisho Z, Crompton D, Anderson JE, Nichols M. Effect of Activated Carbon's Pore Size Distribution on Oxygen Induced Heel Build-up. *Journal of Hazardous Materials*. Published online August 13, 2021:126905. doi:10.1016/J.JHAZMAT.2021.126905

10.	Jahandar Lashaki M, Atkinson JD, Hashisho Z, Phillips JH, Anderson JE, Nichols M. The role of beaded activated carbon's pore size distribution on heel formation during cyclic adsorption/desorption of organic vapors. *Journal of Hazardous Materials*. 2016;315:42-51. doi:10.1016/J.JHAZMAT.2016.04.071

11.	Jahandar Lashaki M, Fayaz M, Wang H, et al. Effect of Adsorption and Regeneration Temperature on Irreversible Adsorption of Organic Vapors on Beaded Activated Carbon. *Environmental Science and Technology*. 2012;46:7. doi:10.1021/es3000195

12.	Mosavari Nezamabad N. Effect of Surface Oxygen Groups on Irreversible Adsorption of Volatile Organic Compounds on Beaded Activated Carbon. Published online 2017. doi:10.7939/R3M03Z893

13.	Feizbakhshan M, Amdebrhan B, Hashisho Z, et al. Effects of oxygen impurity and desorption temperature on heel build-up in activated carbon. *Chemical Engineering Journal*. 2021;409:128232. doi:10.1016/J.CEJ.2020.128232

14.	Mojtaba Hashemi S, Jahandar Lashaki M, Hashisho Z, Phillips JH, Anderson JE, Nichols M. Oxygen impurity in nitrogen desorption purge gas can increase heel buildup on activated carbon. *Separation and Purification Technology*. 2019;210:497-503. doi:10.1016/J.SEPPUR.2018.08.035

15. Maulud DH, Mohsin Abdulazeez A. A Review on Linear Regression Comprehensive in Machine Learning. *Journal of Applied Science and Technology Trends*. 2020;01(04):140-147. doi:10.38094/jastt1457

16. Yu C, Yao W. Robust linear regression: A review and comparison. *Communications in Statistics-Simulation and Computation*. 2017;46(8):6261-6282. doi:10.1080/03610918.2016.1202271

17. Refaeilzadeh P, Tang L, H Liu. Cross-validation. *Encyclopedia of database systems 5*. Published online 2009:532-538. doi:10.1007/978-1-4899-7993-3_565-2

18. Sutter JM, Kalivas JH. Comparison of Forward Selection, Backward Elimination, and Generalized Simulated Annealing for Variable Selection. *Microchemical Journal*. 1993;47(1-2):60-66. doi:10.1006/MCHJ.1993.1012

19. Feizbakhshan M, Hashisho Z, Crompton D, Anderson JE, Nichols M. Effect of Activated Carbon's Pore Size Distribution on Oxygen Induced Heel Build-up. *Journal of Hazardous Materials*. Published online August 13, 2021:126905. doi:10.1016/J.JHAZMAT.2021.126905

20. Chen SG, Yang RT. Theoretical Investigation of Relationships between Characteristic Energy and Pore Size for Adsorption in Micropores. *Journal of Colloid and Interface Science*. 1996;177(2):298-306. doi:10.1006/JCIS.1996.0035

21. McEnaney B. Estimation of the dimensions of micropores in active carbons using the Dubinin-Radushkevich equation. *Carbon*. 1987;25(1):69-75. doi:10.1016/0008-6223(87)90041-8

4. CHAPTER 4: Results and Discussions

4.1 Long-term Experimental Results

4.1.1 Long-term cyclic adsorption breakthrough curve and capacity

Long-term cyclic adsorption/regeneration experiments were conducted on three different activated carbon adsorbents under experimental conditions explained in the previous chapter. The cyclic experiment was continued until the 20th cycle for all but one experimental scenario, G-70R BAC at 0.5 SLPM purge gas flowrate, in which G-70R was exhausted long before the 20th cycle was reached. For the rest of the cyclic experiments, the breakthrough curves of every five cycles are presented in **Figure 4.1**, for clarity and better visualization of breakthrough results.
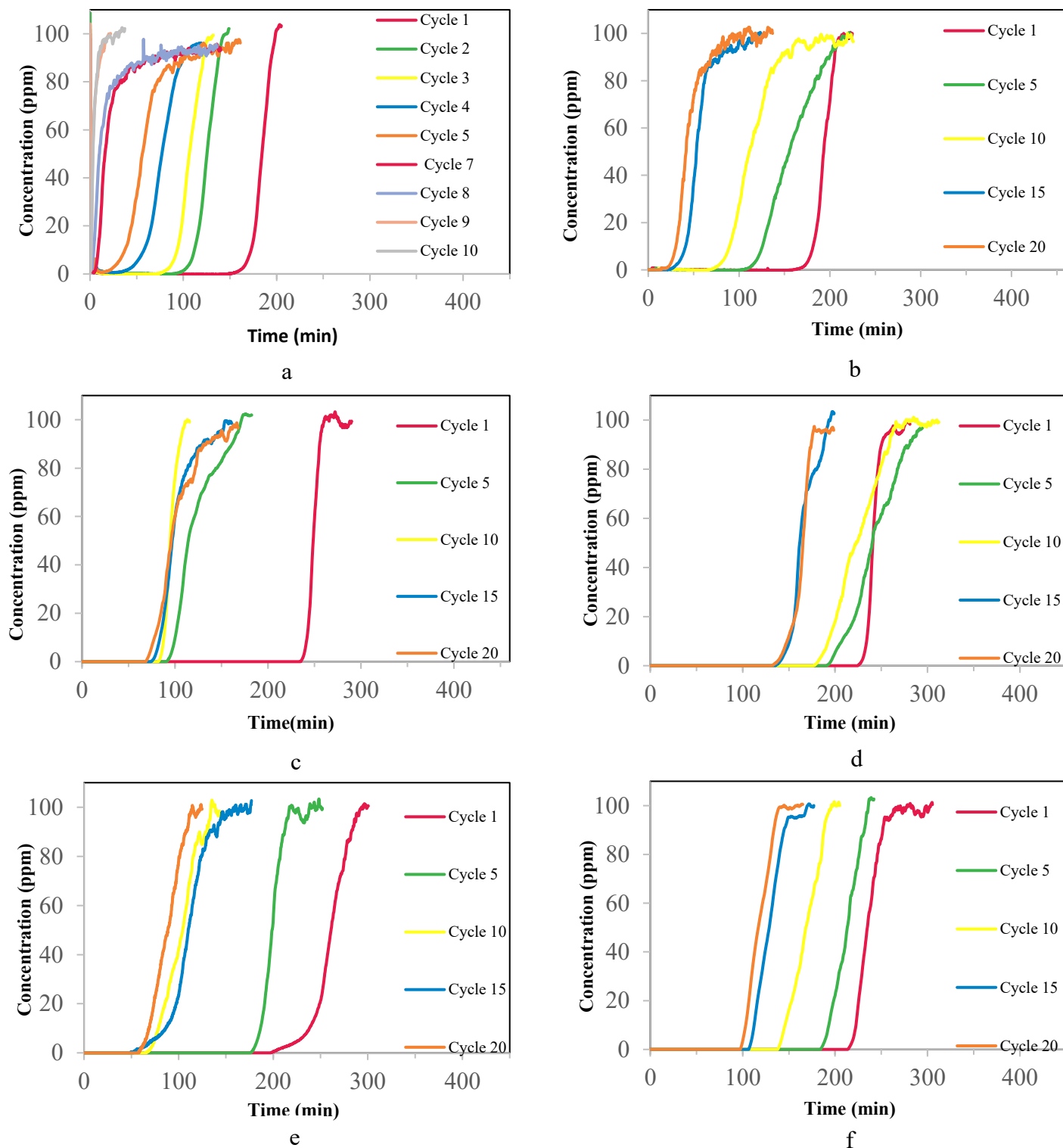
Figure 4.1. Adsorption breakthrough curves of 1,2,4-TMB on three adsorbents at various purge gas flow rates. a) G-70R at 0.5 SLPM, b) G-70R at 5 SLPM, c) B101412 at 0.5 SLPM, d) B101412 at 5 SLPM, e) B100772 at 0.5 SLPM, and f) B100772 at 5 SLPM.

As observed in **Figure 4.1**, the first cycle breakthrough time remained constant for the same adsorbent between various experiments since they were sourced from the same pre-regenerated batch. The longest first cycle breakthrough time was seen in B101412 (236 minutes). B100772 and G-70R were ranked second (223 minutes) and third (172 minutes) respectively. Since adsorption capacity can be calculated using the area under the breakthrough curves, the same trend can be expected for the first cycle adsorption capacities (**Figure 4.2-A**). The trend in breakthrough times and adsorption capacities of the first adsorption cycle agrees with surface area and porosity data in **Table 3.2**, where B101412 has the highest total pore volume and surface area.

For all experiments, regardless of the adsorbent or the purge gas flow rate used, breakthrough times, and thus adsorption capacities, decreased with cyclic use, indicating that regenerative conditions selected such as the selected temperature of 288°C, or the purge gas used and duration of the regeneration were not able to completely remove the adsorbed organic vapors and restore the adsorption capacity of the adsorbent, resulting in heel formation. The most noticeable drop in adsorption capacity and breakthrough time is seen for G-70R adsorbent when purged with 0.5 SLPM of dry air. In this case, after only ten cycles, an immediate breakthrough of 1,2,4- TMB was recorded, and BAC appears fully exhausted. On the other hand, the lowest drop in adsorption capacity with cyclic adsorption/regeneration is seen in the highly mesoporous B101412 activated carbon when purged with 5 SLPM dry air, where the difference between the first cycle and 20th cycle breakthrough time was only 71 minutes ($\Delta T_{1,20}$ =71 min), only 30% drop in breakthrough time.

In general, the decline of adsorption capacity and breakthrough time, as seen in **Figure 4.2-A**, are much less substantial when 5 SLPM of purge gas is utilized instead of 0.5 SLPM.
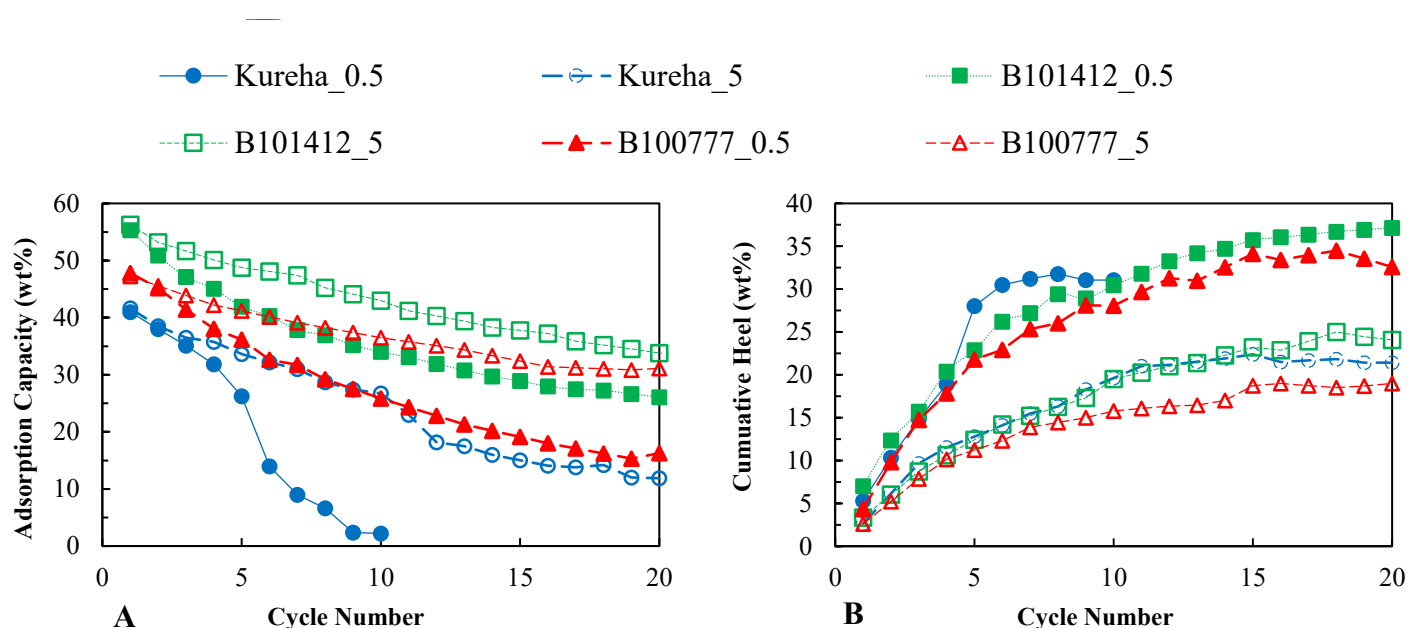
Figure 4.2. Adsorption capacity (A) and heel formation (B) during long-term cyclic adsorption/regeneration.

The rank order of the adsorption capacity remained the same throughout all the experiments. B101412 having the highest total pore volume and surface area, always had the highest adsorption capacity, as seen in **Figure 4.2-A**. Furthermore, it appears that for a specific adsorbent, the adsorption capacities of the first two cycles are very close regardless of the purge gas flow rate. This could mainly be attributed to the small, cumulative heel build-up even at a low purge gas flow rate.

As **Figure 4.2-B** shows, for all adsorbents at both flow rates, a considerable amount of heel was accumulated throughout cyclic adsorption experiments. Thus, it can be concluded that the experimental conditions and parameters (e.g., temperature, purge gas flow rate, type of purge gas) utilized for regeneration of the adsorbent were not sufficient to desorb the VOC adsorbed in each cycle completely. However, the large cumulative heel build-up was expected based on previous studies using dry air as the purge gas. Feizbakhshan et al. [1]. studied the effect of oxygen-induced regeneration and reported substantial heel build-up especially compared to the sample regenerated with Nitrogen gas.

Taking a closer look at **Figure 4.2-B,** two very separate groupings start to appear at higher cycle numbers. Ones regenerated with 0.5 SLPM dry air and those regenerated with 5 SLPM dry air. The difference in cumulative heel builds up amongst adsorbents, though, appear to be less noticeable. Based on these observations, purge gas flowrate appears to be more determinant in heel build-up at higher cycle numbers.

4.1.2 Effect of adsorbent's physical properties

Physical properties of the three activated carbon adsorbents used, such as their total and micropore volume, have a noticeable impact on their breakthrough times and adsorption capacities, as demonstrated in **Figure 4.1** and **Figure 4.2-A**, respectively. As noted before, B101412 having the highest total pore volume, offered the highest adsorption capacity regardless of the purge gas flow rate used. This is consistent with a previous study by Jahandar Lashaki et al. [2]. where it was concluded that the adsorption capacity of an adsorbent is highly correlated with its total pore volume.

In the first five cycles, it appears that adsorbents with higher micropore volume experienced a larger drop in their adsorption capacity. As seen in **Figure 4.2-A**, this trend is much more apparent at 0.5 SLPM purge gas. The drop in breakthrough time from the 1st to the 5th cycle is almost the same for B101412 and G-70R. Regardless of the adsorbent used, in later cycles, adsorption capacity changes slowed down noticeably, and its variation from one cycle to the next became less prominent. By comparing **Figure 4.2-A** and **Figure 4.2-B**, the reduction in adsorption capacity decrease is accompanied by a slower rate of heel formation at later cycles.

The cumulative heel build-up at the first five cycles for the experiments using the same purge gas flow rate is very similar. This could be argued to be a result of similar micropore volumes for all three adsorbents. Micropore volume can increase heel formation because of the strong overlapping attractive forces from opposing walls, increasing adsorption energy drastically[3]. Previous studies on the 5-cycle adsorption regeneration experiments also reported a high correlation between micropore volume of the adsorbent and the cumulative heel build with an R^2 of 0.91[2]. To further strengthen this argument, it can be seen in F**igure 4.2-B,** that B100772 having a slightly lower

micropore volume (0.43 as opposed to 0.50 for G-70R and B101412), is experiencing marginally less cumulative heel build up in the first five cycles.

However, from cycle five onward, a difference appears amongst adsorbents in their heel build accumulation, which was not observed in most studies that focused only on the first five cycles. As **Figure 4.2-B** demonstrates, this difference is more apparent when 0.5 SLPM purge gas is utilized. This different behavior between adsorbents in the later cycles of adsorption/regeneration stems from the exhaustion of the majority of micropores. As explained, in the first five cycles, micropores, having higher adsorption energy, participate extensively in heel formation. In the most extreme case, this phenomenon is much more apparent for G-70R which is mainly comprised of micropores. After the 5th cycle, the micropore volumes are mostly exhausted and blocked. This blockage is further proven by the sudden drop in adsorption capacity for G-70R when going from cycle number 5 to 6. When using 0.5 SLPM as purge gas, adsorption capacity of G-70R is halved (from 26% to 13%). The drop in adsorption capacity is less noticeable in the other two adsorbents due to their lower microporosity (86%, 60%, and 44% for G-70R, B100772, and B101412 in that order). By the 10th cycle, G-70R being 86% micropores is fully exhausted while the other adsorbents can continue adsorption using meso and macropores that are still available. Nevertheless, because meso and macropores do not contribute in a major way to heel formation, the cumulative heel builds up rates slows down.

It can be deducted from the aforementioned changes in cumulative heel build-up; after the first few cycles, larger pores such as macro and mesopores can help overcome the transport limitations present in micropores. Thus, if the target is to conduct a long-term cyclic adsorption/ regeneration on activated carbon adsorbents, selecting adsorbents with a hierarchal pore structure containing micropores and mesopores becomes more critical.

4.1.3 Effect of purge gas flow rate

In general, a higher purge gas flowrate can help desorb more VOCs off the surface of the adsorbent. High flow rates during regeneration can decrease the desorption concentration and, as a result, expose less adsorbate to the high regeneration temperature of 288°C [4]. Due to this low exposure, there is a lower chance of adsorbate thermal decomposition and oxidation, which could lead to the formation of chemisorbed species, especially in the presence of oxygen[5].

Figure 4.2-B demonstrate that when 0.5 SLPM flowrate of dry air was used as the purge gas, heel build-up for the three adsorbents was markedly different compared to samples regenerated at higher flowrate. At the low purge gas flow rate, after 20 cycles of adsorption/regeneration, final cumulative heel values of around 30% were observed for all the activated carbon adsorbents regardless of their physical properties. On the other hand, when 5 SLPM dried air was used, final cumulative heel values were in the range of 20%.

The effect of purge gas flow rate seems more apparent towards the later cycles. In early cycles, the differences between cumulative heel build-ups, when different flowrate is utilized, are not prominent, as shown in **Figure 4.2-B.** As reported in previous investigations, one of the contributing factors to heel formation is mass transfer limitations that are at play during regeneration[4]. As discussed in the previous section, micropores, due to their intense adsorption energy, offer more transport limitations that need to be overcome for adsorbent regeneration [1], and it is known that flowrate increase reduces the heel build-up on all pores as demonstrated in Figure 4.2-**B**. However, due to the mentioned mass transfer limitations in the micropore region, this beneficial effect of purge gas flowrate increase is less impactful compared with its impact in the larger mesopore and macropore regions. Unfortunately, after the first few cycles, when micropore volumes are greatly reduced the flowrate increase can have a much more

meaningful effect in desorbing the adsorbed species in the mesopores with lower adsorption energy. Based on these results, it can be reasonably argued that for early cycles, the microporosity of the adsorbent and its micropore volume are important factors in heel formation. In contrast, purge gas flowrate becomes a decisive factor in heel formation at higher cycle numbers where micropores are no longer dominant.

4.1.4 Nitrogen adsorption analysis

Since purge gas flowrate mainly affects the adsorbents' final cumulative heel formed, samples were chosen based on their cumulative heel build-up to investigate the changes occurring in the pore size of the three adsorbents. For each adsorbent, three samples were selected at various stages of heel build-up. BET surface area, micropore volume, and total pore volume of BAC samples before and after regeneration are listed in **Table 4.1**. As the data demonstrates, heel formation drastically reduced all three parameters. However, by taking a closer look at the data in **Table 4.1** and the pore size distributions shown in **Figure 4.2**, it becomes apparent that pore loss mainly occurred in micropores for all three adsorbents regardless of the total pore volume. Although the presence of mesopores and a hierarchal structure of pores certainly eases the desorption and reduces heel build-up in the cases studied, in general, changes in the mesopore region are negligible compared to the micropores. For example, a 28% cumulative heel build-up on the highly microporous G-70R sample reduced its micropore volume by 92%. In contrast, 24% cumulative heel build-up on the mesoporous B101412 reduced its micropore volume by only 54%.

As expressed in **Figure 4.2**, 28% heel build for G-70R BAC corresponds with the point of exhaustion for this specific adsorbent. As seen in **Table 4.1**, at this point, the micropore volume of the adsorbent is almost reduced to zero. still, even at this point, around 0.17 $(\frac{cm^3}{g})$ of meso

and macropores are left. This further proves that even though adsorption capacity correlates more closely with total pore volume, the presence of micropores is essential for adsorption, and the absence of micropores can seriously hamper the adsorption capabilities of an activated carbon adsorbent.

Table 4.1. Physical characterization of virgin and regenerated BAC samples.

Adsorbent	Micropore Volume (cm^3/g)	Total pore Volume (cm^3/g)	BET surface area (m^2/g)
G-70R_Virgin	0.50	0.58	1331
G-70R_10%	0.37	0.48	961
G-70R_28%	0.04	0.17	118
B101412_Virgin	0.49	1.1	1640
B101412_11%	0.35	0.93	1240
B101412_24%	0.21	0.57	700
B100772_Virgin	0.43	0.72	1400
B100772_10%	0.33	0.47	1229
B100772_19%	0.12	0.28	405
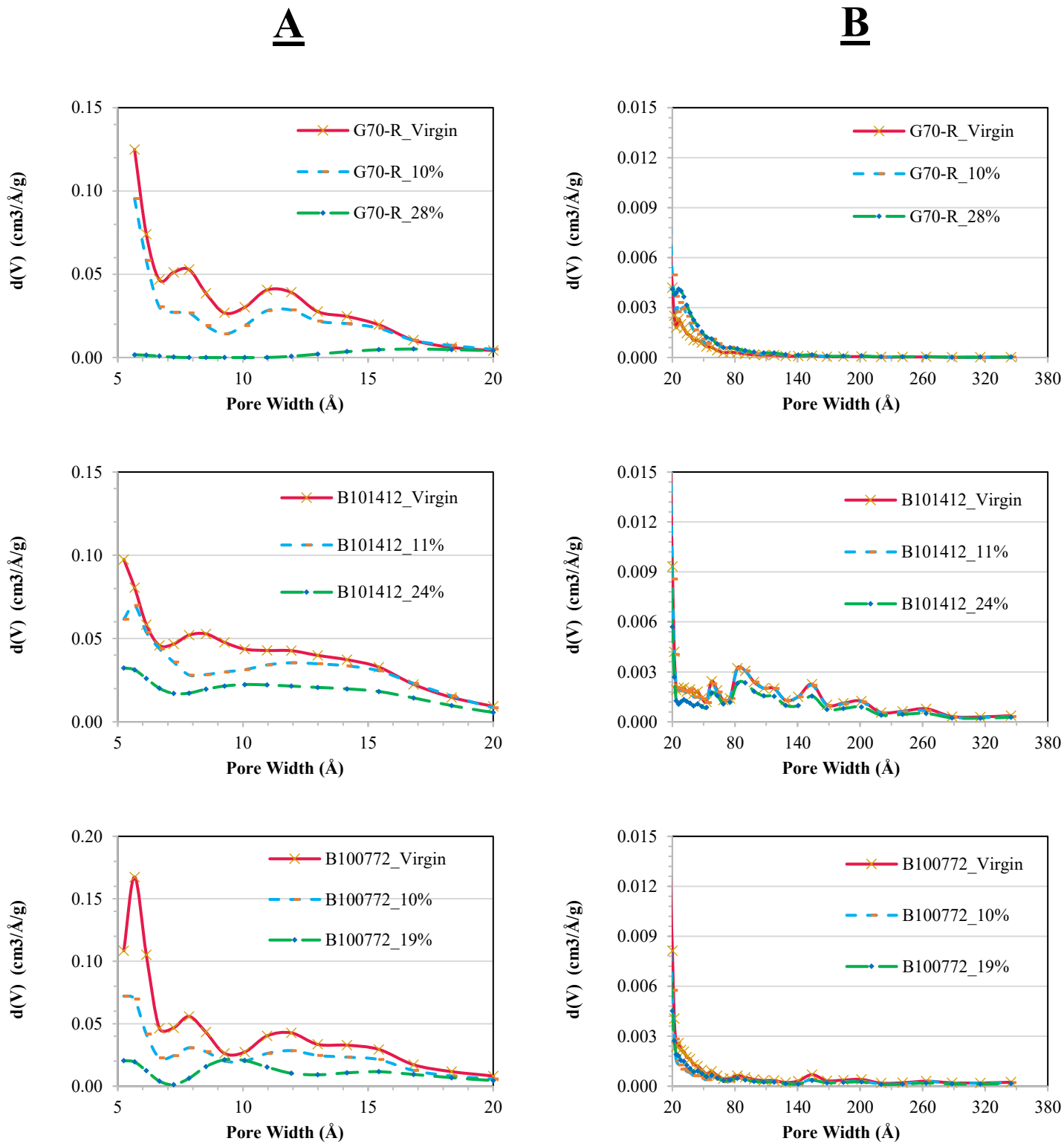
Figure 4.3. PSD analysis of BACs: (A) micropore (≤20 Å) and (B) mesopore (20–500 Å) regions.

4.1.5 Thermogravimetric analysis

TGA and DTG analysis can be valuable tools in understanding the nature of the heel formed. The heel formation mechanism is influenced by various factors such as characteristics of the adsorbate (boiling point, kinetic diameter, and molecular structure) [3], operating conditions (e.g., purge gas flowrate, and regeneration temperature)[6–8], and physical properties of the adsorbent as well [1]. The physisorbed part of the heel usually comprises adsorbates that cannot be completely removed due to their high boiling point and large molecular size [9]. Eventually, given enough time, these none-desorbed adsorbates might be converted into heavier species through thermal oxidation in presence of oxygen. In the end, it has been reported that if the compound undergoes many cyclic reactions, heel species can be converted into char[5]. In **Figure 4.4.** DTG results for the virgin and regenerated samples of the final cycle of each experiment can be observed. For all cases, a first peak is seen below 100 °C, due to desorption of adsorbed moisture[10]. Beyond 100 °C to around 300°C, a flat region is observed where no desorption occurs; species that could have been desorbed in this range has already done so during the last regeneration cycle.

In almost all cases, a peak appears at 400°C, though it is more distinct and apparent in some cases such as the first cycle regenerated samples using 0.5 SLPM dry air. This peak is due to the physisorbed compounds, and thus the existence of the mentioned peak signifies physisorbed heel formation[11].Because all samples were regenerated with dry air there is a much greater chance of chemical reaction occurring with the oxygen molecules present in the purge air. Most of the samples, however, show a third peak at 550°C-600°C. This peak is attributed to chemisorbed species. Next, an additional peak is observed at 650°C which is more apparent for cases where 5 SLPM dry air was utilized. This peak can be attributed to heavy polymeric

species formed through thermal oxidation of non-desorbed organic species[5]. Ultimately, 800°C

is the temperature at which carbon loss would occur, so the tests were limited to this point.
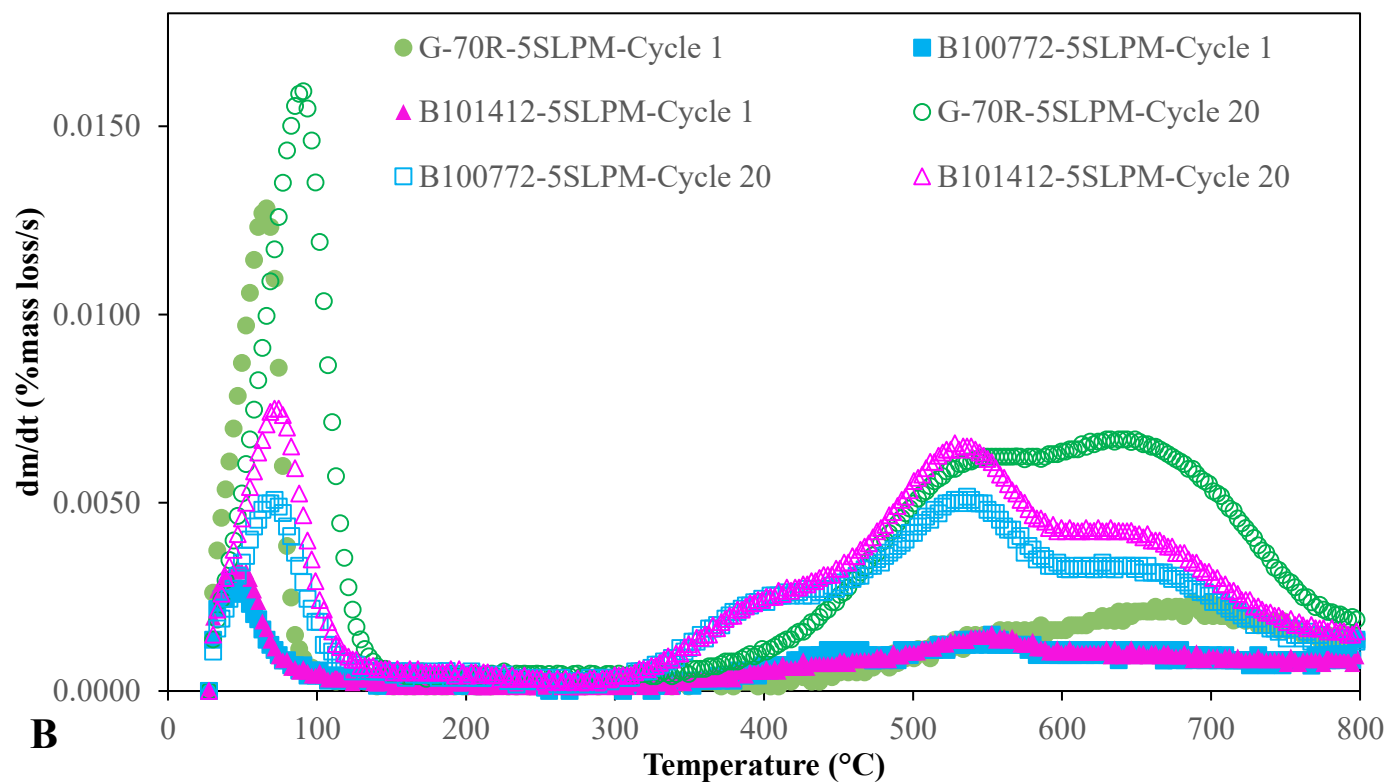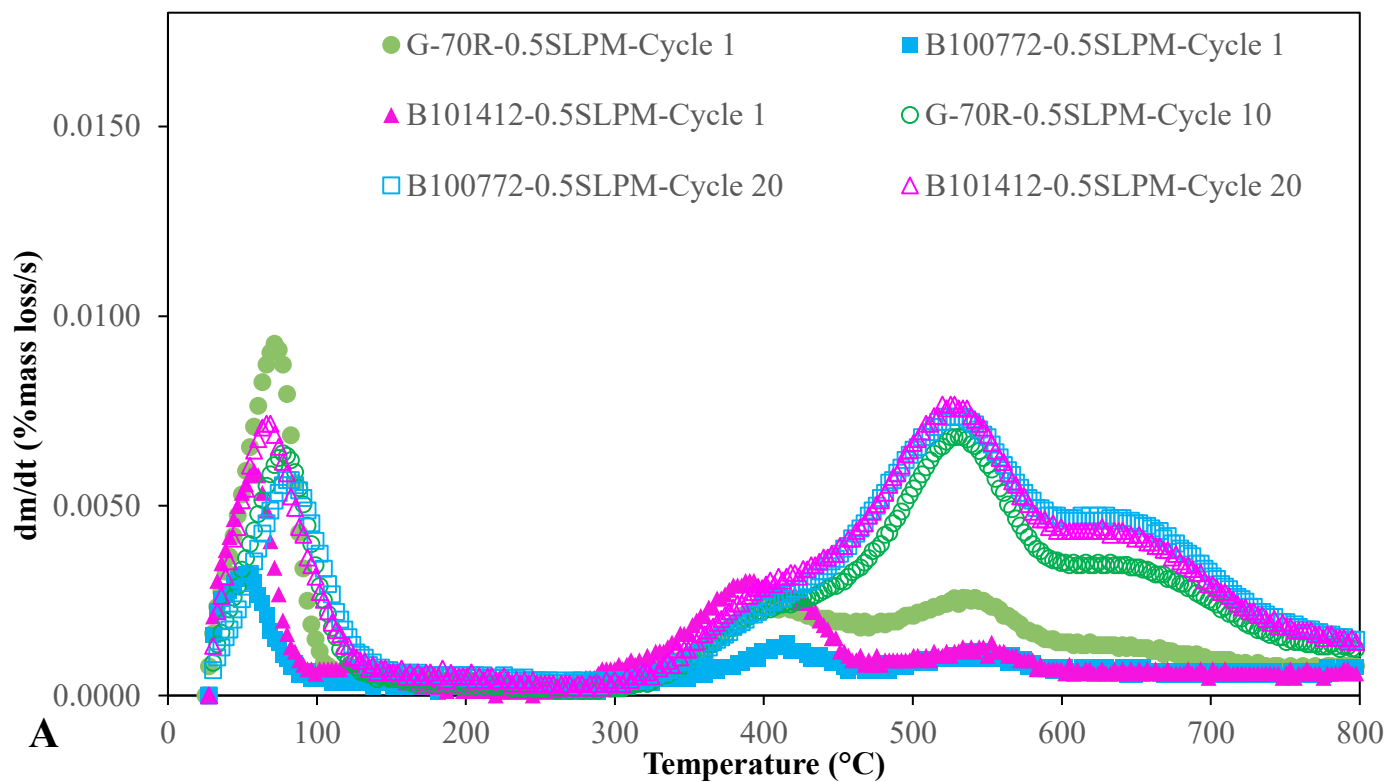
Figure 4.4. DTG analysis of samples regenerated with A) 0.5 SLPM, B) 5 SLPM dried air at the first and final cycle of adsorption/regeneration.

As it can be seen in **Figure 4.4.-A**, for the cases where 0.5 SLPM purge gas flowrate was utilized, in all three adsorbents, two very separate peaks representing physisorbed and chemisorbed species could be detected. However, when these cyclic experiments progressed and reached the final cycle, the peak located in the 550 to 700 °C region which represents the chemisorbed and polymeric species becomes the much more noticeable peak. This result shows that with culmination of the cyclic experiment and continuous contact of the physisorbed species with oxygen at high temperature (288°C), more and more of those weakly attached compounds underwent thermal oxidation, and thus the nature of the heel began to change. This transformation of the heel from physisorbed into chemisorbed can be much better examined in **Figure 4.5** where the DTG of G-70R is shown at three stages during its cyclic adsorption/regeneration. In this case, at almost the midway point (cycle 6), there are still two separate visible peaks at 400°C at 550°C; however, at the 10th cycle the height of the peak at 550°C almost experienced no change while the peak previously observed at 400°C was reduced markedly. Also an increase is seen at around 600°C-650°C. It can be concluded that for each case that 0.5SLPM purge gas was used, a gradual change was in progress in which physiosorbed slowly transforms into more strongly attached chemiosorbed heel. Thus, at early cycles, heel is much more easily removed since it is mostly physiosorbed; however; the removal of heel gradually becomes more and more difficult as nature of the heel changes[5].
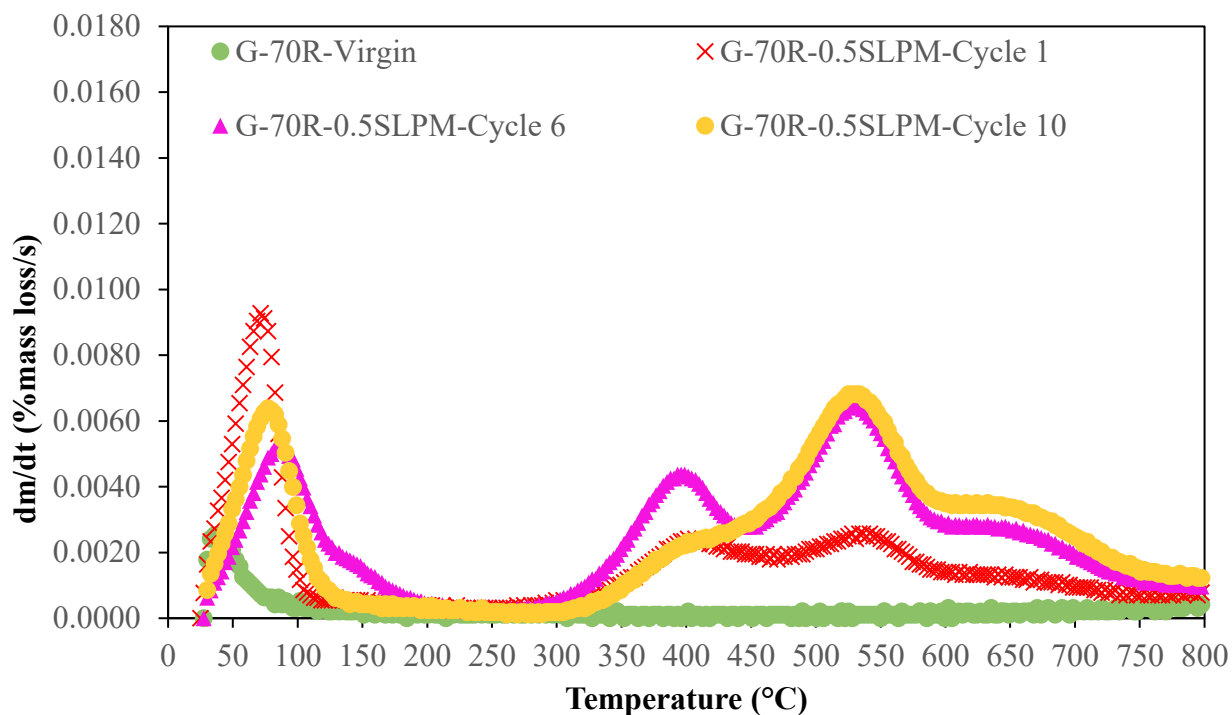
Figure 4.5. DTG of G-70 R sample at various stages of the ten cycle adsorption/regeneration when 0.5 SLPM purge gas was used.

Interestingly, as can be seen in **Figure 4.4.-B** in samples where 5 SLPM purge gas was utilized, regardless of the adsorbent type, the DTG shows a much larger and more apparent chemisorbed peak at the 500-600°C region, and this trend continues into the final cycle with a peak over the 500-600°C region. Higher purge gas flow reduced heel build-up for all the adsorbents, but the heel's nature was also transformed into heavier compounds requiring more energy to desorb. This could arguably be the result of more oxygen being introduced into the adsorbent with higher flowrates. The increased oxygen presence could intensify chemical reactions between adsorbed species and oxygen, resulting in heavier compounds.

Finally, taking different adsorbents into account, it appears that at the first cycle regenerated with 0.5 SLPM dry air, B101412 has a greater portion of physisorbed compounds than the other two adsorbents. This may be related to the difference in microporosity (86%, 60%, and 44% for G-70R, B100772, and B101412, respectively) and the larger pores available for B101412 with an

average micropore pore width of 9.0 Å. The narrower slit-shaped pores in G-70R and B100772, with an average micropore pore width of 7.8 and 8.0 Å respectively, are much more likely to trap the products of the reactions with oxygen, resulting in a heel that requires more energy to be removed. These findings are in agreement with a previous study by Feizbakhshan et al [1] who reported higher weight loss at (350-400 °C) for B-100777, a mesoporous AC, and at 500-550 °C for G-70R, which are used in this study. Other than this specific case for all other samples, the differences among adsorbents seem to be negligible. Considering this, it can be concluded that the purge gas flowrate is more determinant in the nature of the heel formed than the physical property of the adsorbent used.

4.1.6 XPS analysis

The XPS analysis was conducted to determine the virgin and regenerated surface atomic composition of the BACs. The primary purpose of this analysis was to investigate whether the change in the surface elemental composition of adsorbents is similar after a long-term cyclic experiment or significant changes can occur based on their microporosity and surface physical properties. The results of the XPS analysis are shown in **Table 4.2**.

Table 4.2. The surface atomic composition of virgin and used activated carbon.

Adsorbent	Carbon (%)	Oxygen (%)	Sulfur (%)
B101412_Virgin	92.81	6.45	0.74
B100772_Virgin	92.03	7.22	0.74
G-70R_Virgin	93.41	6.59	Negligible
B101412_20th cycle_5SLPM	82.05	17.83	0.12
B100772_20th cycle_5SLPM	86.29	13.45	0.26
G-70R_20th cycle_5SLPM	85.77	14.23	Negligible

As seen in **Table 4.2**, all three adsorbents had very similar surface elemental composition at the start of the experiment, with a dominant presence of carbon and then oxygen. However, after the cyclic experiments, a sharp increase in oxygen accompanied by a decrease in carbon can be seen for all samples. This increase of oxygen on the surface of samples indicates that a significant part of the heel formed was due to thermal oxidation of adsorbate. Additionally, B101412, having the highest total cumulative heel (24% as opposed to 19% and 21% for B100772 and G-70R, respectively), experienced a more prominent presence of oxygen atoms on the surface subsequent to cyclic regeneration.

4.2 Modeling Results

In the following section results of the two Machine learning methods chosen in chapter 3 are brought. Subsequently a comparison is made on the accuracy of each method to arrive at the best method suited for our objective which is prediction of the micropore volume reduction. Firstly

regression tree method was utilized and its result are shown and then compared with the multivariable linear regression method. Important to mention that prior to the utilization of the Machine learning method, some initial methods were utilized to predict changes occurring in the pore volume of the adsorbent. The most significant of these methods was one in which the total pore volume of the adsorbent was reduced equal to the volume of the cumulative heel existing on it. Next this pore volume reduction was considered to be uniform across all pores regardless of their pore width. Needless to say, due the simplistic assumptions existing in this method, large relative error was observed in the predictions. The two main problem with this method were 1) assuming volume reduction is uniform across all pores and 2) the size of the adsorbate had no impact. Both of these issues were rectified in the Machine Learning method.

4.2.1 Comparison of Decision tree and MLR Model in Predicting AC Micropore Volume

For the decision tree prediction model, there is a need to choose a criterion based on which the split value is optimized. Since we are working with numeric data, the criterion chosen was the least square. With this criterion, an attribute is selected for splitting, which minimizes the squared distance between the average values in the nodes regarding true value[12]. A summary of the least square decision tree parameters can be seen in **Table 4.3**.

Table 4.3. Design parameters for the regressive decisions tree predictive model.

Decision tree Parameters	
Criterion	Least Square
Maximum Depth	10
Minimal Gain	0.01
Minimal leaf size	2

The decision tree was designed to have a maximum depth of 10. Based on the size and characteristics of the example set, various depth values were attempted for the decision tree model, and the scores were compared. A maximum depth of 10 was decided upon since it showed the minimum error value while avoiding overfitting of the data. Other parameters were selected on a similar trial and error basis to produce the most suitable model possible for the selected dataset. A small section of the decision tree model (as deep as 5th depth) closer to the root of the tree can be observed in **Figure 4.6**. A complete graph of the decision tree is brought in the appendix.
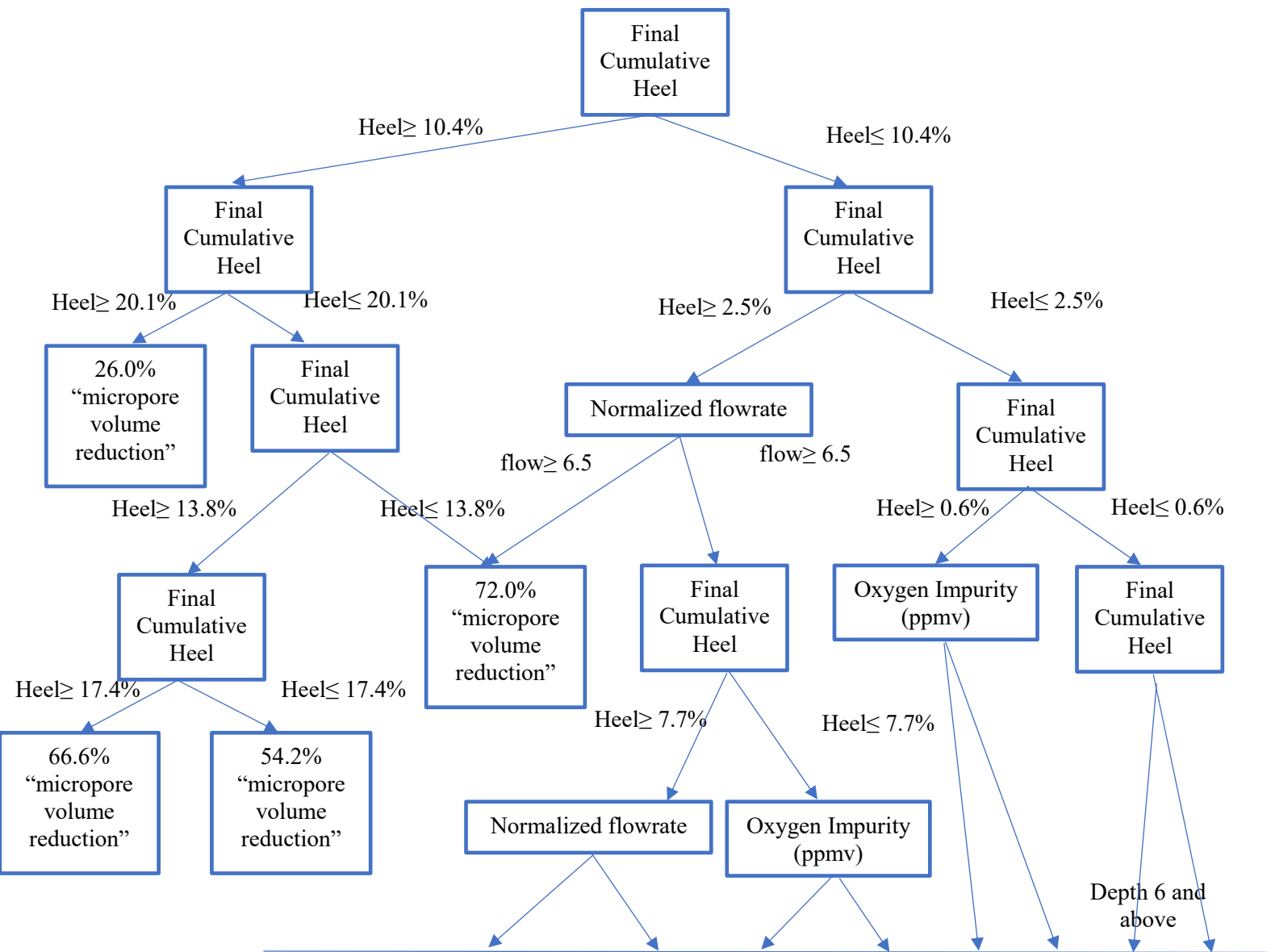
Figure 4.6. Plot of the regression tree devoted for micropore reduction prediction shown as deep as 5 layers.

96

As explained in the methodology section in chapter 3, a forward selection technique was conducted on the data set prior to model application. The forward selection model reduced the influential features from the initial 16 to only 4: final cumulative heel, normalized flowrate, oxygen impurity, and electronic polarization of the test adsorbate.

One important observation that can be made from even the small section of the regression tree (Figure 4.6) is the fact that the most repeated node is the final cumulative heel. This means that the most influential feature in determining how much micropores are reduced is the amount of heel accumulated during cycling adsorption/regeneration experiments. This conclusion is in line with previous studies that demonstrated micropores are highly affected by heel formation[2,13].

A 5-fold cross-validation technique was utilized to test the model's generalizability and performance. R^2, MAE, and RMSE values were selected to evaluate the performance of the model. **Figure 4.7** shows the final predictions of the regression tree for micropore volume reduction versus the actual micropore volume reductions obtained via surface analysis. The micropore volume reduction targeted for prediction by the ML algorithm is expressed as:

$$\frac{\textit{micropore volume available after cyclic adsorption/regenration}}{\textit{micorpore volume availabe for virgin sample}} \times 100 \qquad 4\text{-}1$$

Many samples in the dataset had a large reduction in micropore volume, as observed in **Figure 4.7**, with the accumulation of points on the top right corner. This accumulation creates the false impression of a relatively good R^2 at first glance. However, high deviation from the trendline at lower points reduces the average R^2 of the model drastically. It can be reported that the model has a R^2 of 0.76 ± 0.12 with a micro average of 0.58.
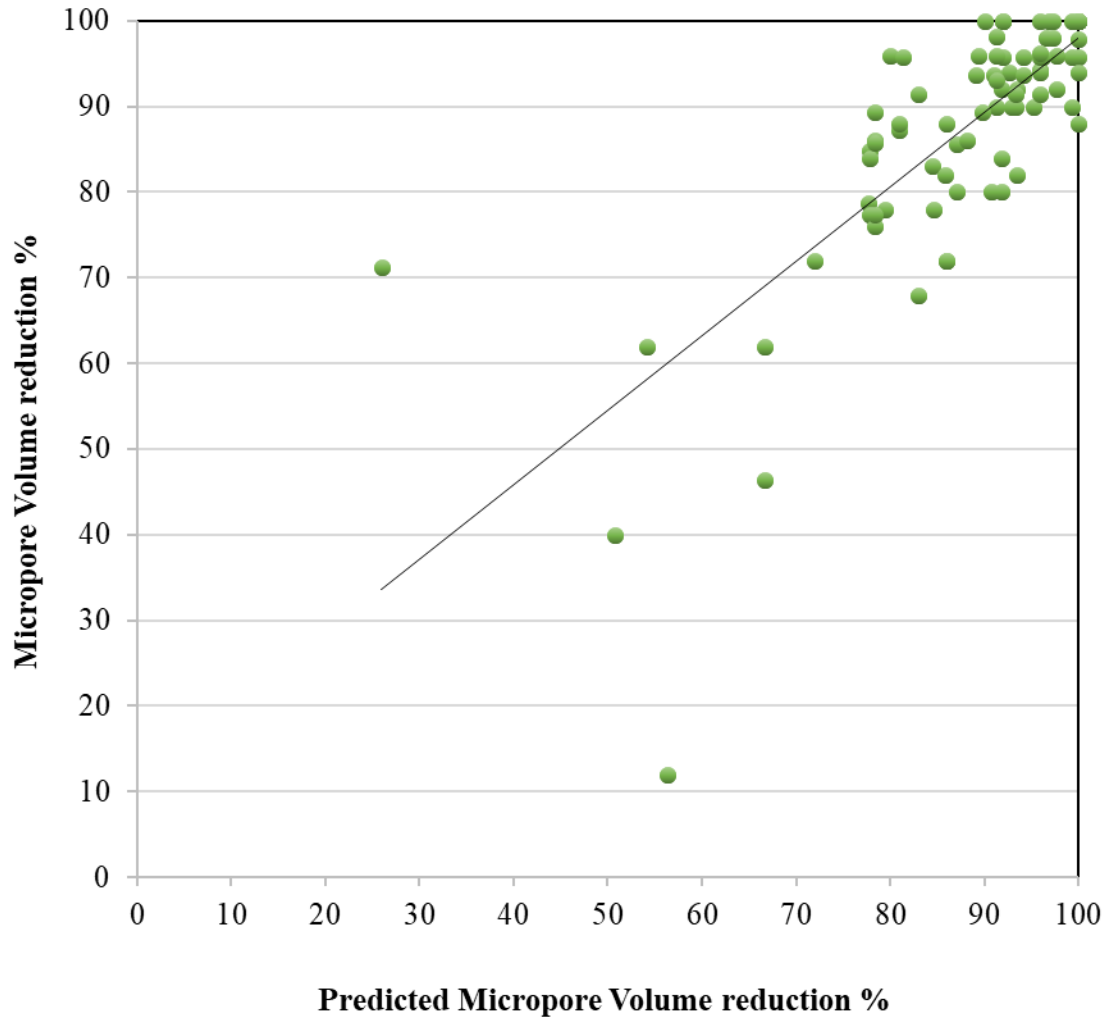
Figure 4.7. The regression tree predicted values of micropore reduction (micropore final/micropore initial %) vs. the experimentally obtained values.

The regression tree model also had an RMSE of 8.84 ± 2.86 and an MAE of 5.40 ± 0.95. The high deviation of predictions from actual values makes this model an unreliable predictive method for this dataset.

The multivariable linear regression model (MLR) was developed in conjunction with the same forward selection and cross-validation techniques as the previous decision tree model. However, the forward selection had a much larger impact on the outcome of the MLR model and managed to reduce the contributing features from 15 to only 2, final cumulative heel and molar volume of the adsorbate. The linear regression model suggested for micropore volume prediction is as follows:

$$\frac{micropore\ volume\ available\ after\ cyclic\ adsorption/regenration}{micorpore\ volume\ availabe\ for\ virgin\ sample} \times 100 =$$

$$-13.265 \times Final\ Cumulative\ Heel\ (wt\%) - 1.016 \times molar\ volume\ \left(\frac{m^3}{kmol}\right) + 88.210$$

4-2

The above equation puts a high focus on the final cumulative heel accumulated on the adsorbent as a cause of micropore volume reduction which is in agreement with both previous studies and the regressive tree model's results [2,13]. However, an interesting fact is the role of the adsorbate's molar volume, which was absent in the regressive tree model. As expressed in previous studies, the molar volume and the kinetic diameter of the adsorbate can appreciably impact the adsorption capacity of an adsorbent and thus the micropore volume reduction[14,15]. Larger adsorbate molecules cannot enter the narrow micropores. As a result, instead of filling the narrow micropores from within, they will immediately block off the entrance to the pore and remove that pore's volume from the total available micropore volumes. With this explanation in mind, the negative coefficient for molar volume is acceptable and demonstrates that larger adsorbate volumes will result in a more considerable loss of available micropores volume.

The comparison of the predicted micropore volume reductions versus the experimentally obtained values can be observed in **Figure 4.8**.
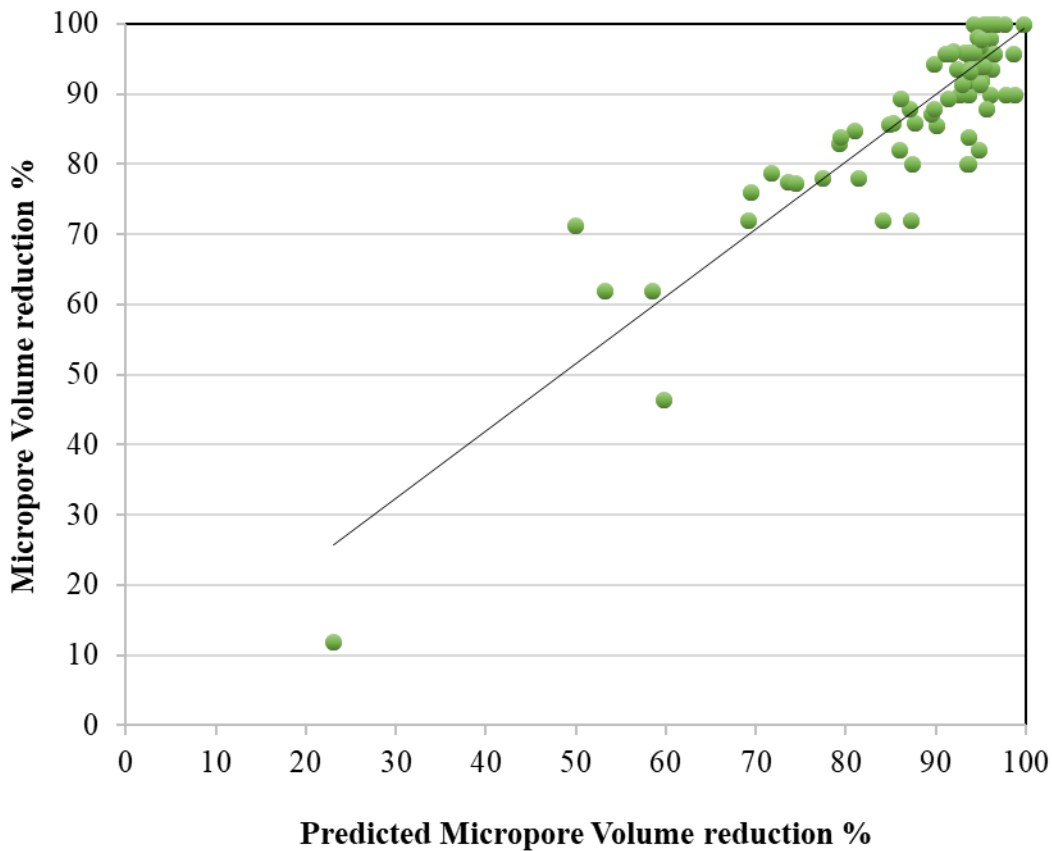
Figure 4.8. The MLR predicted values of micropore reduction (micropore final/micropore initial %) vs. the experimentally obtained values.

The first noticeable change in **Figure 4.8** compared to **Figure 4.7** is a much tighter spread of the points around the trendline, which notably improves the prediction capability. Obtaining the performance values further proves the overall better performance of the MLR model compared to the regressive tree model. The MLR model had an R^2= 0.85 ± 0.08 with a micro average of 0.84, an RMSE of 5.64± 1.19, and an MAE of 4.27 ± 0.77. Based on these performance criteria, the MLR model appeared to be a reliable model for micropore volume prediction and was thus chosen as the primary model for future applications.

4.2.2. PSD modeling

The MLR prediction model chosen was incorporated into the previously developed mathematical model (**equation 4-1).** This newly improved model is capable of predicting the pore size distribution of activated carbon adsorbents after cycles of adsorption/regeneration. To test the model, three activated carbons with various physical properties were chosen. Each of these activated carbons had undergone a long-term cyclic adsorption/regeneration explained in detail in the previous section. For each activated carbon, three samples containing a wide range of heel build-ups were chosen. These nine samples were collected from several long-term adsorption/regeneration experiments. All operating conditions of these experiments were the same except for the flow rate of the purge gas used during desorption which was either 0.5 or 5 SLPM of dried air. The change in desorption flow rate was used to produce wide ranges of heel build-up. A summary of these operating conditions can be observed in **Table 4.4**. The heel-build ups were carefully selected to represent three ranges of low heel, medium heel, and high heel build-up. The model was used to predict each sample's pore size distribution, and the results are presented below. In addition, the result of the pore size distribution prediction is subsequently used in the DRL equation to obtain the adsorption capacity of the adsorbent at the specific experimental concentration of 100 ppm 1,2,4- TMB.

Table 4.4. Operating conditions of the long-term cyclic adsorption/regeneration experiments previously conducted on all three BAC adsorbents.

Adsorption	Regeneration
Injection port Temperature: 40 °C	Bed Temperature: 288 °C
Flow: 10 SLPM	Flow: 0.5/5 SLPM
Flow Gas: Air	Flow Gas: Air
Injection: 100 ppm of 1,2,4-TMB	Duration: 180 min

G-70R

G-70 R, is a highly microporous activated carbon adsorbent (86% microporosity), as demonstrated previously. During the long-term cyclic adsorption/regeneration experiments, nine total samples at various stages of cumulative heel development were collected as demonstrated in **Figure 4.9** out of these nine samples; three were chosen, for further study and model comparison, representing low, medium, and high heel build-up, distinguished in **Figure 4.9** by green triangles. These samples had 6.0%, 11.5%, and 18.9 % mass balance cumulative heel build-up, in that order. More information regarding the samples, such as the desorption purge gas flowrate and the cycle number from which they were collected, can be found in **Table 4.5.**
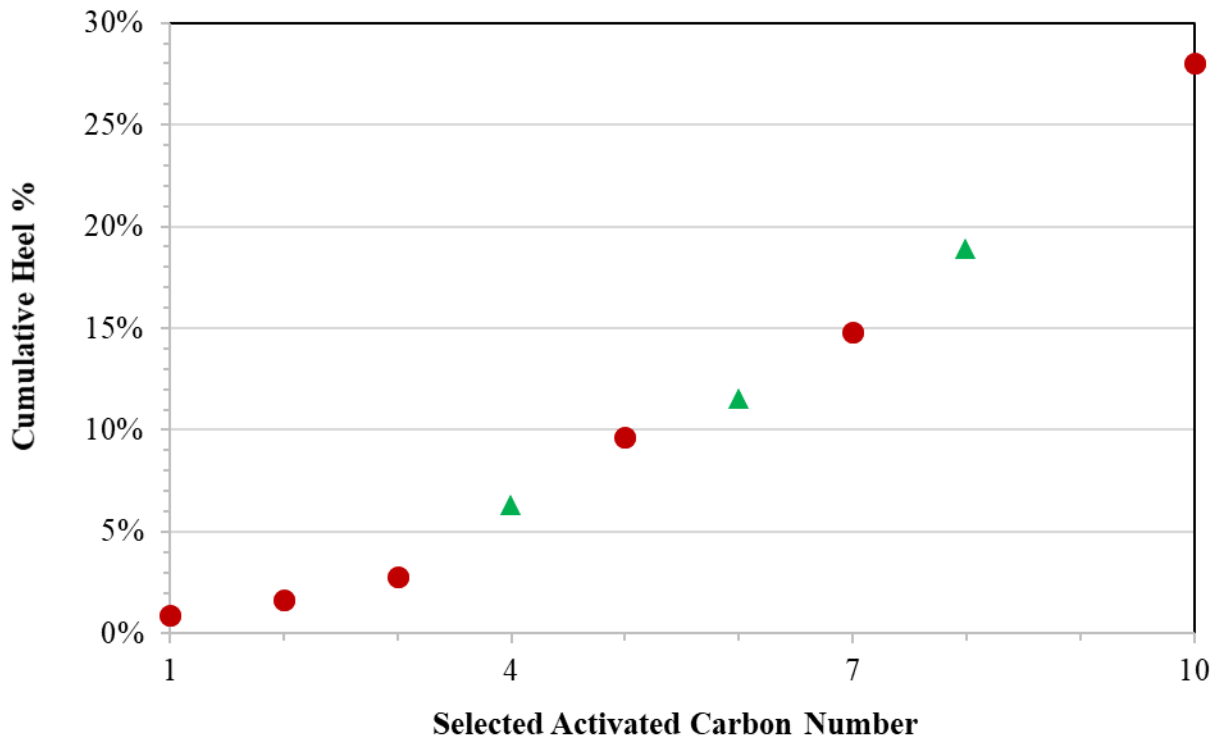
Figure 4.9. Samples collected from long-term cyclic adsorption/regeneration experiments on G-70R and their corresponding heel-buildup. Green triangles distinguish samples chosen for model comparison.

Table 4.5. G-70R Collected samples' information

Sample Tag	Desorption Flow (SLPM)	Cycle Number	Cumulative Heel (wt.%)
A	5	3	6.3
B	5	4	11.5
C	0.5	4	18.9
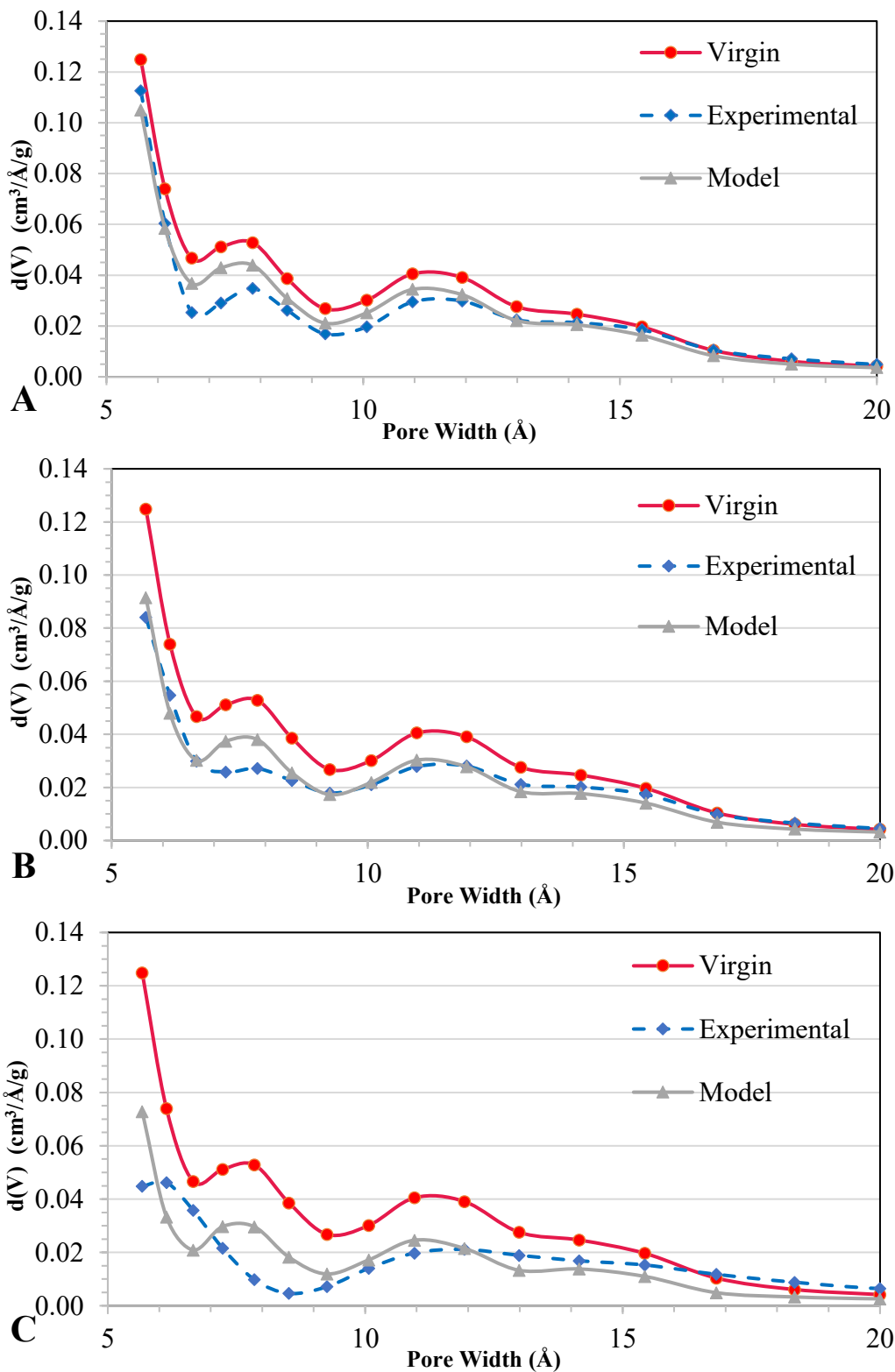
Figure 4.10. PSD of virgin, experimental, and model predicted for G-70R. Sample A, B, and C.

Table 4.6. Experimental measurement and model prediction of micropore volume, volume of pores below 32Å, and adsorption capacity for G-70R samples

Physical properties				
Sample A	**Micropore volume (cm³/g)**	**V32 (cm³/g)**	**Adsorption Capacity (wt.%)**	**Cumulative heel (wt.%)**
Experimental	0.32	0.35	36.4	
Model	0.34	0.37	35.2	
				6.3
Absolute relative error %	7.5	5.14	3.32	

Physical properties				
Sample B	**Micropore volume (cm³/g)**	**V32 (cm³/g)**	**Adsorption Capacity (wt.%)**	**Cumulative heel (wt.%)**
Experimental	0.29	0.32	33.0	
Model	0.29	0.31	30.9	
				11.5
Absolute relative error %	0.80	1.70	6.21	

Physical properties				
Sample C	**Micropore volume (cm³/g)**	**V32 (cm³/g)**	**Adsorption Capacity (wt.%)**	**Cumulative heel (wt.%)**
Experimental	0.23	0.26	26.2	
Model	0.22	0.24	25.00	
				18.9
Absolute relative error %	3.11	7.69	4.76	

Most of the data available in our dataset for the MLR model was collected from cyclic adsorption/regeneration experiments conducted on G-70R adsorbent. Since micropore prediction directly results from the MLR model, it was expected to see micropore volume reduction predictions with great accuracy for the G-70R sample. The results from **Table 4.6** proved our assumption with a Mean Relative Absolute Error (MRAE) of 3.5% and a Mean Absolute Error (MAE) of only $0.01 \frac{cm^3}{g}$ for G-70R micropore volume prediction. The first sample which was in the low heel build-up range showed to most error for micropore volume prediction with an Absolute Relative Error (ARE) of 7.5 %. This is in agreement with the MLR model results as observed in **Figure 4.8**, where the biggest dispersion of values around the trendline was observed for low micropore volume reductions (low heel build-up region). Furthermore, V32 had been defined as the volume of pores below 32 Å plus a constant value of 0.055616; hence the same error values as micropore volume for V32 predictions were expected. The final results prove this point and a MRAE of 5.5% and an MAE of $0.02 \frac{cm^3}{g}$ for V32 prediction was observed. Taking into account the PSD predictions, it appears that the model predicted PSD closely follows the trend of the experimental PSD. However, narrower micropore regions show some deviation, best seen in Figure 4.10-**B** at around the 7 Å and below. In this area, the model overpredicts the available volume when it has actually been reduced much more due to the heel build-up. This inaccuracy can be the result of pore blockage. The adsorbate used, 1,2,4- TMB, has a kinetic diameter of around 6.8 Å[14], as a result, it can easily block the entrance to these narrow micropores and remove a large section of the mentioned narrow micropores from the total micropore volume even with a low amount of accumulated heel. The model is incapable of predicting this occurrence which results in over-prediction. MAE and MRAE were calculated for the result of the adsorption capacity prediction at 100 ppm concentration of the adsorbate to help us better evaluate the new

DRL model's performance in capacity prediction. The model had an MAE of 1.50 wt.% and a MRAE of 4.8 %.

Blucher 100772

Blucher 100772 is the second adsorbent chosen for experiments. This adsorbent has lower total micropore volume and microporosity than G-70R (0.43 $\frac{cm^3}{g}$ and 60%, respectively), as demonstrated in the previous section. During the long-term cyclic adsorption/regeneration experiments, six total samples at various stages of cumulative heel development were collected, as demonstrated in **Figure 4.11**, out of which three were chosen for further study, same as G-70R. These three samples had 4.4%, 10.1%, and 14.7% mass balance cumulative heel build-up. The same procedure of surface analysis and comparison of experimental results to the model predicted values was conducted on these three samples. Table 4.7 displays more information about these samples. Important to note that samples with high cumulative heel build-up, such as 19%, were not chosen since in industrial usage, when the BAC reaches these values of heel build-up, it has lost most of its adsorption capabilities and is thus of no practical usage, and since our model was developed with the goal of industrial adsorption in mind, these samples were excluded.
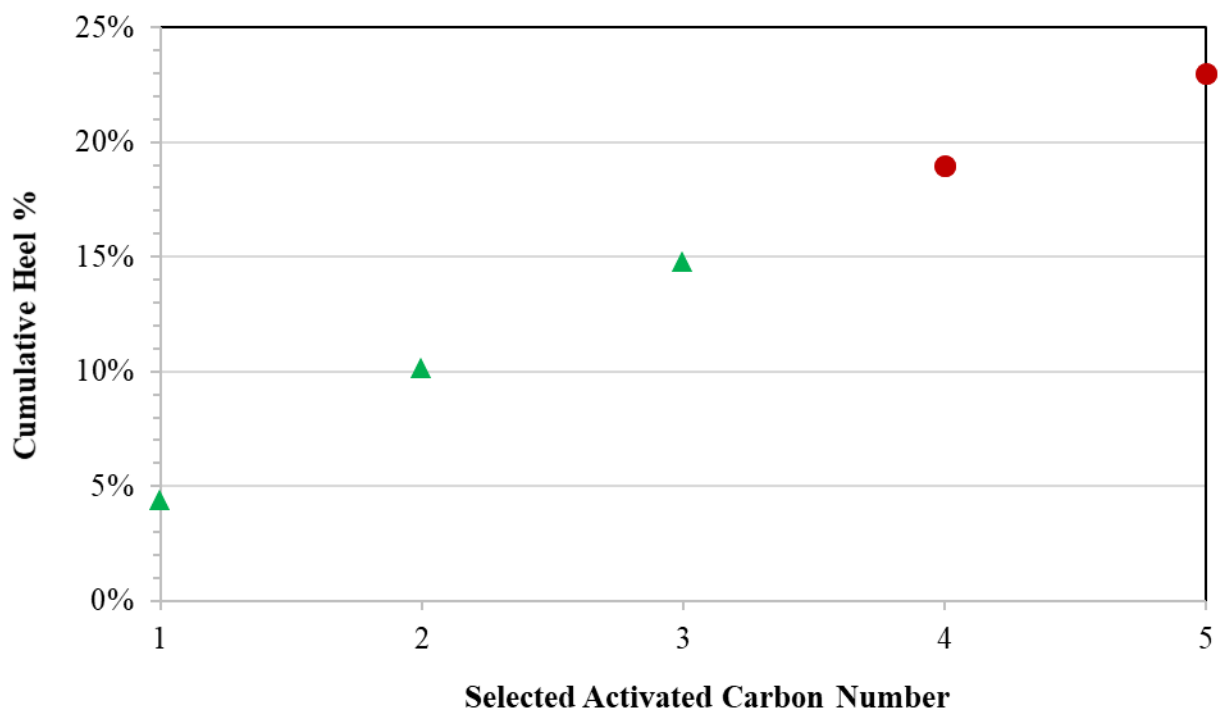
Figure 4.11. Samples collected from long-term cyclic adsorption/regeneration experiments on B100772 and their corresponding heel-buildup. Green triangles distinguish samples chosen for model comparison.

Table 4.7. B100772 Collected samples' information

Sample Tag	Desorption Flow (SLPM)	Cycle Number	Cumulative Heel (wt.%)
A	0.5	1	4.4
B	5	4	10.1
C	0.5	3	14.7
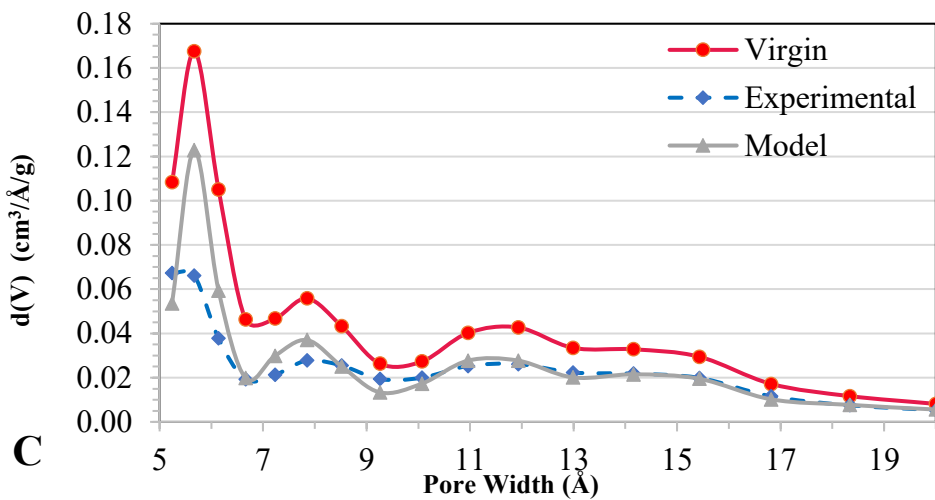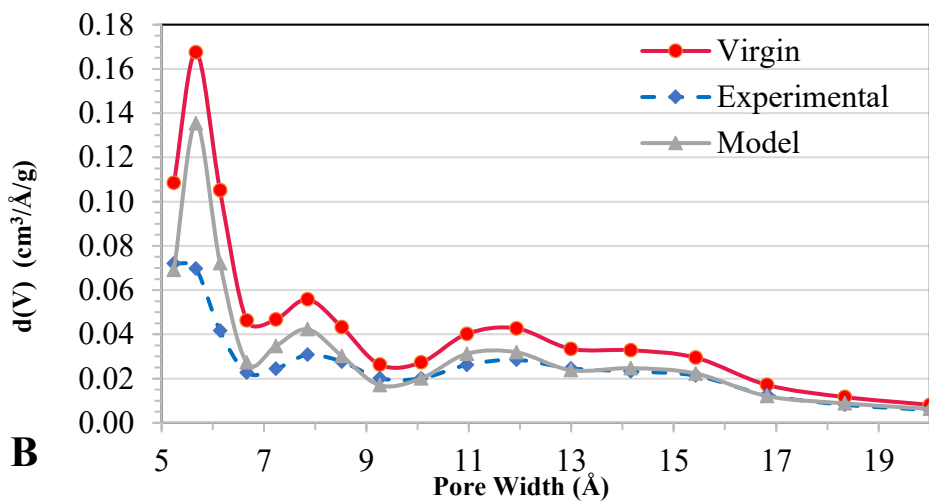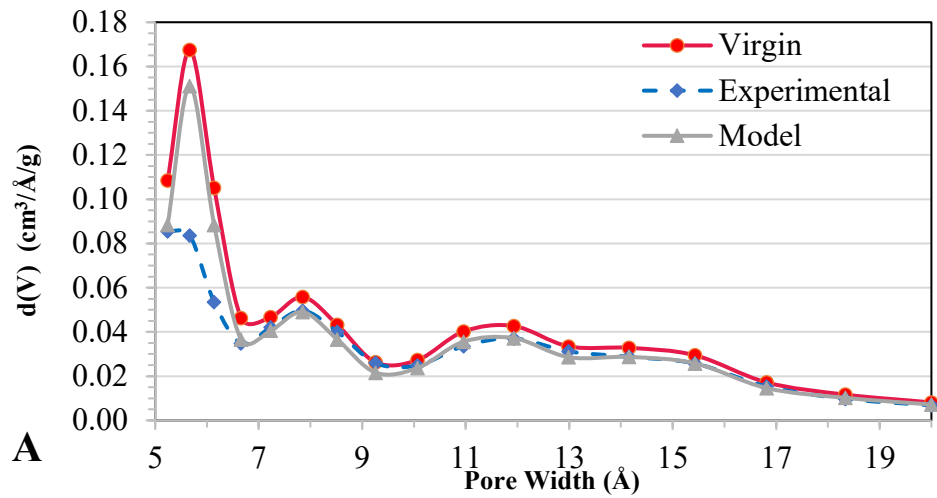
Figure 4.12. PSD of virgin, experimental, and model predicted for B100772. Sample A, B, C.

Table 4.8. Experimental measurement and model prediction of micropore volume, volume of

pores below 32Å, and adsorption capacity for B100772 samples

Physical properties				
Sample A	**Micropore volume (cm³/g)**	**V32 (cm³/g)**	**Adsorption Capacity (wt.%)**	**Cumulative heel (wt.%)**
Experimental	0.44	0.47	45.1	
Model	0.48	0.51	47.4	
				4.4
Absolute relative error %	9.1	10.05	5.03	

Physical properties				
Sample B	**Micropore volume (cm³/g)**	**V32 (cm³/g)**	**Adsorption Capacity (wt.%)**	**Cumulative heel (wt.%)**
Experimental	0.37	0.39	43.2	
Model	0.41	0.44	41.1	
				10.1
Absolute relative error %	10.81	12.16	4.62	

Physical properties				
Sample C	**Micropore volume (cm³/g)**	**V32 (cm³/g)**	**Adsorption Capacity (wt.%)**	**Cumulative heel (wt.%)**
Experimental	0.31	0.33	38.1	
Model	0.36	0.38	36.7	
				14.7
Absolute relative error %	14.41	16.57	3.52	

Blucher 101412

Blucher 101412 is the final adsorbent chosen for experiments. This adsorbent is highly mesoporous and has the lowest microporosity (44%) between all three BAC adsorbents chosen for this study. However, it has almost the same total micropore volume as G-70R (0.50 $\frac{cm^3}{g}$). Ten samples were gathered during the long-term cyclic adsorption/regeneration experiments, and three were selected for model validation. These three samples had 10.6%, 15.7%, and 24.4% mass balance cumulative heel build-up, respectively. Table 4.9 displays more information about the three chosen samples. As mentioned above, B101412 is highly mesoporous while having the same micropores volume as G-70R. As a result, B101412 has a much higher adsorption capacity and thus heel build-up accumulation. This high adsorption capacity is why samples gathered here had notably more heel build-up accumulated than previous BACs.
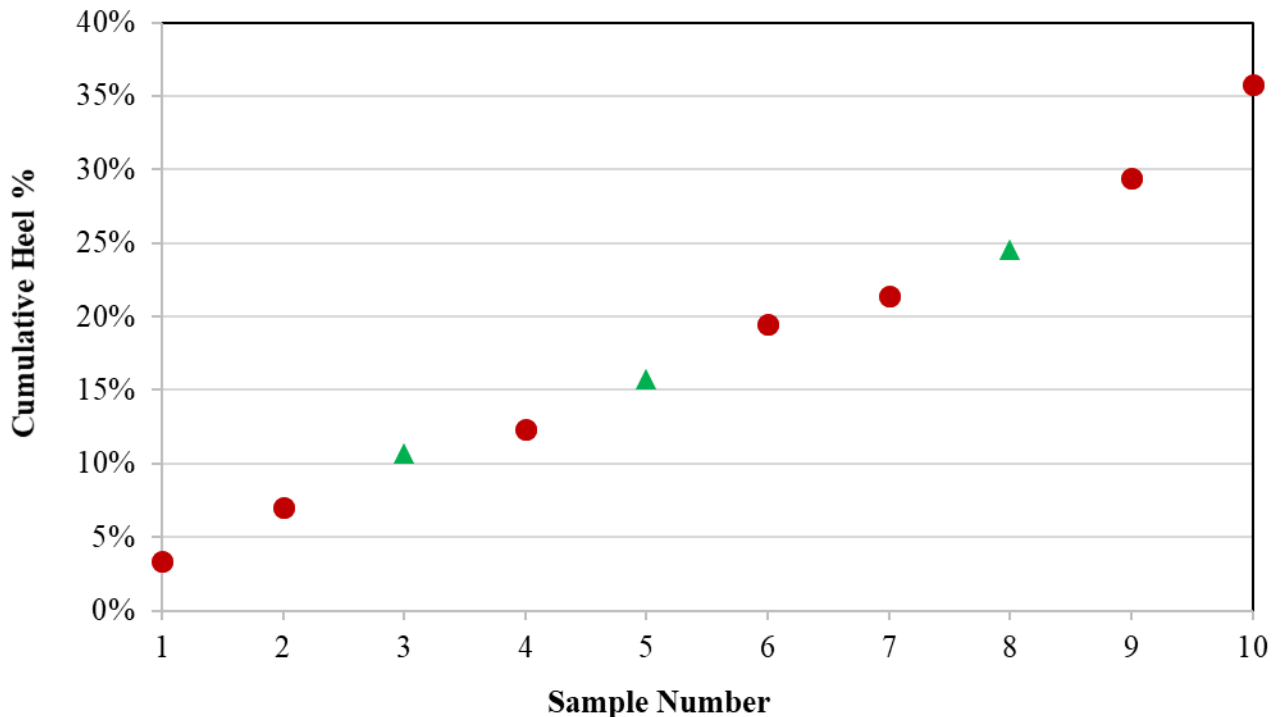
Figure 4.13. Samples collected from long-term cyclic adsorption/regeneration experiments on B101412 and their corresponding heel-buildup. Green triangles distinguish samples chosen for model comparison.

111

Table 4.9. B101412 Collected samples' information.

Sample Number	Desorption Flow (SLPM)	Cycle Number	Cumulative Heel (wt.%)
A	5	4	10.6
B	0.5	3	15.7
C	5	19	24.4
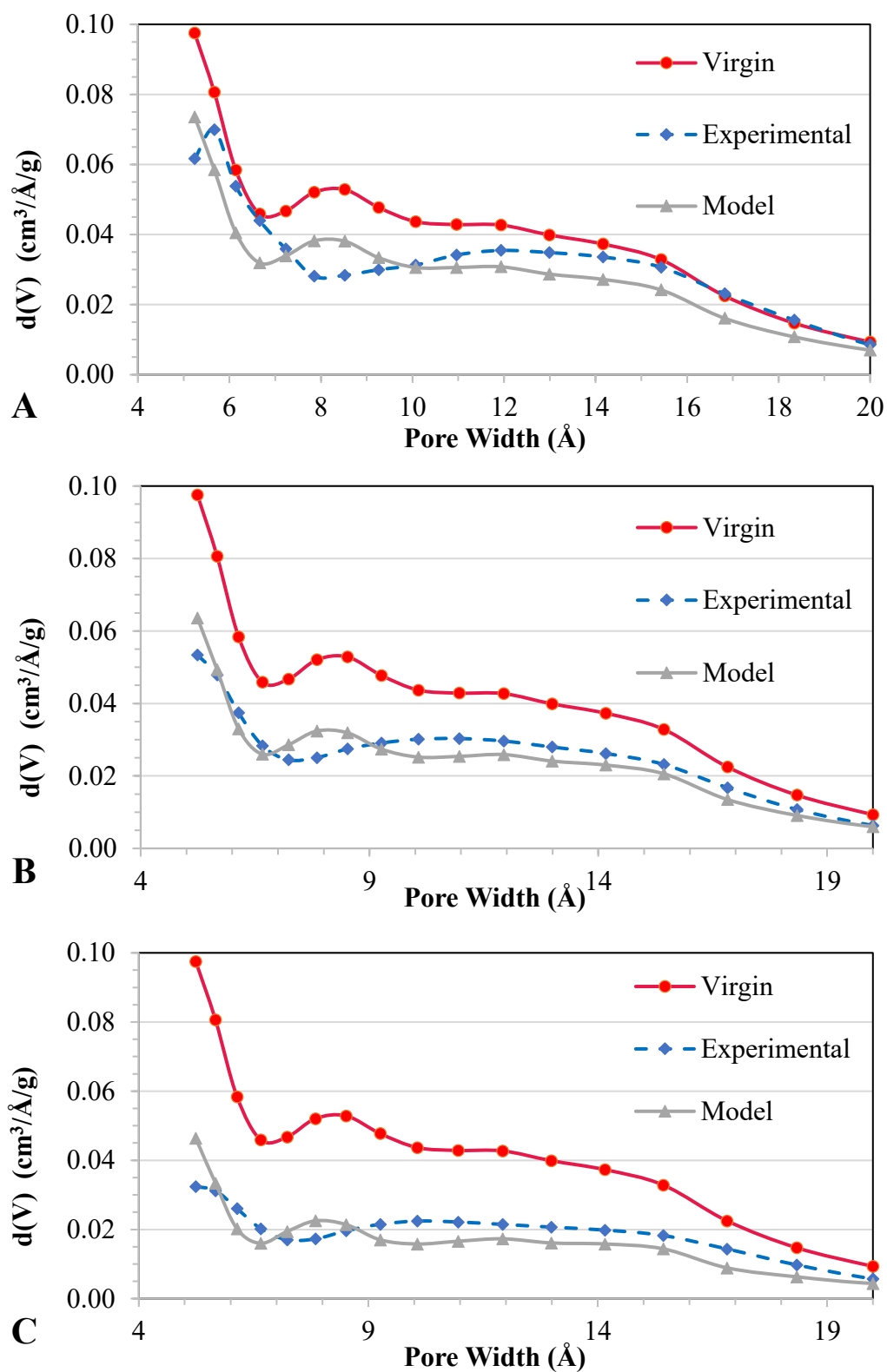
Figure 4.14. PSD of virgin, experimental, and model predicted for B101412. Sample A, B, C.

Table 4.10. Experimental measurement and model prediction of micropore volume, volume of pores below 32Å, and adsorption capacity for B101412 samples

Sample A	Physical properties			
	Micropore volume (cm³/g)	V32 (cm³/g)	Adsorption Capacity (wt.%)	Cumulative heel (wt.%)
Experimental	0.48	0.51	50.1	
Model	0.43	0.46	43.1	
				10.6
Absolute relative error %	9.42	8.97	13.98	

Sample B	Physical properties			
	Micropore volume (cm³/g)	V32 (cm³/g)	Adsorption Capacity (wt.%)	Cumulative heel (wt.%)
Experimental	0.39	0.41	45.1	
Model	0.36	0.39	37.2	
				15.7
Absolute relative error %	5.40	3.61	17.46	

Sample C	Physical properties			
	Micropore volume (cm³/g)	V32 (cm³/g)	Adsorption Capacity (wt.%)	Cumulative heel (wt.%)
Experimental	0.28	0.30	34.5	
Model	0.24	0.27	27.2	
				24.4
Absolute relative error %	14.23	10.61	21.25	

Since both Blucher BAC adsorbents, with higher mesoporosity, were not represented equally in the data set used for the MLR learning algorithm and the dataset mostly contained samples with high microporosity, a higher range of error values was expected to be observed across the board for them. The final observation was in line with expectations of the model's capabilities. Model's micropore predictions for Blucher 100772 had a MAE of 0.04 $\frac{cm^3}{g}$ and a MRAE of 12.0%. Interestingly the error values for Blucher 101412 were quite comparable with Blucher 100772 with a MAE of 0.04 $\frac{cm^3}{g}$ and a MRAE of 10.8%. This similarity in micropore prediction capability indicates that the root of the issue is the under-representation of the adsorbent in the learning algorithm and not an inherent problem with the model itself. By adding more data into the data set, the error values for micropore volume prediction could be expected to drop to the levels of G-70R. Additionally, V32 predictions for both adsorbents followed the same trend as micropore predictions, and for Blucher 100772, a MAE of 0.05 $\frac{cm^3}{g}$ and an MRAE of 12.1% was observed, while for the mesoporous Blucher 101412, slightly lower values of 0.033 $\frac{cm^3}{g}$ and 8.2% for MAE and MRAE were obtained, respectively.

Taking a gander at micropore volume predictions for all nine samples, it can be concluded that the least ARE was obtained for the medium heel region in all three adsorbents. This variation in error among heel regions can be due to the occurrence of pore blockage. In low heel build-up regions, since the adsorbate used has a sizeable kinetic diameter (about 6.8 [14]), and the adsorbents utilized have many narrow micropores well below this size, there is a good chance that a sudden blockage of one of these narrow micropores might ensue, reducing the available micropore volume drastically. However, the model can not take this sudden blockage into account and, considering the low mass of the accumulated heel, makes false predictions. As explained before, this is also

why the model predicted PSD plot has the most deviation from the experimentally obtained PSD at narrower micropores. These pore blockages reduce the available micropore volume of the BAC more than the model anticipates based on the mass of the heel accumulated. In conclusion, the medium heel region is where the model works best at making micropore volume predictions. Nevertheless, its answers are still useful for all regions.

The adsorption capacity of Blucher samples at an inlet concentration of 100 ppm 1,2,4-TMB was predicted as well. For Blucher 100772, the adsorption capacity was predicted with a MAE of 1.9 wt.%, and MRAE of 4.4%, whereas for B101412, much higher error values of 7.4 wt.% and 17.6% were observed for MAE and MRAE, respectively. The first thing to note is that the prediction accuracy for G-70R and Blucher 100772 are very similar, with a MARE of 4.7% and 4.4% for G-70R and Blucher 100772, correspondingly. However, they have considerably different error values for V32 predictions (MARE of 5.51 and 12.16 for G-70R and Blucher 100772, respectively). This observation could be explained by how the DLR equation is formulated.

$$W = W_0 \, exp(-kA^2) \qquad 4\text{-}3$$

$$A = RT \, ln(P_0/P) \qquad 4\text{-}4$$

In the equation above, W_0 represents V32 and thus the micropore volume available in the adsorbent, while A, known as adsorption potential, is the only parameter here affected directly by the inlet concentration. It can be understood that the larger the inlet concentration becomes, the more impactful the micropore volume will be. At low concentrations such as 100 ppm used in the tests, the impact of available micropore volume is reduced, and thus relatively large errors in V32 predictions cannot translate directly into substantial error for predictions of adsorption capacity. With the above mentioned fact in mind, what becomes essential in adsorption capacity prediction at low concentrations of adsorbate, is the initial value of the physical properties of the adsorbent,

such as initial micropore volume, since changes in the micropores and V32 are minimal compared with the initial value and as a result are not enormously influential in the final prediction errors. As suggested in a previous study by Jahandar Lashaki et al.[2], adsorption capacity is much more closely correlated with the total pore volume rather than micropore of the adsorbent, at the investigated concentration; thus, G-70R and Blucher 100772 having close total pore volume initially ($0.58 \frac{cm^3}{g}$ and $0.72 \frac{cm^3}{g}$ for G-70R and Blucher 100772 respectively) are expected to show similar adsorption capacities, which agrees with the results obtained, and the model performs at the same accuracy for both of them.

Furthermore, for the highly mesoporous Blucher 101412, with a much greater total pore volume of $1.10 \frac{cm^3}{g}$, the model is having great difficulty in capacity prediction. This issue could be the result of another important factor influencing the model's accuracy: the definition of the W_0 parameter in the DRL equation. Urano et al.[16] considered W_0 to be only a function of micropore volume thus the adsorption is mainly limited by the available micropore volume of the adsorbent regardless of how much meso and macro pores are available. This conclusion directly contrasts with results from this study and previous studies[1,2] where Blucher 101412 and G-70R, while having very close initial micropore volume, showed drastically different first cycle adsorption capacity. The limitation is W_0 parameter definition causes the model not to consider adsorption done in adsorbents with large mesopores volume such as B101412, resulting in the under-prediction of the BAC's capacity.

In conclusion, the more microporous the adsorbent, the better the prediction of the adsorption capacity of the model becomes. This is apparent when comparing MRAE of adsorption capacity prediction for all three adsorbents where the most microporous sample G-70R showed a minor ARE (1.5%) and the least microporous Blucher 101412 showed the highest ARE (7.5%).

4.2.3. Adsorption Capacity Prediction at various concentrations

In the previous section, all the results were provided for the same inlet concentration of 100 ppm 1,2,4-TMB. This limitation constrains any investigation into the model's performance at different inlet concentrations of adsorbates. To rectify this problem, three samples, one from each adsorbent, were chosen. These samples each had a medium amount of cumulative heel build-up on them. The heel build-up amounts were 14.1% (cycle 3), 20.6% (cycle 5), and 19.0% (cycle 5) for G-70R, B101412, and B100772, respectively. These samples were obtained separate from the previous experiments and were chosen to be in the same heel build-up region. The experimental condition of which were explained in chapter 3. The adsorption capacity of these used samples was experimentally obtained at 50, 100, 500 and 1000 ppm inlet concentrations of 1,2,4-TMB. Additionally, the virgin samples of each adsorbent were put through the same test for further investigation into the model's performance.

As reflected in **Figure 4.15** for all adsorbents, whether virgin or used, increased inlet concentration resulted in a more considerable deviation between the model predicted adsorption capacity values and those obtained experimentally. This deviation is mainly due to the different adsorption mechanisms at low and high inlet concentrations. As reported by Mangun et al [17]. the adsorbate does not condense in the narrow micropores at low concentrations and remains in a tightly bound gas phase. Hence only a small volume of a pore is occupied, and the total available pore volume is not a limitation. However, at high inlet concentrations, the adsorbate prefers to condense inside the meso and macro pores. In this case, the total available pore volume becomes a limiting factor rather than the adsorption energy of the pores. As a result of the mentioned difference, at high inlet concentrations, meso and macropores, which have a much larger pore volume and in them adsorption takes place through capillary condensation, become much more valuable and help in

118

increasing the maximum adsorption capacity of the adsorbent. In contrast, they are much less noticeable at low inlet concentrations, and micropores with higher adsorption energy and the mechanism of volume filling are primarily at play [18].
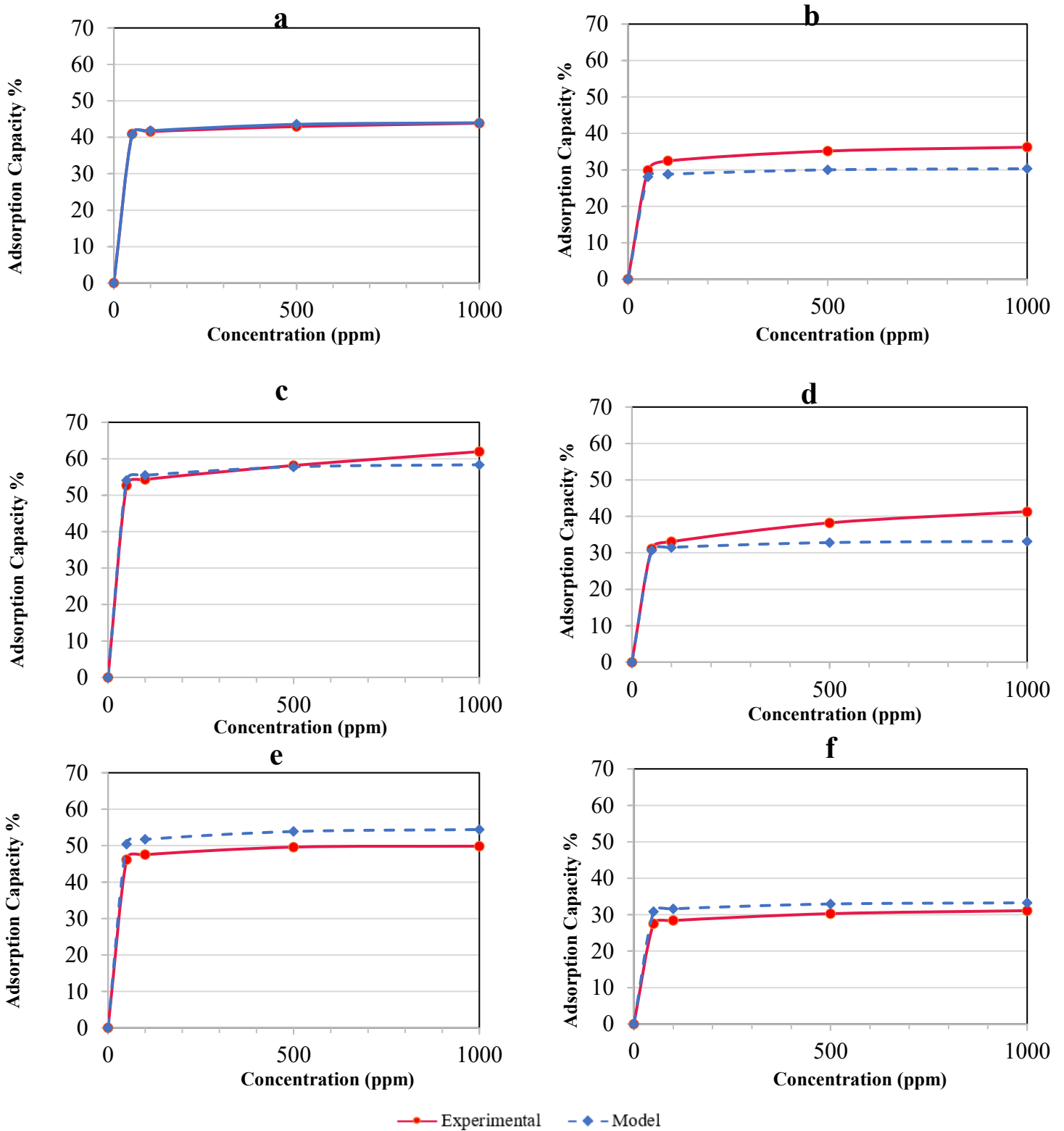
Figure 4.15. Modeled and experimentally obtained adsorption capacities at various inlet concentrations for (a) Virgin G-70R, (b) Used G-70R, (c) Virgin B101412, (d) Used B101412, (e) Virgin B100772, and (f) Used B100772.

Nevertheless, the above-mentioned difference in adsorption at low and high inlet concentrations has not been defined in the basic DRL model proposed by Hung et al[19]. As a result, for all three BACs experimented, the model predicts a negligible rise in adsorption capacity with an increase in adsorbate concentration (**Figure 4.15**). The most significant noticeable deviation is seen for the used Blucher 101412 in **Figure 4.15-d**. This considerable deviation is due to the fact that this adsorbent is highly mesoporous. For G-70R, as seen in **Figure 4.15 (a)** and **(b)**, the deviation is much smaller since the G-70R is highly microporous and does not contain a large volume of mesopores to contribute in the adsorption process compared to the other two adsorbents.

In general, as expected, the predictions were more accurate for virgin adsorbents since no additional error caused by micropore volume prediction was involved. A MAE of 0.3 wt.%, 4.3 wt.%, and 1.6 wt.% was observed for G-70R, B100772, and B101412, respectively. On the other hand, for the used samples, the error values were generally greater than the virgin samples with a MAE of 4.6 wt.%, 3.0 wt.%, and 3.9 wt.% for G-70R, B100772, and B101412, respectively. The only exception is B100772, where a smaller MAE was seen for the used sample. However, this variation can be explained by **Figure 4.15-f**. For Blucher 100772, the model predicted values were greater than those experimentally obtained. Since micropores were mainly occupied by the heel accumulated in the previous cycles in the used sample, the mesopores played a more considerable role in adsorption. As a result, with increased adsorption capacity at higher concentrations, the slope of the experimental plot is increased compared to the virgin sample. This increase in slope combined with the aforementioned overprediction present in this specific samples concludes in the gap between the model and actual values growing smaller relative to the adsorption capacity values obtained for the virgin B100772, and thus the average error is reduced.

In the end, the model made adsorption capacity prediction for all three samples with an average MAE of 3.8 at the lower end of inlet concentrations, these error values were much less considerable for all three samples tested. It appears that if the adsorbent being used is highly mesoporous, it is best to use the model only at lower inlet concentrations to decrease error in calculations.

4.4 References

1. Feizbakhshan M, Hashisho Z, Crompton D, Anderson JE, Nichols M. Effect of Activated Carbon's Pore Size Distribution on Oxygen Induced Heel Build-up. *Journal of Hazardous Materials*. Published online August 13, 2021:126905. doi:10.1016/J.JHAZMAT.2021.126905

2. Jahandar Lashaki M, Atkinson JD, Hashisho Z, Phillips JH, Anderson JE, Nichols M. The role of beaded activated carbon's pore size distribution on heel formation during cyclic adsorption/desorption of organic vapors. *Journal of Hazardous Materials*. 2016;315:42-51. doi:10.1016/J.JHAZMAT.2016.04.071

3. Yun JH, Choi DK, Moon H. Benzene adsorption and hot purge regeneration in activated carbon beds. *Chemical Engineering Science*. 2000;55(23):5857-5872. doi:10.1016/S0009-2509(00)00189-5

4. Niknaddaf S, Atkinson JD, Gholidoust A, et al. Influence of Purge Gas Flow and Heating Rates on Volatile Organic Compound Decomposition during Regeneration of an Activated Carbon Fiber Cloth. Published online 2020. doi:10.1021/acs.iecr.9b06070

5. Jahandar Lashaki M, Hashisho Z, Phillips JH, Crompton D, Anderson JE, Nichols M. Mechanisms of heel buildup during cyclic adsorption-desorption of volatile organic compounds in a full-scale adsorber-desorber. *Chemical Engineering Journal*. 2020;400:124937. doi:10.1016/J.CEJ.2020.124937

6. Niknaddaf S, Atkinson JD, Shariaty P, et al. Heel formation during volatile organic compound desorption from activated carbon fiber cloth. *Carbon*. 2016;96:131-138. doi:10.1016/J.CARBON.2015.09.049

7. Lashaki MJ, Fayaz M, Wang H (Helena), et al. Effect of Adsorption and Regeneration Temperature on Irreversible Adsorption of Organic Vapors on Beaded Activated Carbon. *Environmental Science and Technology*. 2012;46(7):4083-4090. doi:10.1021/ES3000195

8. Jahandar Lashaki M, Atkinson JD, Hashisho Z, et al. Effect of desorption purge gas oxygen impurity on irreversible adsorption of organic vapors. *Carbon*. 2016;99:310-317. doi:10.1016/J.CARBON.2015.12.037

9. Fayaz M. Adsorption and Microwave Regeneration for Controlling Volatile Organic Compounds Emissions from Automotive Paint Booths. Published online 2016. doi:10.7939/R3VH5CP7K

10. Çalişkan E, Bermúdez JM, Parra JB, Menéndez JA, Mahramanlioĝlu M, Ania CO. Low temperature regeneration of activated carbons using microwaves: Revising conventional wisdom. *Journal of Environmental Management*. 2012;102:134-140. doi:10.1016/J.JENVMAN.2012.02.016

11. Hashemi SM. Effect of Desorption Purge Gas Oxygen Impurity on Heel Formation During Regeneration of Beaded Activated Carbon Saturated with Organic Vapors. Published online 2017. doi:10.7939/R3WD3QD3Q

12. Myles AJ, Feudale RN, Liu Y, Woody NA, Brown SD. An introduction to decision tree modeling. *Journal of Chemometrics*. 2004;18(6):275-285. doi:10.1002/CEM.873

13. Feizbakhshan M, Hashisho Z, Crompton D, Anderson JE, Nichols M. Effect of Activated Carbon's Pore Size Distribution on Oxygen Induced Heel Build-up. *Journal of Hazardous Materials*. 2021;409. doi:10.1016/J.JHAZMAT.2021.126905

14. Lashaki M, Fayaz M, … SNJ of hazardous, 2012 undefined. Effect of the adsorbate kinetic diameter on the accuracy of the Dubinin–Radushkevich equation for modeling adsorption of organic vapors on activated carbon. *Elsevier*. Accessed September 26, 2021.

https://www.sciencedirect.com/science/article/pii/S030438941200948X?casa_token=W3qoAV2

GTHsAAAAA:EhA1hPJbtQFvK_K1k8redJalGFxmH7BJMGB7RrU8hhIMXh6MppbQ095PbY

Ib7jHXuGnmOg9Y

15. Huang MC, Chou CH, Teng H. Pore-size effects on activated-carbon capacities for volatile organic compound adsorption. *AIChE Journal*. 2002;48(8):1804-1810. doi:10.1002/AIC.690480820

16. Urano K, Omori S, Yamamoto E. Prediction Method for Adsorption Capacities of Commercial Activated Carbons in Removal of Organic Vapors. *Environmental Science and Technology*. 1982;16(1):10-14. doi:10.1021/ES00095A006

17. Mangun C, Daley M, Braatz R, Economy J. Effect of pore size on adsorption of hydrocarbons in phenolic-based activated carbon fibers. *Carbon*. 1998;36(1-2):123-129. doi:10.1016/S0008-6223(97)00169-3

18. Bansal RC, Goyal M. Activated Carbon Adsorption. Published online May 24, 2005. doi:10.1201/9781420028812

19. Hung HW, Lin TF. Prediction of the Adsorption Capacity for Volatile Organic Compounds onto Activated Carbons by the Dubinin–Radushkevich–Langmuir Model. *Journal of the Air & Waste Management Association*. 2012;57(4):497-506. doi:10.3155/1047-3289.57.4.497

5. CHAPTER 5: Conclusions and Recommendations

5.1 Conclusions

The experiments performed on G-70R Kureha BAC, Blucher 101412, and Blucher 100772 evaluated the performance of these adsorbents for 20-cycle adsorption/regeneration of 1,2,4-TMB under two different purge gas flowrates. This research has added to the understanding of the long-term performance of activated carbons beyond the common five cycle studies usually conducted. Additionally, the results of the mentioned long-term investigations were further utilized to develop a mathematical model capable of predicting both the pore size distribution and the adsorption capacity of the BAC adsorbents throughout the cyclic experiment.

The combined effect of purge gas flow rate and porosity of activated carbon on the long-term performance of 1,2,4-TMB on BAC was investigated. 6 different scenarios made up of a combination of three different activated carbon adsorbents with various porosity and physical properties and two different purge gas flow rates (0.5 and 5 SLPM) were studied. Initially, the effect of the porosity and the available micropore volume of adsorbents were more determinants in the performance of the BAC and the final cumulative heel build-up. In the first five cycles, G-70R and B101412 had almost the same initial micropore volume (0.50 and 0.49 $\frac{cm^3}{g}$ respectively) demonstrated a very similar heel formation rate and B100772, which had the lowest micropore volume (0.43 $\frac{cm^3}{g}$) lagged in heel formation in comparison with the other two adsorbents. However, the adsorption capacities had a much better correlation with the total pore volume, and the highly mesoporous B101412 (40% microporosity) showed a much higher adsorption capacity than the other two. With the progression of the adsorption/regeneration experiments to higher cycle numbers, however, the effect of purge gas flowrate became much more significant, and a clear separation was observed in both heel formation and adsorption capacity among samples regenerated using 0.5 SLPM of dried air and those regenerated with 5 SLPM. It was reported that

at higher cycle numbers, due to the elimination of a majority of micropores in adsorbents, microporosity of the adsorbent is reduced and its effect diminishes greatly, and purge gas flow rate increase can be much more effective in the removal of the adsorbed species in the larger mesopores. At the final cycles, samples regenerated with 0.5 SLPM all had an average cumulative heel of 31 %, and those regenerated with 5 SLPM had a cumulative heel build-up average of 21%, signifying the importance of purge gas flow rate in heel reduction in later cycles.

Interestingly the DTG results showed that even though higher purge gas flow rates reduce the magnitude of heel build-up, it also transforms the heel into heavier chemically formed compounds. Additionally, the PSD of the virgin and regenerated samples were compared, and it was demonstrated that micropores are mostly exhausted in the first few cycles, and this effect is exasperated the more microporous a sample is. In the extreme case of using a 0.5 SLPM purge gas flow rate, G-70R was utterly exhausted, and its micropore volume of 0.50 $\frac{cm^3}{g}$ reduced to almost zero by the 10th cycle, however, the mesoporous B100772 under the same operating condition lasted 20 cycles and only lost 50% of its initial micropore volume. This difference indicates that selecting activated carbon with a hierarchal pore structure containing micropores and mesopores helps to lengthen the lifetime of the adsorbent in cyclic adsorption/ regeneration processes.

In the second section, a model was developed to predict the pore size distribution of activated carbon adsorbents after going through cyclic adsorption/regeneration. At first, using machine learning and multivariable linear regression, a mathematical regression model was found, based on data points existing in the literature and also ones gathered in this study, to predict the micropore volume of activated carbon based on the cumulative mass heel formed on it and the molar volume of the adsorbate. This newly acquired micropore volume was utilized to finalize the pore size distribution model. The PSD prediction model was then tested on nine different samples from the

three activated carbon adsorbents forming different level of heel. The PSD model better predicted the micropore volume and PSD of the G-70R adsorbent with a mean relative absolute error (MRAE) of 3.5%. In contrast, the micropore prediction for B101412 and B100772 had a MRAE of 10.8% and 12.0%, respectively. The difference in accuracy was due to under-representing the more mesoporous adsorbents in the machine learning training data set.

Finally, the PSD prediction model was utilized to enhance the existing DRL isotherm model to predict the adsorption capacity of used activated carbon samples with various amounts of cumulative heel build-up on them. The accuracy and capabilities of the enhanced DRL model were tested on three virgin samples, and three used samples of the G-70R, B100772, and B101412. As expected, virgin samples' adsorption capacity prediction errors were much lower for all three adsorbents than their used counterparts. For example, virgin B101412 had an MRAE of 2.68%, while used B101412 had an MRAE of 10%. This variation was expected since no errors from PSD prediction were involved in virgin isotherms.

Furthermore, the enhanced DRL model demonstrated greater deviation from experimental values as the inlet concentration was increased. The deviation was mainly due to the different mechanisms of adsorption at low and high concentrations of VOC. It was concluded that the more mesoporous the adsorbent becomes, the larger this deviation at high inlet concentration grows. Thus, it is best to use the model at low to mid concentration of volatile organic compounds, especially if the adsorbent has significant meso and macropores.

This study demonstrated how impactful the choice of adsorbent and purge gas flow rate could be on the long-term cyclic performance of activated carbon. Furthermore, the model developed could help understand the changes occurring throughout the cyclic adsorption/regeneration and thus provide the operator with a reasonable estimation of how different adsorbents could perform prior

to the start of the actual operation. Based on the model results, a well-informed choice can be made on proceeding with cyclic adsorption.

As a final comment, the model developed for adsorption capacity prediction combined with the automated setup has the capability to substantially reduce the time and effort required to obtain isotherms and pore size distribution for various VOC/adsorbent combinations. For example, one can conduct a 30 cycle analysis over a short duration and have 30 isotherms for adsorption of the targeted compound at various inlet concentrations. This preliminary data can help improve industrial processes to understand better the changes occurring in the adsorption capacity of their selected activated carbon adsorbent as the cyclic adsorption/regeneration process progresses. With this deeper understanding, it is possible to plan for how long an adsorbent can be used before immediate replacement is required and how much each adsorbent can be used before the risk of going over applicable limits can occur. As a result, less time and energy will be spent replacing the adsorbent, and a reduced amount of waste will be generated.

Furthermore, the pore size distribution changes can also be easily predicted with this model. PSDs are invaluable in understanding how each adsorbate with its distinct kinetic diameter interacts with narrow pores of the selected activated carbon. The knowledge gained from these interactions could be used to predict the capability of adsorbents when used with new compounds with similar or larger kinetic diameters.

5.2. Recommendations

One crucial limitation faced in this study was the lack of cyclic adsorption/regeneration data on more mesoporous adsorbents. Most of the data set used in this study involved G-70R Kureha BAC, and as a result, the PSD and adsorption capacity models were more accurate for G-70R compared to other adsorbents. To overcome this issue and increase the model's generalizability, the long-

term performance of activated carbons with various porosities could be conducted. By adding more data from these adsorbents into the training dataset of the model, its accuracy will increase. Furthermore, for better optimization of the long-term performance of activated carbons, the same investigation method of this study could be utilized to observe the effect of other operating parameters such as regeneration duration or temperature. Design experiment (DOE) methods such as "Taguchi methods" could be applied to investigate and optimize long-term performance of the adsorbent.

Bibliography:

1. HaiLin W, Lie N, Jing L, et al. Characterization and assessment of volatile organic compounds (VOCs) emissions from typical industries. *Chinese Science Bulletin*. 2013;58(7):724-730. doi:10.1007/s11434-012-5345-2

2. Technical Overview of Volatile Organic Compounds | US EPA. Accessed September 19, 2021. https://www.epa.gov/indoor-air-quality-iaq/technical-overview-volatile-organic-compounds

3. EUR-Lex - 31999L0013 - EN - EUR-Lex. Accessed September 19, 2021. https://eur-lex.europa.eu/legal-content/EN/TXT/?uri=celex%3A31999L0013

4. EUR-Lex - 32001L0081 - EN - EUR-Lex. Accessed September 19, 2021. https://eur-lex.europa.eu/legal-content/EN/TXT/?uri=celex%3A32001L0081

5. Toxic substances list: volatile organic compounds - Canada.ca. Accessed September 19, 2021. https://www.canada.ca/en/environment-climate-change/services/management-toxic-substances/list-canadian-environmental-protection-act/volatile-organic-compounds.html

6. Nurmatov UB, Tagiyeva N, Semple S, Devereux G, Sheikh A. Volatile organic compounds and risk of asthma and allergy: a systematic review. *European Respiratory Review*. 2015;24(135):92-101. doi:10.1183/09059180.00000714

7. Paciência I, Madureira J, Rufo J, Moreira A, Fernandes E de O. A systematic review of evidence and implications of spatial and seasonal variations of volatile organic compounds (VOC) in indoor human environments. *http://dx.doi.org/101080/1093740420151134371*. 2016;19(2):47-64. doi:10.1080/10937404.2015.1134371

8. Canada Gazette, Part 1, Volume 153, Number 27: Volatile Organic Compound Concentration Limits for Certain Products Regulations. Accessed September 19, 2021. https://gazette.gc.ca/rp-pr/p1/2019/2019-07-06/html/reg1-eng.html

9. Kim BR. VOC Emissions from Automotive Painting and Their Control: A Review. *Environmental Engineering Research*. 2011;16(1):1-9. doi:10.4491/eer.2011.16.1.001

10. Piccot SD, Watson JJ, Jones JW. A Global Inventory of Volatile Organic Compound Emissions From Anthropogenic Sources. *Journal of Geophysical Research: Atmospheres*. 1992;97(D9). doi:10.1029/92JD00682

11. Guenther A, Hewitt CN, Erickson D, et al. A global model of natural volatile organic compound emissions. *Journal of Geophysical Research: Atmospheres*. 1995;100. doi:10.1029/94JD02950

12. Tie X, Li G, Ying Z, Guenther A, Madronich S. Biogenic emissions of isoprenoids and NO in China and comparison to anthropogenic emissions. *Science of the Total Environment*. 2006;371:238-251. doi:10.1016/j.scitotenv.2006.06.025

13. Canada's Air Pollutant Emissions Inventory - Open Government Portal. Accessed September 19, 2021. https://open.canada.ca/data/en/dataset/fa1c88a8-bf78-4fcb-9c1e-2a5534b92131

14. Khan FI, Kr Ghoshal A. Removal of Volatile Organic Compounds from polluted air. *Journal of Loss Prevention in the Process Industries*. 2000;13(6):527-545. doi:10.1016/S0950-4230(00)00007-3

15. Rani Parmar G, Rao NN. Emerging Control Technologies for Volatile Organic Compounds. *Critical Reviews in Environmental Science and Technology*. 2008;39(1):41-78. doi:10.1080/10643380701413658

16. Zhang X, Gao B, Creamer AE, Cao C, Li Y. Adsorption of VOCs onto engineered carbon materials: A review. *Journal of Hazardous Materials*. 2017;338:102-123. doi:10.1016/J.JHAZMAT.2017.05.013

17. Yang C, Miao G, Pi Y, et al. Abatement of various types of VOCs by adsorption/catalytic oxidation: A review. *Chemical Engineering Journal*. 2019;370:1128-1153. doi:10.1016/J.CEJ.2019.03.232

18. Carratalá-Abril J, Lillo-Ródenas MA, Linares-Solano A, Cazorla-Amorós D. Regeneration of activated carbons saturated with benzene or toluene using an oxygen-containing atmosphere. *Chemical Engineering Science*. 2010;65(6):2190-2198. doi:10.1016/J.CES.2009.12.017

19. Moreno-Castilla C, Rivera-Utrilla J, Joly JP, López-Ramón M v., Ferro-García MA, Carrasco-Marín F. Thermal regeneration of an activated carbon exhausted with different substituted phenols. *Carbon*. 1995;33(10):1417-1423. doi:10.1016/0008-6223(95)00090-Z

20. Martin RJ, Ng WJ. Chemical regeneration of exhausted activated carbon—I. *Water Research*. 1984;18(1):59-73. doi:10.1016/0043-1354(84)90048-4

21. Ivancev-Tumbas I, Dalmacija B, Tamas Z, Karlovic E. Reuse of biologically regenerated activated carbon for phenol removal. *Water Research*. 1998;32(4):1085-1094. doi:10.1016/S0043-1354(97)00337-0

22. Hwang KS, Choi DK, Gong SY, Cho SY. Adsorption and thermal regeneration of methylene chloride vapor on an activated carbon bed. *Chemical Engineering Science*. 1997;52(7):1111-1123. doi:10.1016/S0009-2509(96)00470-8

23. Jahandar Lashaki M, Hashisho Z, Phillips JH, Crompton D, Anderson JE, Nichols M. Mechanisms of heel buildup during cyclic adsorption-desorption of volatile organic compounds in a full-scale adsorber-desorber. *Chemical Engineering Journal*. 2020;400:124937. doi:10.1016/J.CEJ.2020.124937

24. Weber WJ, Smith EH. Simulation and design models for adsorption processes. *Environmental Science and Technology*. 1987;21(11):1040-1050. doi:10.1021/ES00164A002

25.   Suzuki M, Suzuki M. *Adsorption Engineering*. Vol 14. Kodansha; 1990. Accessed September 21, 2021. https://www.academia.edu/download/56981223/AdsorptionEngineering.pdf

26.   Bansal RC, Goyal M. Activated Carbon Adsorption. Published online May 24, 2005. doi:10.1201/9781420028812

27.   Thommes M, Kaneko K, Neimark A v., et al. Physisorption of gases, with special reference to the evaluation of surface area and pore size distribution (IUPAC Technical Report). *Pure and Applied Chemistry*. 2015;87(9-10):1051-1069. doi:10.1515/PAC-2014-1117

28.   Rufford T, Zhu J, Hulicova-Jurcakova D. *Green Carbon Materials: Advances and Applications*.; 2019.

29.   Hu H, Xu K. Physicochemical technologies for HRPs and risk control. *High-Risk Pollutants in Wastewater*. Published online January 1, 2020:169-207. doi:10.1016/B978-0-12-816448-8.00008-3

30.   Barrer RM, McKenzie N, Reay JSS. Capillary condensation in single pores. *Journal of Colloid Science*. 1956;11(4-5):479-495. doi:10.1016/0095-8522(56)90164-7

31.   Huang MC, Chou CH, Teng H. Pore-size effects on activated-carbon capacities for volatile organic compound adsorption. *AIChE Journal*. 2002;48(8):1804-1810. doi:10.1002/AIC.690480820

32.   Mokhatab S, Poe WA, Mak JY. Handbook of natural gas transmission and processing: Principles and practices. *Handbook of Natural Gas Transmission and Processing: Principles and Practices*. Published online January 1, 2018:1-826. doi:10.1016/C2017-0-03889-2

33.   Vidic RD, Suidan MT. Role of Dissolved Oxygen on the Adsorptive Capacity of Activated Carbon for Synthetic and Natural Organic Matter. *Environ Sci Technol*. 1991;25(9):1612-1618. doi:10.1021/ES00021A013

34. Marsh H, Rodríguez-Reinoso F. Characterization of Activated Carbon. *Activated Carbon*. Published online January 1, 2006:143-242. doi:10.1016/B978-008044463-5/50018-2

35. Huang ZH, Kang F, Liang KM, Hao J. Breakthrough of methyethylketone and benzene vapors in activated carbon fiber beds. *Journal of Hazardous Materials*. 2003;98(1-3):107-115. doi:10.1016/S0304-3894(02)00284-4

36. Das D, Gaur V, Verma N. Removal of volatile organic compound by activated carbon fiber. *Carbon*. 2004;42(14):2949-2962. doi:10.1016/J.CARBON.2004.07.008

37. Lashaki MJ, Fayaz M, Wang H (Helena), et al. Effect of Adsorption and Regeneration Temperature on Irreversible Adsorption of Organic Vapors on Beaded Activated Carbon. *Environmental Science and Technology*. 2012;46(7):4083-4090. doi:10.1021/ES3000195

38. Jr KS, Dunn R, Ternes M. *Air Pollution Control Technology Handbook*. Vol 62.; 2015. doi:10.1595/205651318X696657

39. Wang H, Lashaki MJ, Fayaz M, et al. Adsorption and Desorption of Mixtures of Organic Vapors on Beaded Activated Carbon. *Environmental Science and Technology*. 2012;46(15):8341-8350. doi:10.1021/ES3013062

40. Niknaddaf S, Atkinson JD, Gholidoust A, et al. Influence of Purge Gas Flow and Heating Rates on Volatile Organic Compound Decomposition during Regeneration of an Activated Carbon Fiber Cloth. Published online 2020. doi:10.1021/acs.iecr.9b06070

41. Babu B v, Gupta S. Modeling and Simulation of Fixed bed Adsorption column: Effect of Velocity Variation. *Engineering Technology*. Published online 2005:30923-34748. Accessed December 21, 2021. http://discovery.bits-pilani.ac.in/discipline/chemical/BVb/index.html;

42. Aktaş Ö, Çeçen F. Effect of type of carbon activation on adsorption and its reversibility. *Journal of Chemical Technology and Biotechnology*. 2006;81(1):94-101. doi:10.1002/JCTB.1363

43. Leng CC, Pinto NG. Effects of surface properties of activated carbons on adsorption behavior of selected aromatics. *Carbon*. 1997;35(9):1375-1385. doi:10.1016/S0008-6223(97)00091-2

44. Lillo-Ródenas MA, Cazorla-Amorós D, Linares-Solano A. Behaviour of activated carbons with different pore size distributions and surface oxygen groups for benzene and toluene adsorption at low concentrations. *Carbon*. 2005;43(8):1758-1767. doi:10.1016/J.CARBON.2005.02.023

45. Cal MP, Larson SM, Rood MJ. Experimental and modeled results describing the adsorption of acetone and benzene onto activated carbon fibers. *Environmental Progress*. 1994;13(1):26-30. doi:10.1002/EP.670130114

46. Mangun C, Daley M, Braatz R, Economy J. Effect of pore size on adsorption of hydrocarbons in phenolic-based activated carbon fibers. *Carbon*. 1998;36(1-2):123-129. doi:10.1016/S0008-6223(97)00169-3

47. Jahandar Lashaki M, Atkinson JD, Hashisho Z, Phillips JH, Anderson JE, Nichols M. The role of beaded activated carbon's pore size distribution on heel formation during cyclic adsorption/desorption of organic vapors. *Journal of Hazardous Materials*. 2016;315:42-51. doi:10.1016/J.JHAZMAT.2016.04.071

48. Feizbakhshan M, Hashisho Z, Crompton D, Anderson JE, Nichols M. Effect of Activated Carbon's Pore Size Distribution on Oxygen Induced Heel Build-up. *Journal of Hazardous Materials*. 2021;409. doi:10.1016/J.JHAZMAT.2021.126905

49. TIPNIS PR, HARRIOTT P. THERMAL REGENERATION OF ACTIVATED CARBONS. *Chemical Engineering Communications*. 1986;46(1-3):11-28. doi:10.1080/00986448608911393

50. Canet X, Gilles F, Su BL, de weireld guy, Frere M. Adsorption of alkanes and aromatic compounds on various faujasites in the Henry domain. 1. Compensating cation effect on zeolites Y. *Journal of Chemical & Engineering Data* . 2007;52(6):2127-2137. doi:10.1021/je700214v

51. Ghiaci M, Abbaspur A, Kia R, Seyedeyn-Azad F. Equilibrium isotherm studies for the sorption of benzene, toluene, and phenol onto organo-zeolites and as-synthesized MCM-41. *Separation and Purification Technology*. 2004;40(3):217-229. doi:10.1016/J.SEPPUR.2004.03.001

52. Vasanth Kumar K, Sivanesan S. Sorption isotherm for safranin onto rice husk: Comparison of linear and non-linear methods. *Dyes and Pigments*. 2007;72(1):130-133. doi:10.1016/J.DYEPIG.2005.07.020

53. El-Khaiary MI. Least-squares regression of adsorption equilibrium data: Comparing the options. *Journal of Hazardous Materials*. 2008;158(1):73-87. doi:10.1016/J.JHAZMAT.2008.01.052

54. Foo KY, Hameed BH. Insights into the modeling of adsorption isotherm systems. *Chemical Engineering Journal*. 2010;156(1):2-10. doi:10.1016/J.CEJ.2009.09.013

55. Langmuir I. THE CONSTITUTION AND FUNDAMENTAL PROPERTIES OF SOLIDS AND LIQUIDS. PART I. SOLIDS. *Journal of the American Chemical Society*. 2002;38(11):2221-2295. doi:10.1021/JA02268A002

56. Do D. *Adsorption Analysis: Equilibria and Kinetics (with Cd Containing Computer MATLAB Programs)*. Vol 2. World Scientific; 1998.

57. Al-Ghouti MA, Da'ana DA. Guidelines for the use and interpretation of adsorption isotherm models: A review. *Journal of Hazardous Materials*. 2020;393:122383. doi:10.1016/J.JHAZMAT.2020.122383

58. Freundlich H. Über die Adsorption in Lösungen. *Zeitschrift für Physikalische Chemie*. 1907;57U(1):385-470. doi:10.1515/ZPCH-1907-5723

59. Hung HW, Lin TF. Prediction of the Adsorption Capacity for Volatile Organic Compounds onto Activated Carbons by the Dubinin–Radushkevich–Langmuir Model. *Journal of the Air & Waste Management Association*. 2012;57(4):497-506. doi:10.3155/1047-3289.57.4.497

60. Urano K, Omori S, Yamamoto E. Prediction Method for Adsorption Capacities of Commercial Activated Carbons in Removal of Organic Vapors. *Environmental Science and Technology*. 1982;16(1):10-14. doi:10.1021/ES00095A006

61. Qi S, Hay KJ, Rood MJ, Cal MP. Carbon Fiber Adsorption Using Quantitative Structure-Activity Relationship. *Journal of Environmental Engineering*. 2000;126(9):865-868. doi:10.1061/(ASCE)0733-9372(2000)126:9(865)

62. Crittenden JC, Cortright RD, Rick B, Tang SR, Perram D. Using GAC to Remove VOCs From Air Stripper Off-Gas. *Journal - American Water Works Association*. 1988;80(5):73-84. doi:10.1002/J.1551-8833.1988.TB03040.X

63. Prakash J, Nirmalakhandan N, Speece RE. Prediction of Activated Carbon Adsorption Isotherms for Organic Vapors. *Environmental Science and Technology*. 1994;28(8):1403-1409. doi:10.1021/ES00057A005

64. Reucroft PJ, Simpson WH, Jonas LA. Sorption properties of activated carbon. *Journal of Physical Chemistry*. 1971;75(23):3526-3531. doi:10.1021/J100692A007

65. Noll K. *Adsorption Technology for Air and Water Pollution Control*. CRC Press; 1991.

66. Nirmalakhandan NN, Speece RE. Prediction of Activated Carbon Adsorption Capacities for Organic Vapors Using Quantitative Structure—Activity Relationship Methods. *Environmental Science and Technology*. 1993;27(8):1512-1516. doi:10.1021/ES00045A004

67. Jahandar Lashaki M, Atkinson JD, Hashisho Z, et al. Effect of desorption purge gas oxygen impurity on irreversible adsorption of organic vapors. *Carbon*. 2016;99:310-317. doi:10.1016/J.CARBON.2015.12.037

68. Friday DK, LeVan MD. Hot purge gas regeneration of adsorption beds with solute condensation: Experimental studies. *AIChE Journal*. 1985;31(8):1322-1328. doi:10.1002/AIC.690310811

69. Salvador F, Martin-Sanchez N, Sanchez-Hernandez R, Sanchez-Montero MJ, Izquierdo C. Regeneration of carbonaceous adsorbents. Part I: Thermal Regeneration. *Microporous and Mesoporous Materials*. 2015;202:259-276. doi:10.1016/J.MICROMESO.2014.02.045

70. Niknaddaf S, Atkinson JD, Shariaty P, et al. Heel formation during volatile organic compound desorption from activated carbon fiber cloth. *Carbon*. 2016;96:131-138. doi:10.1016/J.CARBON.2015.09.049

71. Fayaz M, Shariaty P, Atkinson JD, et al. Using Microwave Heating To Improve the Desorption Efficiency of High Molecular Weight VOC from Beaded Activated Carbon. *Environmental Science and Technology*. 2015;49(7):4536-4542. doi:10.1021/ES505953C

72. Ania CO, Parra JB, Menéndez JA, Pis JJ. Microwave-assisted regeneration of activated carbons loaded with pharmaceuticals. *Water Research*. 2007;41(15):3299-3306. doi:10.1016/J.WATRES.2007.05.006

73. Guo D, Shi Q, He B, Yuan X. Different solvents for the regeneration of the exhausted activated carbon used in the treatment of coking wastewater. *Journal of Hazardous Materials*. 2011;186(2-3):1788-1793. doi:10.1016/J.JHAZMAT.2010.12.068

74. Martin RJ, Ng WJ. The repeated exhaustion and chemical regeneration of activated carbon. *Water Research*. 1987;21(8):961-965. doi:10.1016/S0043-1354(87)80014-3

75. Aktaş Ö, Çeçen F. Bioregeneration of activated carbon: A review. *International Biodeterioration & Biodegradation*. 2007;59(4):257-272. doi:10.1016/J.IBIOD.2007.01.003

76. Goeddertz JG, Matsumoto MR, Scott Weber A. Offline Bioregeneration of Granular Activated Carbon. *Journal of Environmental Engineering*. 1988;114(5):1063-1076. doi:10.1061/(ASCE)0733-9372(1988)114:5(1063)

77. Kim DJ, Miyahara T, Noike T. Effect of C/N ratio on the bioregeneration of biological activated carbon. *Water Science and Technology*. 1997;36(12):239-249. doi:10.1016/S0273-1223(97)00720-8

78. Sirotkin AS, Koshkina LY, Ippolitov KG. The BAC-process for treatment of waste water Containing non-ionogenic synthetic surfactants. *Water Research*. 2001;35(13):3265-3271. doi:10.1016/S0043-1354(01)00029-X

79. Wang H, Jahandar Lashaki M, Fayaz M, et al. Adsorption and desorption of mixtures of organic vapors on beaded activated carbon. *Environmental Science and Technology*. 2012;46(15):8341-8350. doi:10.1021/ES3013062

80. Jahandar Lashaki M, Atkinson JD, Hashisho Z, Phillips JH, Anderson JE, Nichols M. The role of beaded activated carbon's surface oxygen groups on irreversible adsorption of organic vapors. *Journal of Hazardous Materials*. 2016;317:284-294. doi:10.1016/J.JHAZMAT.2016.05.087

81. Feizbakhshan M, Hashisho Z, Crompton D, Anderson JE, Nichols M. Effect of Activated Carbon's Pore Size Distribution on Oxygen Induced Heel Build-up. *Journal of Hazardous Materials*. Published online August 13, 2021:126905. doi:10.1016/J.JHAZMAT.2021.126905

82. Jahandar Lashaki M, Fayaz M, Wang H, et al. Effect of Adsorption and Regeneration Temperature on Irreversible Adsorption of Organic Vapors on Beaded Activated Carbon. *Environmental Science and Technology*. 2012;46:7. doi:10.1021/es3000195

83. Feizbakhshan M, Amdebrhan B, Hashisho Z, et al. Effects of oxygen impurity and desorption temperature on heel build-up in activated carbon. *Chemical Engineering Journal*. 2021;409:128232. doi:10.1016/J.CEJ.2020.128232

84. Jiang W, Xing X, Li S, Zhang X, Wang W. Synthesis, characterization and machine learning based performance prediction of straw activated carbon. *Journal of Cleaner Production*. 2019;212:1210-1223. doi:10.1016/J.JCLEPRO.2018.12.093

85. Mullainathan S, Spiess J. Machine Learning: An Applied Econometric Approach. *Journal of Economic Perspectives*. 2017;31(2):87-106. doi:10.1257/JEP.31.2.87

86. Li J, Zhu X, Li Y, Tong YW, Ok YS, Wang X. Multi-task prediction and optimization of hydrochar properties from high-moisture municipal solid waste: Application of machine learning on waste-to-resource. *Journal of Cleaner Production*. 2021;278:123928. doi:10.1016/J.JCLEPRO.2020.123928

87. Guo H nan, Wu S biao, Tian Y jie, Zhang J, Liu H tao. Application of machine learning methods for the prediction of organic solid waste treatment and recycling processes: A review. *Bioresource Technology*. 2021;319:124114. doi:10.1016/J.BIORTECH.2020.124114

88. Zhu X, Wang X, Ok YS. The application of machine learning methods for prediction of metal sorption onto biochars. *Journal of Hazardous Materials*. 2019;378:120727. doi:10.1016/J.JHAZMAT.2019.06.004

89. Kim B, Lee S, Kim J. Inverse design of porous materials using artificial neural networks. *Science Advances*. 2020;6(1). doi:10.1126/SCIADV.AAX9324

90. Zhang K, Zhong S, Zhang H. Predicting Aqueous Adsorption of Organic Compounds onto Biochars, Carbon Nanotubes, Granular Activated Carbons, and Resins with Machine Learning. *Environmental Science & Technology*. 2020;54(11):7008-7018. doi:10.1021/ACS.EST.0C02526

91. Foroughi M, Ahmadi Azqhandi MH, Kakhki S. Bio-inspired, high, and fast adsorption of tetracycline from aqueous media using Fe3O4-g-CN@PEI-β-CD nanocomposite: Modeling by response surface methodology (RSM), boosted regression tree (BRT), and general regression

neural network (GRNN). *Journal of Hazardous Materials*. 2020;388:121769. doi:10.1016/J.JHAZMAT.2019.121769

92. Yuan X, Suvarna M, Low S, et al. Applied Machine Learning for Prediction of CO2 Adsorption on Biomass Waste-Derived Porous Carbons. *Environmental Science & Technology*. 2021;55(17):11925-11936. doi:10.1021/ACS.EST.1C01849

93. Xiao J, Li C, Fang L, et al. Machine learning–based optimization for hydrogen purification performance of layered bed pressure swing adsorption. *International Journal of Energy Research*. 2020;44(6):4475-4492. doi:10.1002/ER.5225

94. Avhale A, Kaya D, Mabande GTP, et al. Defect-free zeolite membranes of the type BEA for organic vapour separation and membrane reactor applications. *Studies in Surface Science and Catalysis*. 2008;174(SUPPL. PART A):669-672. doi:10.1016/S0167-2991(08)80287-X

95. Mosavari Nezamabad N. Effect of Surface Oxygen Groups on Irreversible Adsorption of Volatile Organic Compounds on Beaded Activated Carbon. Published online 2017. doi:10.7939/R3M03Z893

96. Mojtaba Hashemi S, Jahandar Lashaki M, Hashisho Z, Phillips JH, Anderson JE, Nichols M. Oxygen impurity in nitrogen desorption purge gas can increase heel buildup on activated carbon. *Separation and Purification Technology*. 2019;210:497-503. doi:10.1016/J.SEPPUR.2018.08.035

97. Maulud DH, Mohsin Abdulazeez A. A Review on Linear Regression Comprehensive in Machine Learning. *Journal of Applied Science and Technology Trends*. 2020;01(04):140-147. doi:10.38094/jastt1457

98. Yu C, Yao W. Robust linear regression: A review and comparison. *Communications in Statistics-Simulation and Computation*. 2017;46(8):6261-6282. doi:10.1080/03610918.2016.1202271

99.   Refaeilzadeh P, Tang L, H Liu. Cross-validation. *Encyclopedia of database systems 5*. Published online 2009:532-538. doi:10.1007/978-1-4899-7993-3_565-2

100.   Sutter JM, Kalivas JH. Comparison of Forward Selection, Backward Elimination, and Generalized Simulated Annealing for Variable Selection. *Microchemical Journal*. 1993;47(1-2):60-66. doi:10.1006/MCHJ.1993.1012

101.   Chen SG, Yang RT. Theoretical Investigation of Relationships between Characteristic Energy and Pore Size for Adsorption in Micropores. *Journal of Colloid and Interface Science*. 1996;177(2):298-306. doi:10.1006/JCIS.1996.0035

102.   McEnaney B. Estimation of the dimensions of micropores in active carbons using the Dubinin-Radushkevich equation. *Carbon*. 1987;25(1):69-75. doi:10.1016/0008-6223(87)90041-8

103.   Yun JH, Choi DK, Moon H. Benzene adsorption and hot purge regeneration in activated carbon beds. *Chemical Engineering Science*. 2000;55(23):5857-5872. doi:10.1016/S0009-2509(00)00189-5

104.   Fayaz M. Adsorption and Microwave Regeneration for Controlling Volatile Organic Compounds Emissions from Automotive Paint Booths. Published online 2016. doi:10.7939/R3VH5CP7K

105.   Çalişkan E, Bermúdez JM, Parra JB, Menéndez JA, Mahramanlioĝlu M, Ania CO. Low temperature regeneration of activated carbons using microwaves: Revising conventional wisdom. *Journal of Environmental Management*. 2012;102:134-140. doi:10.1016/J.JENVMAN.2012.02.016

106.   Hashemi SM. Effect of Desorption Purge Gas Oxygen Impurity on Heel Formation During Regeneration of Beaded Activated Carbon Saturated with Organic Vapors. Published online 2017. doi:10.7939/R3WD3QD3Q

107. Myles AJ, Feudale RN, Liu Y, Woody NA, Brown SD. An introduction to decision tree modeling. *Journal of Chemometrics*. 2004;18(6):275-285. doi:10.1002/CEM.873

Appendix: Supplementary Information for Chapter 4

A. Machine Learning Process Flowchart
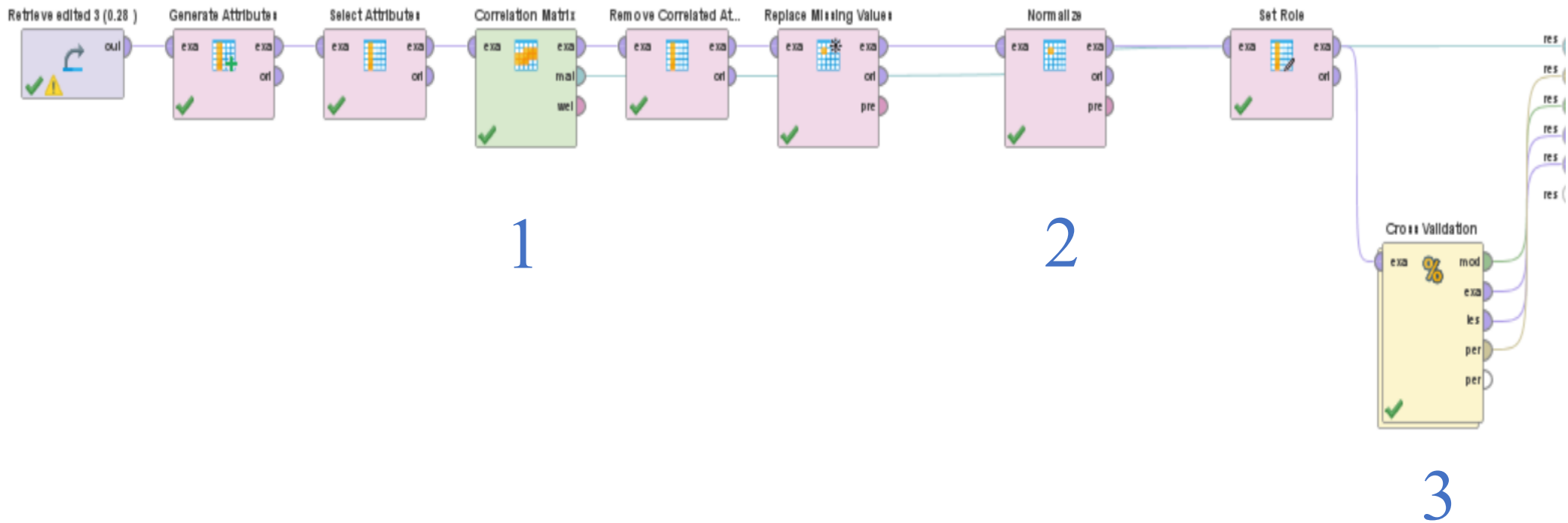
Figure A.1. Basic schematic of the first layer of the process showing the preprocessing stages and the final cross validation.
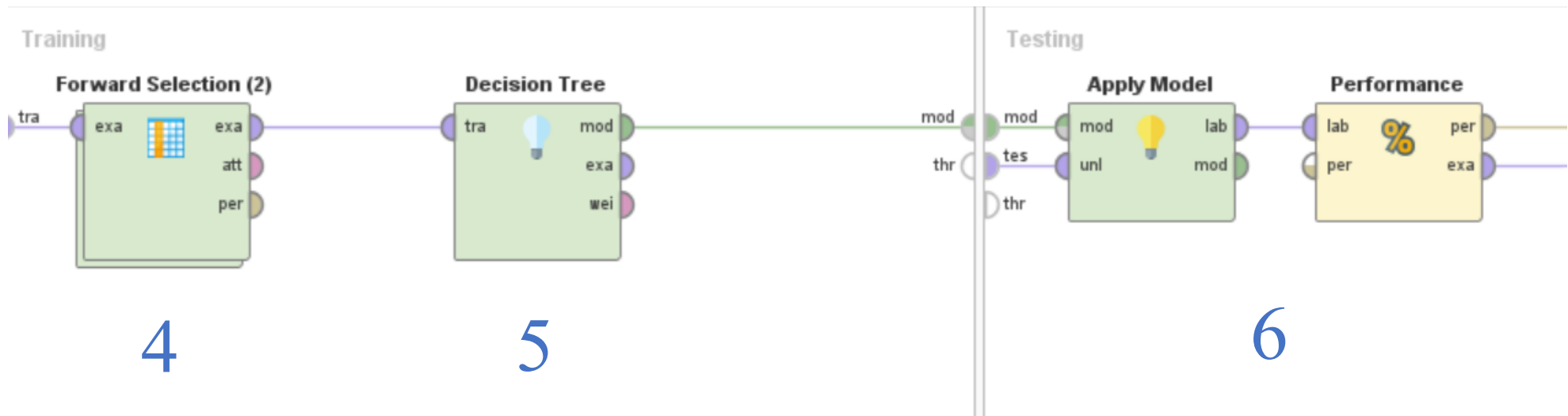
Figure A.2. Basic schematic of the second layer, nested inside cross-validation, shows the forward selection and the decision tree model's

application.

1) In this section, we use the Pearson Correlation Coefficient (PCC) to measure the linear dependency between any two features using the below equation: $r = \dfrac{\sum (x-\bar{X})(y-\bar{Y})}{\sqrt{\left[\sum (x-\bar{X})^2\right]\left[\sum (y-\bar{Y})^2\right]}}$

   where $\bar{X}$ or $\bar{Y}$ are the averages of variable x or y. Using the calculated correlations, any two features that are highly correlated, more than 0.95, are filtered out. This will reduce the number of features to 14.

2) In this stage, all the variables except the target value were normalized using the Z-transformation method into the range of 0.1-0.9.

$$x_i^* = 0.1 + \frac{0.8(x_i - x_{min})}{(x_{max} - x_{min})}$$

3) This section is the main cross-validation in which model training and testing occur. Nested inside this stage are the forward selection method and the decision tree model.

4) Forward selection is a feature importance technique; Feature importance refers to techniques that assign a score to input features based on how useful they are at predicting a target variable. In this method, we start with one feature, and other features are added one by one to select the best combination of features for accurate prediction.

5) The decision tree and linear regression prediction model are applied to the selected features and examples.

6) The targeted feature is defined as $\left(\dfrac{Final\ Micropore\ Volume}{Initial\ Micropore\ Volume} * 100\right)$

7) Models performance evaluations for predictability and generalizability are acquired.

$$R^2 = 1 - \frac{\sum_{i=i}^{N}(Y_i^{experiment} - Y_i^{prediction})^2}{\sum_{i=i}^{N}(Y_i^{experiment} - \hat{Y}_{average}^{prediction})^2}$$

$$RMSE = \sqrt{\frac{1}{N}\sum_{i=i}^{N}(Y_i^{experiment} - Y_i^{prediction})^2}$$

B. Dataset for the ML model

- 90 experiments were chosen as sample data (Excluding the experimental data gathered in this study). These experiments varied in many ways, for example: type of adsorbent, adsorbate, and purge gas to name a few however they shared several similarities that made them suitable for our purpose.

- All the experiments have been done using 10 SLPM air.

- In all the experiment the adsorbate was a single compound, and no mixture was used; this is important for us since the developed isotherm prediction model requires a single compound adsorbate.

- Regeneration for all the cases was done using the same technique of wrapping the reactor with heating tape and the duration of heating was also 3 hours for all.

- Properties of tests utilized in this dataset can be seen in **Table** B**.1**

- The complete 90 Data point table is also included in **Table** B**.2**.

Table B.1. Collected samples properties to be used in machine learning algorithms.

Adsorbate (VOC) used in the experiments:

n-butanol, xylenes, p-xylene, n-decane, 2-heptanone, n-butyl acetate, 2-butoxyethanol, 4-methyl-2, pentanone /Methylisobutylketone, n-Heptane, Diethanolamine (dissolved in tetrahydrofuran 13.94 wt%), Methyldiethanolamine (dissolved in tetrahydrofuran 19.24 wt.%), Methyldiethanolamine (dissolved in tetrahydrofuran 20 wt.%), isopropylbenzene, Naphthalene (dissolved in Tetrahydrophuran 11.58%wt), 1-Ethyl-2-Methylbenzene, neopentylbenzene, Pentamethylbenzene(Solid; dissolved in tetrahydrofurane (THF) (83.61% wt.)), (TXIB) dissolved in THF (20.87 wt. %), Indan, 2-Amino-2-Methylpropanol dissolved in THF (42.77 wt.%), benzene, ethylbenzene, butylbenzene, Tetrahydrofuran, Butyl propionate/ Propanoic acid, Butyl isobutyrate

Adsorbents used in the experiments:

Blucher 100777, Heat treated BAC, BAC-H (Hydrogen treated BAC), BAC-O-400 (Oxygen Functionalized BAC), BAC Kureha, ACFC-"20"

Purge gas oxygen impurity (ppmv) used in the experiments:

5, 208, 625, 1250, 2500, 5000, 10000, 20000, 21500 ,210000

Regeneration Temperature (°C) used in the experiments:

200, 288, 400

Table B.2. Datapoints used in the ML algorithm. The first 6 features.

Source	Adsorbent	Adsorbate	Adsorption capacity (wt.%)	Cumulative Heel (wt.%)	Flow (SLPM) / Cross sectional Area(cm2)	O_2 impurity PPMV
1st-quarter-Ford Report	Kureha BAC	n-butanol	38.66	0.00	0.61	5
1st-quarter-Ford Report	Kureha BAC	xylenes	42.37	0.00	0.61	5
1st-quarter-Ford Report	Kureha BAC	xylenes	42.55	0.00	0.61	5
2nd-quarter-Ford report	Kureha BAC	xylenes	42.61	0.25	0.61	5
2nd-quarter-Ford report	Kureha BAC	n-butyl acetate	41.96	0.00	0.61	5
2nd-quarter-Ford report	Kureha BAC	4-methyl-2-pentanone /Methylisobutylketone	37.69	0.00	0.61	5
2nd-quarter-Ford report	Kureha BAC	n-Heptane	31.98	0.00	0.61	5
2nd-quarter-Ford report	Kureha BAC	Tetrahydrofuran	29.28	0.00	0.61	5
2nd-quarter-Ford report	Kureha BAC	Butyl propionate/ Propanoic acid	41.46	0.00	0.61	5
2nd-quarter-Ford report	Kureha BAC	Butyl isobutyrate	41.32	0.00	0.61	5
3d-quarter- Ford report	Kureha BAC	Methyldiethanolamine (dissolved in tetrahydrofuran 19.24 wt.%)	30.62	8.35	0.61	5
3d-quarter-Ford reprot	Kureha BAC	(TXIB) dissolved in THF (20.87 wt. %)	22.70	16.27	0.61	5
3d-quarter-Ford reprot	Kureha BAC	1-Ethyl-2-Methylbenzene	44.00	2.11	0.61	5
3d-quarter-Ford reprot	Kureha BAC	Pentamethylbenzene(Solid; dissolved in tetrahydrofurane (THF) (83.61% wt.))	26.30	4.92	0.61	5
3d-quarter-Ford reprot	Kureha BAC	Indan	46.10	1.39	0.61	5
3d-quarter-Ford reprot	Kureha BAC	Naphthalene (dissolved in	22.25	0.70	0.61	5

		Tetrahydrophuran 11.58%wt)				
3d-quarter-Ford reprot	Kureha BAC	Diethanolamine (dissolved in tetrahydrofuran 13.94 wt%)	20.59	3.29	0.61	5
3d-quarter-Ford reprot	Kureha BAC	2-Amino-2-Methylpropanol dissolved in THF (42.77 wt.%)	32.70	0.96	0.61	5
5th-quarter-Ford reprot	Kureha BAC	2-Amino-2-Methylpropanol dissolved in THF (20 wt.%)	22.73	0.71	0.61	5
Keivan Rahmani's Thesis	Kureha BAC	1,2,4-TMB	43.49	34.57	0.06	215000
Keivan Rahmani's Thesis	Kureha BAC	1,2,4-TMB	43.55	21.11	0.61	215000
Keivan Rahmani's Thesis	Kureha BAC	1,2,4-TMB	43.51	19.13	0.06	10000
Keivan Rahmani's Thesis	Kureha BAC	1,2,4-TMB	43.43	4.10	6.13	10000
Keivan Rahmani's Thesis	Kureha BAC	1,2,4-TMB	44.09	11.94	0.61	10000
Keivan Rahmani's Thesis	Kureha BAC	1,2,4-TMB	43.55	5.50	6.13	215000
Keivan Rahmani's Thesis	Kureha BAC	1,2,4-TMB	42.70	4.02	0.06	5
Keivan Rahmani's Thesis	Kureha BAC	1,2,4-TMB	43.00	4.72	0.01	5
Keivan Rahmani's Thesis	Kureha BAC	1,2,4-TMB	41.80	0.48	0.61	5
Keivan Rahmani's Thesis	Kureha BAC	1,2,4-TMB	42.84	0.17	6.13	5
Mohammad Feizbakhshan's Thesis	Kureha BAC	1,2,4-TMB	43.59	9.53	1.22	210000

Mohammad Feizbakhshan's Thesis	Kureha BAC	1,2,4-TMB	43.68	6.42	1.22	210000
Mohammad Feizbakhshan's Thesis	Kureha BAC	1,2,4-TMB	45.36	6.55	1.22	10000
Mohammad Feizbakhshan's Thesis	ACFC-20"	1,2,4-TMB	61.10	18.61	1.22	210000
Mohammad Feizbakhshan's Thesis	Kureha BAC	1,2,4-TMB	43.74	2.07	1.22	10000
Mohammad Feizbakhshan's Thesis	Kureha BAC	1,2,4-TMB	44.31	1.58	1.22	5
Mohammad Feizbakhshan's Thesis	Kureha BAC	1,2,4-TMB	43.80	0.49	1.22	5
Mohammad Feizbakhshan's Thesis	ACFC-20"	1,2,4-TMB	61.20	0.89	1.22	5
Mohammad Feizbakhshan's Thesis	B-100777"	1,2,4-TMB	66.30	9.59	1.22	210000
Mohammad Feizbakhshan's Thesis	B-100777"	1,2,4-TMB	66.20	0.42	1.22	5
Nastaran Mosavari Thesis	BAC-H	n-decane	35.29	0.71	0.61	5
Nastaran Mosavari Thesis	BAC-O-400.	2-heptanone	38.23	2.18	0.61	5
Nastaran Mosavari Thesis	BAC-O-400.	1,2,4-TMB	44.38	4.34	0.61	5
Nastaran Mosavari Thesis	BAC-H	2-heptanone	38.07	0.32	0.61	5
Nastaran Mosavari Thesis	BAC-O-400.	2-butoxyethanol	42.58	1.62	0.61	5
Nastaran Mosavari Thesis	BAC-H	1,2,4-TMB	41.60	0.32	0.61	5
Nastaran Mosavari Thesis	BAC-O-400.	p-xylene	39.41	3.28	0.61	5
Nastaran Mosavari Thesis	BAC-O-400.	n-decane	35.24	1.24	0.61	5
Nastaran Mosavari Thesis	heat treated BAC (BAC-400)	1,2,4-TMB	45.08	0.73	0.61	5
Nastaran Mosavari Thesis	BAC-H	p-xylene	39.52	0.61	0.61	5

Nastaran Mosavari Thesis	heat treated BAC (BAC-400)	2-butoxyethanol	44.97	1.10	0.61	5
Nastaran Mosavari Thesis	BAC-H	2-butoxyethanol	42.35	0.74	0.61	5
Nastaran Mosavari Thesis	BAC-H	n-butanol	35.32	0.30	0.61	5
Nastaran Mosavari Thesis	BAC-O-400.	n-butanol	34.77	0.57	0.61	5
Nastaran Mosavari Thesis	heat treated BAC (BAC-400)	n-decane	36.68	0.72	0.61	5
Nastaran Mosavari Thesis	BAC-H	ethylbenzene	38.61	0.05	0.61	5
Nastaran Mosavari Thesis	BAC-O-400.	ethylbenzene	39.36	1.41	0.61	5
Nastaran Mosavari Thesis	heat treated BAC (BAC-400)	p-xylene	41.54	0.39	0.61	5
Nastaran Mosavari Thesis	heat treated BAC (BAC-400)	2-heptanone	40.26	0.46	0.61	5
Nastaran Mosavari Thesis	BAC-H	n-butyl acetate	40.00	0.00	0.61	5
Nastaran Mosavari Thesis	BAC-O-400.	n-butyl acetate	39.62	0.37	0.61	5
Nastaran Mosavari Thesis	heat treated BAC (BAC-400)	ethylbenzene	41.07	0.25	0.61	5
Nastaran Mosavari Thesis	heat treated BAC (BAC-400)	n-butanol	36.45	0.25	0.61	5
Nastaran Mosavari Thesis	heat treated BAC (BAC-400)	n-butyl acetate	41.56	0.17	0.61	5
Seyed Mojtaba Hashemi's Thesis	Kureha BAC	1,2,4-TMB	43.90	15.80	0.61	20000
Seyed Mojtaba Hashemi's Thesis	Kureha BAC	isopropylbenzene	45.80	11.20	0.61	10000
Seyed Mojtaba Hashemi's Thesis	Kureha BAC	1,2,4-TMB	43.60	6.30	0.61	1250
Seyed Mojtaba Hashemi's Thesis	Kureha BAC	1,2,4-TMB	44.30	8.80	0.61	2500

155

Seyed Mojtaba Hashemi's Thesis	Kureha BAC	1,2,4-TMB	43.30	11.80	0.61	5000
Seyed Mojtaba Hashemi's Thesis	Kureha BAC	n-butyl acetate	41.10	1.30	0.61	10000
Seyed Mojtaba Hashemi's Thesis	Kureha BAC	isopropylbenzene	44.40	4.60	0.61	5
Seyed Mojtaba Hashemi's Thesis	Kureha BAC	ethylbenzene	40.80	1.50	0.61	10000
Seyed Mojtaba Hashemi's Thesis	Kureha BAC	butylbenzene	43.20	0.80	0.61	5
Seyed Mojtaba Hashemi's Thesis	Kureha BAC	n-butyl acetate	42.60	1.30	0.61	5
Seyed Mojtaba Hashemi's Thesis	Kureha BAC	butylbenzene	41.90	7.00	0.61	10000
Seyed Mojtaba Hashemi's Thesis	Kureha BAC	1,2,4-TMB	44.40	4.20	0.61	625
Seyed Mojtaba Hashemi's Thesis	Kureha BAC	2-heptanone	39.30	2.90	0.61	10000
Seyed Mojtaba Hashemi's Thesis	Kureha BAC	ethylbenzene	40.60	0.10	0.61	5
Seyed Mojtaba Hashemi's Thesis	Kureha BAC	1,2,4-TMB	43.40	1.30	0.61	208
Seyed Mojtaba Hashemi's Thesis	Kureha BAC	n-decane	37.40	3.40	0.61	10000
Seyed Mojtaba Hashemi's Thesis	Kureha BAC	2-butoxyethanol	45.00	1.10	0.61	5
Seyed Mojtaba Hashemi's Thesis	Kureha BAC	neopentylbenzene	41.60	0.70	0.61	5
Seyed Mojtaba Hashemi's Thesis	Kureha BAC	neopentylbenzene	42.00	1.40	0.61	10000
Seyed Mojtaba Hashemi's Thesis	Kureha BAC	2-butoxyethanol	44.70	1.30	0.61	10000

Seyed Mojtaba Hashemi's Thesis	Kureha BAC	2-heptanone	40.30	0.46	0.61	5
Seyed Mojtaba Hashemi's Thesis	Kureha BAC	benzene	27.30	0.20	0.61	10000
Seyed Mojtaba Hashemi's Thesis	Kureha BAC	1-butanol	37.00	0.70	0.61	10000
Seyed Mojtaba Hashemi's Thesis	Kureha BAC	n-decane	36.70	0.70	0.61	5
Seyed Mojtaba Hashemi's Thesis	Kureha BAC	1-butanol	36.40	0.20	0.61	5
Seyed Mojtaba Hashemi's Thesis	Kureha BAC	benzene	26.70	0.00	0.61	5

Table B.3. Datapoints used in the ML algorithm. The next 6 features.

Source	Initial BET Surface Area (m2/g)	Initial Micropore volume (cm3/g)	Initial Total Pore volume (cm3/g)	Molar mass (g/mol)	Density (g/ml)	Boiling point °C
1st-quarter-Ford Report	1307.30	0.47	0.55	74.12	0.81	117.70
1st-quarter-Ford Report	1307.30	0.47	0.55	106.17	0.86	138.50
1st-quarter-Ford Report	1307.30	0.47	0.55	106.17	0.86	138.50
2nd-quarter-Ford report	1307.30	0.47	0.55	106.17	0.86	138.50
2nd-quarter-Ford report	1307.30	0.47	0.55	116.20	0.88	126.00
2nd-quarter-Ford report	1307.30	0.47	0.55	100.16	0.80	116.50
2nd-quarter-Ford report	1307.30	0.47	0.55	100.21	0.68	98.50
2nd-quarter-Ford report	1307.30	0.47	0.55	72.11	0.89	66.00
2nd-quarter-Ford report	1307.30	0.47	0.55	130.18	0.88	145.00
2nd-quarter-Ford report	1307.30	0.47	0.55	144.21	0.86	155.50
3d-quarter- Ford report	1307.30	0.47	0.55	119.16	1.04	247.00
3d-quarter-Ford reprot	1307.30	0.47	0.55	286.41	0.94	380.00
3d-quarter-Ford reprot	1307.30	0.47	0.55	120.19	0.88	165.20
3d-quarter-Ford reprot	1307.30	0.47	0.55	148.24	0.92	232.00
3d-quarter-Ford reprot	1307.30	0.47	0.55	116.16	0.97	177.90
3d-quarter-Ford reprot	1307.30	0.47	0.55	128.17	1.14	217.90
3d-quarter-Ford reprot	1307.30	0.47	0.55	105.14	1.09	217.00
3d-quarter-Ford reprot	1307.30	0.47	0.55	89.14	0.93	165.00
5th-quarter-Ford reprot	1307.30	0.47	0.55	89.14	0.94	165.50
Keivan Rahmani's Thesis	1372.00	0.50	0.57	120.19	0.88	169.38

Keivan Rahmani's Thesis	1372.00	0.50	0.57	120.19	0.88	169.38
Keivan Rahmani's Thesis	1372.00	0.50	0.57	120.19	0.88	169.38
Keivan Rahmani's Thesis	1372.00	0.50	0.57	120.19	0.88	169.38
Keivan Rahmani's Thesis	1372.00	0.50	0.57	120.19	0.88	169.38
Keivan Rahmani's Thesis	1372.00	0.50	0.57	120.19	0.88	169.38
Keivan Rahmani's Thesis	1372.00	0.50	0.57	120.19	0.88	169.38
Keivan Rahmani's Thesis	1372.00	0.50	0.57	120.19	0.88	169.38
Keivan Rahmani's Thesis	1372.00	0.50	0.57	120.19	0.88	169.38
Keivan Rahmani's Thesis	1372.00	0.50	0.57	120.19	0.88	169.38
Mohammad Feizbakhshan's Thesis	1380.00	0.53	0.62	120.19	0.88	169.38
Mohammad Feizbakhshan's Thesis	1380.00	0.53	0.62	120.19	0.88	169.38
Mohammad Feizbakhshan's Thesis	1380.00	0.53	0.62	120.19	0.88	169.38
Mohammad Feizbakhshan's Thesis	1940.00	0.73	0.80	120.19	0.88	169.38
Mohammad Feizbakhshan's Thesis	1380.00	0.53	0.62	120.19	0.88	169.38
Mohammad Feizbakhshan's Thesis	1380.00	0.53	0.62	120.19	0.88	169.38
Mohammad Feizbakhshan's Thesis	1380.00	0.53	0.62	120.19	0.88	169.38

Mohammad Feizbakhshan's Thesis	1940.00	0.73	0.80	120.19	0.88	169.38
Mohammad Feizbakhshan's Thesis	1745.00	0.66	1.78	120.19	0.88	169.38
Mohammad Feizbakhshan's Thesis	1745.00	0.66	1.78	120.19	0.88	169.38
Nastaran Mosavari Thesis	1296.00	0.47	0.55	142.29	0.73	174.00
Nastaran Mosavari Thesis	1288.00	0.47	0.56	114.18	0.80	151.00
Nastaran Mosavari Thesis	1288.00	0.47	0.56	120.19	0.88	169.38
Nastaran Mosavari Thesis	1296.00	0.47	0.55	114.18	0.80	151.00
Nastaran Mosavari Thesis	1288.00	0.47	0.56	118.17	0.90	168.00
Nastaran Mosavari Thesis	1296.00	0.47	0.55	120.19	0.88	169.38
Nastaran Mosavari Thesis	1288.00	0.47	0.56	106.16	0.86	138.00
Nastaran Mosavari Thesis	1288.00	0.47	0.56	142.29	0.73	174.00
Nastaran Mosavari Thesis	1353.00	0.50	0.54	120.19	0.88	169.38
Nastaran Mosavari Thesis	1296.00	0.47	0.55	106.16	0.86	138.00
Nastaran Mosavari Thesis	1353.00	0.50	0.54	118.17	0.90	168.00
Nastaran Mosavari Thesis	1296.00	0.47	0.55	118.17	0.90	168.00
Nastaran Mosavari Thesis	1296.00	0.47	0.55	74.12	0.81	118.00
Nastaran Mosavari Thesis	1288.00	0.47	0.56	74.12	0.81	118.00
Nastaran Mosavari Thesis	1353.00	0.50	0.54	142.29	0.73	174.00
Nastaran Mosavari Thesis	1296.00	0.47	0.55	106.16	0.87	136.00
Nastaran Mosavari Thesis	1288.00	0.47	0.56	106.16	0.87	136.00
Nastaran Mosavari Thesis	1353.00	0.50	0.54	106.16	0.86	138.00
Nastaran Mosavari Thesis	1353.00	0.50	0.54	114.18	0.80	151.00
Nastaran Mosavari Thesis	1296.00	0.47	0.55	116.16	0.88	126.00

Nastaran Mosavari Thesis	1288.00	0.47	0.56	116.16	0.88	126.00
Nastaran Mosavari Thesis	1353.00	0.50	0.54	106.16	0.87	136.00
Nastaran Mosavari Thesis	1353.00	0.50	0.54	74.12	0.81	118.00
Nastaran Mosavari Thesis	1353.00	0.50	0.54	116.16	0.88	126.00
Seyed Mojtaba Hashemi's Thesis	1371.00	0.50	0.57	120.19	0.88	169.38
Seyed Mojtaba Hashemi's Thesis	1371.00	0.50	0.57	120.20	0.86	152.40
Seyed Mojtaba Hashemi's Thesis	1371.00	0.50	0.57	120.19	0.88	169.38
Seyed Mojtaba Hashemi's Thesis	1371.00	0.50	0.57	120.19	0.88	169.38
Seyed Mojtaba Hashemi's Thesis	1371.00	0.50	0.57	120.19	0.88	169.38
Seyed Mojtaba Hashemi's Thesis	1371.00	0.50	0.57	116.20	0.88	126.00
Seyed Mojtaba Hashemi's Thesis	1371.00	0.50	0.57	120.20	0.86	152.40
Seyed Mojtaba Hashemi's Thesis	1371.00	0.50	0.57	106.20	0.86	136.00
Seyed Mojtaba Hashemi's Thesis	1371.00	0.50	0.57	134.20	0.86	183.00
Seyed Mojtaba Hashemi's Thesis	1371.00	0.50	0.57	116.20	0.88	126.00
Seyed Mojtaba Hashemi's Thesis	1371.00	0.50	0.57	134.20	0.86	183.00
Seyed Mojtaba Hashemi's Thesis	1371.00	0.50	0.57	120.19	0.88	169.38
Seyed Mojtaba Hashemi's Thesis	1371.00	0.50	0.57	114.20	0.81	151.00

Seyed Mojtaba Hashemi's Thesis	1371.00	0.50	0.57	106.20	0.86	136.00
Seyed Mojtaba Hashemi's Thesis	1371.00	0.50	0.57	120.19	0.88	169.38
Seyed Mojtaba Hashemi's Thesis	1371.00	0.50	0.57	142.30	0.73	174.00
Seyed Mojtaba Hashemi's Thesis	1371.00	0.50	0.57	118.17	0.90	171.00
Seyed Mojtaba Hashemi's Thesis	1371.00	0.50	0.57	148.30	0.86	185.00
Seyed Mojtaba Hashemi's Thesis	1371.00	0.50	0.57	148.30	0.86	185.00
Seyed Mojtaba Hashemi's Thesis	1371.00	0.50	0.57	118.17	0.90	171.00
Seyed Mojtaba Hashemi's Thesis	1371.00	0.50	0.57	114.20	0.81	151.00
Seyed Mojtaba Hashemi's Thesis	1371.00	0.50	0.57	78.11	0.87	80.00
Seyed Mojtaba Hashemi's Thesis	1371.00	0.50	0.57	74.12	0.81	117.70
Seyed Mojtaba Hashemi's Thesis	1371.00	0.50	0.57	142.30	0.73	174.00
Seyed Mojtaba Hashemi's Thesis	1371.00	0.50	0.57	74.12	0.81	117.70
Seyed Mojtaba Hashemi's Thesis	1371.00	0.50	0.57	78.11	0.87	80.00

Table B.4. Datapoints used in the ML algorithm. The last 6 features.

Source	Melting point °C	Electronic polarization of the test (cm³/mol)	Molecular parachors	Molar volume (m³/kmol)	polarizability (Å³)	Henrys Law Constant (atm-m3/mole)
1st-quarter-Ford Report	-89.50	22.15	207.00	0.09	8.80	0.00
1st-quarter-Ford Report	-34.00	35.96	284.67	0.12	14.20	0.01
1st-quarter-Ford Report	-34.00	35.96	284.67	0.12	14.20	0.01
2nd-quarter-Ford report	-34.00	35.96	284.67	0.12	14.20	0.01
2nd-quarter-Ford report	-78.00	31.52	294.15	0.13	13.42	0.00
2nd-quarter-Ford report	-84.70	29.81	272.90	0.13	11.80	0.00
2nd-quarter-Ford report	-90.61	35.05	315.93	0.14	13.70	1.80
2nd-quarter-Ford report	-108.40	19.88	181.30	0.26	42.70	0.00
2nd-quarter-Ford report	-89.00	36.15	338.19	0.15	14.40	
2nd-quarter-Ford report	-91.50	41.54	378.86	0.16	16.20	
3d-quarter- Ford report	-21.00	32.28	292.57	0.11	12.70	0.00
3d-quarter-Ford reprot	-70.00	80.37	710.54	0.30	31.50	0.00
3d-quarter-Ford reprot	-81.00	40.00	316.69	0.14	16.10	0.00
3d-quarter-Ford reprot	54.50	47.71	374.17	0.17	20.00	0.00
3d-quarter-Ford reprot	-51.40	39.04	298.08	0.12	15.20	0.00
3d-quarter-Ford reprot	80.26	40.10	283.10	0.13	17.50	0.00
3d-quarter-Ford reprot	28.00	26.72	247.72	0.10	10.80	0.00
3d-quarter-Ford reprot	25.50	25.50	231.30	0.10	10.20	0.00
5th-quarter-Ford reprot	25.50	25.47	231.06	0.10	10.20	

Keivan Rahmani's Thesis	-43.78	40.43	317.92	0.14	16.10	0.01
Keivan Rahmani's Thesis	-43.78	40.43	317.92	0.14	16.10	0.01
Keivan Rahmani's Thesis	-43.78	40.43	317.92	0.14	16.10	0.01
Keivan Rahmani's Thesis	-43.78	40.43	317.92	0.14	16.10	0.01
Keivan Rahmani's Thesis	-43.78	40.43	317.92	0.14	16.10	0.01
Keivan Rahmani's Thesis	-43.78	40.43	317.92	0.14	16.10	0.01
Keivan Rahmani's Thesis	-43.78	40.43	317.92	0.14	16.10	0.01
Keivan Rahmani's Thesis	-43.78	40.43	320.64	0.14	16.10	0.01
Keivan Rahmani's Thesis	-43.78	40.43	317.92	0.14	16.10	0.01
Keivan Rahmani's Thesis	-43.78	40.43	317.92	0.14	16.10	0.01
Mohammad Feizbakhshan's Thesis	-43.78	40.43	317.92	0.14	16.10	0.01
Mohammad Feizbakhshan's Thesis	-43.78	40.43	317.92	0.14	16.10	0.01
Mohammad Feizbakhshan's Thesis	-43.78	40.43	317.92	0.14	16.10	0.01
Mohammad Feizbakhshan's Thesis	-43.78	40.43	317.92	0.14	16.10	0.01
Mohammad Feizbakhshan's Thesis	-43.78	40.43	317.92	0.14	16.10	0.01
Mohammad Feizbakhshan's Thesis	-43.78	40.43	317.92	0.14	16.10	0.01

Mohammad Feizbakhshan's Thesis	-43.78	40.43	317.92	0.14	16.10	0.01
Mohammad Feizbakhshan's Thesis	-43.78	40.43	317.92	0.14	16.10	0.01
Mohammad Feizbakhshan's Thesis	-43.78	40.43	317.92	0.14	16.10	0.01
Mohammad Feizbakhshan's Thesis	-43.78	40.43	317.92	0.14	16.10	0.01
Nastaran Mosavari Thesis	29.70	48.31	428.56	0.20	20.61	5.15
Nastaran Mosavari Thesis	-35.00	35.21	322.81	0.14	14.31	0.00
Nastaran Mosavari Thesis	-43.78	40.43	317.92	0.14	16.10	0.01
Nastaran Mosavari Thesis	-35.00	35.21	322.81	0.14	14.31	0.00
Nastaran Mosavari Thesis	-74.80	33.16	296.89	0.13	14.37	0.00
Nastaran Mosavari Thesis	-43.78	40.43	317.92	0.14	16.10	0.01
Nastaran Mosavari Thesis	13.20	35.96	284.41	0.12	14.20	0.01
Nastaran Mosavari Thesis	29.70	48.31	428.56	0.20	20.61	5.15
Nastaran Mosavari Thesis	-43.78	40.43	317.92	0.14	16.10	0.01
Nastaran Mosavari Thesis	13.20	35.96	284.41	0.12	14.20	0.01
Nastaran Mosavari Thesis	-74.80	33.16	296.89	0.13	14.37	0.00
Nastaran Mosavari Thesis	-74.80	33.16	296.89	0.13	14.37	0.00
Nastaran Mosavari Thesis	-89.80	22.15	206.99	0.09	9.21	0.00
Nastaran Mosavari Thesis	-89.80	22.15	206.99	0.09	9.21	0.00
Nastaran Mosavari Thesis	29.70	48.31	428.56	0.20	20.61	5.15
Nastaran Mosavari Thesis	-94.90	35.80	284.96	0.12	14.20	0.01
Nastaran Mosavari Thesis	-94.90	35.80	284.96	0.12	14.20	0.01
Nastaran Mosavari Thesis	13.20	35.96	284.41	0.12	14.20	0.01

Nastaran Mosavari Thesis	-35.00	35.21	322.81	0.14	14.31	0.00
Nastaran Mosavari Thesis	-78.00	31.51	295.37	0.13	13.42	0.00
Nastaran Mosavari Thesis	-78.00	31.51	295.37	0.13	13.42	0.00
Nastaran Mosavari Thesis	-94.90	35.80	284.96	0.12	14.20	0.01
Nastaran Mosavari Thesis	-89.80	22.15	206.99	0.09	9.21	0.00
Nastaran Mosavari Thesis	-78.00	31.51	295.37	0.13	13.42	0.00
Seyed Mojtaba Hashemi's Thesis	-43.78	40.43	317.92	0.14	16.10	0.01
Seyed Mojtaba Hashemi's Thesis	-96.00	40.39	322.19	0.14	16.00	0.01
Seyed Mojtaba Hashemi's Thesis	-43.78	40.43	317.92	0.14	16.10	0.01
Seyed Mojtaba Hashemi's Thesis	-43.78	40.43	317.92	0.14	16.10	0.01
Seyed Mojtaba Hashemi's Thesis	-43.78	40.43	317.92	0.14	16.10	0.01
Seyed Mojtaba Hashemi's Thesis	-78.00	31.52	294.15	0.13	13.42	0.00
Seyed Mojtaba Hashemi's Thesis	-96.00	40.39	322.19	0.14	16.00	0.01
Seyed Mojtaba Hashemi's Thesis	-93.00	35.95	286.06	0.12	14.20	0.01
Seyed Mojtaba Hashemi's Thesis	-88.00	45.27	365.20	0.16	17.90	0.01
Seyed Mojtaba Hashemi's Thesis	-78.00	31.52	294.15	0.13	13.42	0.00
Seyed Mojtaba Hashemi's Thesis	-88.00	45.27	365.20	0.16	17.90	0.01
Seyed Mojtaba Hashemi's Thesis	-43.78	40.43	317.92	0.14	16.10	0.01

Seyed Mojtaba Hashemi's Thesis	-35.00	34.74	319.79	0.14	14.31	0.00
Seyed Mojtaba Hashemi's Thesis	-93.00	35.95	286.06	0.12	14.20	0.01
Seyed Mojtaba Hashemi's Thesis	-43.78	40.43	317.92	0.14	16.10	0.01
Seyed Mojtaba Hashemi's Thesis	-29.70	48.32	429.19	0.20	19.10	4.83
Seyed Mojtaba Hashemi's Thesis	-74.80	33.16	296.39	0.13	14.37	0.00
Seyed Mojtaba Hashemi's Thesis	-44.72	49.80	400.75	0.17	19.70	
Seyed Mojtaba Hashemi's Thesis	-44.72	49.80	400.75	0.17	19.70	
Seyed Mojtaba Hashemi's Thesis	-74.80	33.16	296.39	0.13	14.37	0.00
Seyed Mojtaba Hashemi's Thesis	-35.00	34.74	319.79	0.14	14.31	0.00
Seyed Mojtaba Hashemi's Thesis	5.50	26.36	206.22	0.09	10.32	0.01
Seyed Mojtaba Hashemi's Thesis	-89.80	22.04	205.97	0.92	9.21	0.00
Seyed Mojtaba Hashemi's Thesis	-29.70	48.32	429.19	0.20	19.10	4.83
Seyed Mojtaba Hashemi's Thesis	-89.80	22.04	205.97	0.92	9.21	0.00
Seyed Mojtaba Hashemi's Thesis	5.50	26.36	206.22	0.09	10.32	0.01

C. MATLAB code for PSD prediction

```matlab
function V20 = Pore_size_changes_Micropores_ML(file_name,Heal_data)
subsetA = xlsread(file_name,1,'A3:B50');
Molar_volume =0.14 ;     %TMB molar volume
Micropore_Volume_percent=- 2.295 * Heal_data*100- 8.418 * Molar_volume+ 97.578;

Pore_width = subsetA(:,1);
Pore_width_below_20 = Pore_width(Pore_width<=20);
dV = subsetA(:,2);
dV20 = dV(1:size(Pore_width_below_20));
Pore_width_below_32 = Pore_width(Pore_width<=32);
Pore_width_20_32 = Pore_width_below_32(Pore_width_below_32>20);
dV = subsetA(:,2);
dV32 = dV(1:size(Pore_width_below_32));
dv21_32 = dV(18:size(Pore_width_20_32,1)+17);
Micropore_volume = trapz(Pore_width_below_20,dV20);
Micropore_voume_final = Micropore_volume*(Micropore_Volume_percent/100);
S = cumtrapz(Pore_width_below_20,dV20);
 Sprime = zeros(length(S),1);
 Sprime(1)=S(1);
 for j=2:length(S)
    Sprime(j)=S(j)-S(j-1);
 end
Sprime(1)=S(2)+0.01;
E0 = Characteristic_Energy_micropore(file_name);
 temp1 = length(Sprime)-length(E0);
 temp2 = ones(temp1,1);
 E = vertcat(E0,temp2);
 MSP= E.* Sprime;
while trapz(Pore_width_below_20,dV20) -
Micropore_voume_final>0.000000000000000000000001
   dV20 = dV20-MSP*0.00001;
   dV20(dV20<0)=0;
end
dV20
dv_new = vertcat(dV20,dv21_32);
V20 = trapz(Pore_width_below_20,dV20);
fprintf('your new available total micropore volume is %10f5\n',V20);
V32 = trapz(Pore_width_below_32,dv_new);
```

```
fprintf('your new available V32 is %10f5\n',V32);
V = trapz(Pore_width,dV);
fprintf('your new available total pore volume is %10f5\n',V);
dV(1:length(dV20)) = dV20;
plot(Pore_width,dV,'r');
axis([0,100,-0.01,0.15]);
grid on;
title('Pore Size Disturbution for cycle ');
ylabel('d(V) (cm3/A/g)');
xlabel('Pore width');
hold off;
end
```

D. Regression Tree graph

170